ONBOARD WAVE FORECASTS

by

Sofia Isilda Nunes de Caires

This thesis is submitted for the degree of Master of Science

Department of Naval Architecture and Ocean Engineering University of Glasgow

March 1997

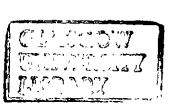

DECLARATION

Except where reference is made to the work of others, this thesis is believed to be original.

DEDICATION

To Father, Aunt Angela and Uncle Lindolfo, who encouraged me to go on studying.

ACKNOWLEDGEMENTS

To Prof. Carlos Guedes Soares, for his supervision, his support, and for the opportunities he gave me for working and studying abroad, now and in the past.

To Dr. K.S. Varyani, for his supervision and patience in reviewing several stages of this thesis.

To JNICT, Junta Nacional de Investigação Científica, who supported the research through the Portuguese Sub-Program Ciência e Tecnologia do 2° Quadro Comunitário de Apoio.

To Dr. Leo Holthuijsen and Dr. Nico Booij, of the Hydraulics Department of Delft University of Technology, for all they did for me during my stay in Delft. The example in Section 5.3 was performed in Delft under the supervision of Leo, who contributed extensively to my formation.

To Prof. Barltrop, Head of the Department, for the helpful suggestions and the review of the thesis.

To Frutuoso, for his precious help in finding batimetry data in the Internet.

To Mr. Selway and Mr. Shields, from OceanRoutes, for the ship routes and weather ship route information provided.

To all the researchers, students and staff at the Secção Autónoma de Engenharia Naval, for their friendship and for the good time spent together during my MSc. Special thanks to Ulla, Ricardo, Marise, Carla, Manolo, and Dulce.

To Mrs. Thelma Will, Mr. David Percival, Mr. David Sinclair, secretary and technicians of the Hydrodynamics Laboratory, for their help during my stay in Glasgow. To my house mates at Acre House for their company and friendship, specially Oguz and Dilek.

To Prof. Faulkner and Mrs. Faulkner for their interest and help.

At last but not at least I would like to thank Zé-tó for every single thing, and acknowledge his help.

SUMMARY

The aim of this thesis is to provide an easy, fast and reliable way of forecasting the wave conditions onboard a ship once the wind fields are provided. The resulting methodology, called BOWFOR, is based on the assimilation of the second generation wave model DOLPHIN with wave observations onboard the ship.

Specifically, BOWFOR is intended as a methodology for providing wave forecasts at any time-space location or set of locations chosen, and in particular along the ship route. It is executed by running a model on a personal computer, and requires wind field forecasts for the trip at the departure of the ship. The forecasts are produced and updated during the journey through the assimilation of DOLPHIN with buoy, satellite or visual observations. In the latter case, the observations are corrected by currently used empirical formulas.

It will be seen that the methodology requires only four daily wave observations to produce good forecasts, and the forecasts are valid for at least two days. In the important situation in which communications are lost, the possibility of assimilating visual observations allows efficient forecasts. Thus the BOWFOR methodology, by regularly providing the captain of the ship with updated information on the wave conditions ahead, permits an optimised route planning.

Setting up BOWFOR involved essentially the choice of an appropriate wave model and an efficient assimilation technique. It also involved the study of the wave theories behind wave models and of assimilation techniques, the adaptation of WAM and DOLPHIN, the wave models chosen for our investigation, the testing of models, analysis of results, and getting sensibility about the relevant variables and parameters, and the choice and acquisition of data and planning of the experiments.

The thesis is divided into seven chapters.

Chapter 1 is introductory. Chapter 2 describes the basics of linear wave theory, and gives an account of the representation of random sea waves by spectral analysis methods. Chapter 3 outlines the history of wind waves theory along with the physics behind wave models.

In Chapter 4 the performances of WAM, a third generation wave model, and of DOLPHIN, a second generation model, are compared. The comparison is made through hindcasts of storms that occurred in the Portuguese coast. The chapter includes some details about the adaptation of the DOLPHIN and WAM models. Both models were run on a personal computer, as a way of providing straightforward comparisons in a realistic environment. It is shown that WAM is to a certain extent more accurate than DOLPHIN, but that it cannot be efficiently run on board ships. The relatively good results provided by DOLPHIN justify its choice as the model to be used by BOWFOR.

Chapter 5 is dedicated to the improvement of DOLPHIN forecasts by a recently introduced assimilation technique. The technique is tested with observations (measured and simulated) made with buoys at the forecast location and upwave of the forecast

location, and with satellite. It is shown that the continuous assimilation of significant wave height and mean wave period is very efficient, providing even better results than WAM.

Chapter 6 describes the BOWFOR methodology and its application to a ship journey from Europe to North America and return. Ship visual observations obtained during the trip are used to assimilate DOLPHIN, providing forecasts for the next points in the route. This application was based on synthetic data. The assimilation procedure used 4 ship observations per day during a 5-day assimilation period, and provided a 2-day forecast. This procedure was continuously performed along the journeys. This context is the most critical one may expect to have in practice, in the sense that there will usually be more information available, *e.g.* more visual observations, other ships' observations, or satellite or buoys observations, which may also be added to the assimilation scheme. Better results are expected if the number of observations of any source is increased, but what is of interest is that even in this critical setting the results were very good, specially on the trip from North America to Europe, when the ship was forerunning the wave conditions.

Chapter 7 gathers achievements, conclusions and suggestions for further work.

CONTENTS

NOMENCLATURE

Notations commonly used in this thesis are described here. However, in certain cases where certain notations are not frequently used, they are described as they appear in respective chapters.

Roman symbols

a	wave amplitude
A	Philips' parameter
B	Miles' parameter
c	wave velocity
c_g	wave group velocity
c_{diss}	DOLPHIN dissipation coefficient
E	wave energy
f	wave frequency
f_m	mean wave frequency
f_p	wave peak frequency
F	wave number spectrum
$F_p(\vec{k},\omega)$	three dimensional spectrum of pressure fluctuations
g	acceleration of gravity
h	water depth
H	wave height
H_s	significant wave height
J	cost function
J^{χ}	misfit between the observed waves and the modelled waves
J^{ψ}	difference between the best-fit control variables and their first-guess value
k	wave number modulus
$\vec{k}$	wave number vector
L	wave length
m_n	nth order spectral moment
N	action spectral density

p	pressure
$R(\vec{X},\tau)$	three-dimensional auto-covariance function
$S(\vec{k},\omega)$	three-dimensional wave spectrum
$S(\omega,\theta)$	directional angular frequency wave spectrum
$S(f,\theta)$	directional frequency wave spectrum
$S(f)$	wave frequency spectrum
S_J	JONSWAP spectrum
S_{PM}	Pierson-Moskowitz spectrum
T	wave period
T_z	mean zero-upcrossing period
u_*	wind friction velocity
z_0	roughness length
U_5	wind speed at a height of five meters above the water surface
U_{10}	wind speed at a height of ten meters above the water surface
w'	waves induced fluctuation in the horizontal component of the mean wind velocity

Greek symbols

α	Phillips' constant
α_c	dimensionless Charnock parameter
$\hat{\alpha}$	a constant, and an integral parameter of the wave steepness
$\hat{\alpha}_{PM}$	integral parameter of the wave steepness for the Pierson-Moskowitz spectrum
β_m	a constant
δ	Dirac function
ε	wave phase angle
ϕ	wind speed direction, longitude
ϕ_J	JONSWAP shape function
ϕ_{PM}	Pierson Moskowitz shape function
Φ_{ds}	dissipation source term
Φ_{in}	wind input source term
Φ_{nl}	non linear interactions source term
Φ	net source term

γ	peak enhancement factor
γ_{in}	growth factor
γ_{ds}	dissipation factor
η	wave profile
κ	von Kármán constant
λ	latitude
μ	dimensionless critical height
φ	velocity potential
θ	wave direction
ρ	water density
ρ_a	air density
σ^2	variance of the sea state
τ	kinematic stress
τ	DOLPHIN decay time scale
τ_w	wave stress
ω	wave angular frequency
$\vec{\psi}$	best-fit control variables
$\vec{\psi}^{fg}$	first-guess control variables

Abbreviations

ND	number of directions in the WAM model
NF	number of frequencies in the WAM model
r.m.s.	root-mean-square error
S.I.	scatter-index
ECMWF	European Centre of Medium Range Weather Forecast

LIST OF FIGURES

LIST OF TABLES

CHAPTER 1

INTRODUCTION

There was a time when sailors went to the sea in fragile vessels, with no knowledge of what wave conditions to expect. Figure *1.1*, a print by the Japanese artist Hokusai, illustrates fragile boats being caught in the middle of a storm with giant waves, a situation probably common in the past.

Nowadays, not only ships and boats are more robust and safer, but also the capability of predicting and of providing information to ships about the wave conditions is greatly developed.

Shipping companies, sometimes through specialised weather routing agencies, regularly provide wave forecasts to ships on route. The wave forecasts are supplied for some days from the ship's departure, and then may or may not be updated during the journey; when the weather conditions deteriorate, the information is almost always updated.

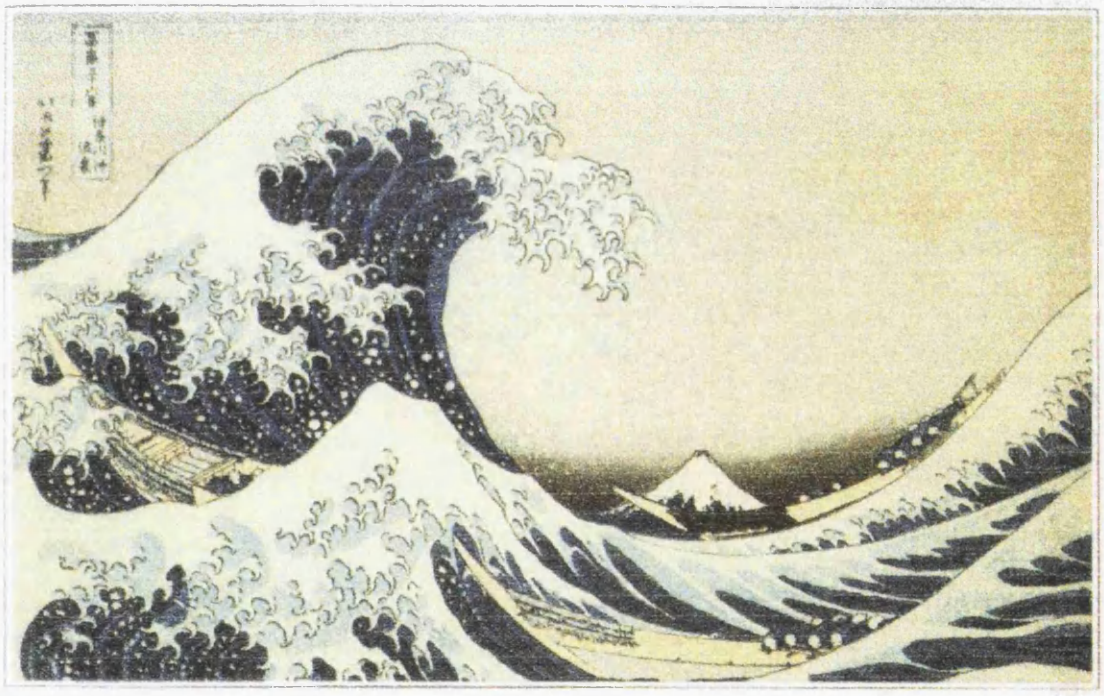

Figure 1.1 - The Wave (three boats battle against a giant wave); by Hokusai (1760-1849).

Navigation companies and routing agencies are often subjected to economical pressures and sometimes it may happen that the urge for a ship to arrive at a harbour on time overcomes the weather safety. The performance of the captain of the ship is thus subjected to the credibility of this external information. On the other hand, the observations of wave conditions onboard ships are necessarily more accurate than the forecasts provided on land, and it seems that the combination of the two types of information could be used to improve the predictions. Since there may be abrupt changes in the weather, changes in the loading conditions of the ship, or communication problems, it is desirable to produce weather forecasts onboard ships rather than relying exclusively on land predictions.

It is believed that wave models, and especially assimilated wave models, can be efficiently used onboard to improve the forecasts, and it is the objective of this thesis to suggest a methodology, BOWFOR, which will serve such a purpose.

This chapter introduces the concepts of wave model and assimilation, and then describes the structure of the thesis, stating its innovative aspects.

The waves generated by the wind on the ocean surface are modelled as a random process characterised by a spectrum, whose evolution is specified by physical laws. On a 'fast' time-space scale, the motion of the sea surface is assumed to be a gaussian, stationary and homogeneous stochastic process, characterised locally by the wave spectrum. On a 'slow' space-time scale this spectrum is allowed to vary in interaction with the environment according to the energy balance equation. The most crucial aspect of a wave model is its ability to specify the directional wave spectrum for realistic wind fields that vary in space and time.

The first generation of wave models, whose formulation was based on the wave energy balance equation, appeared in the 50's. Although the physics behind the process was not correct, these models were capable of providing wave forecasts. The second generation wave models that appeared in the 70's enabled a more accurate evolution of the wave spectrum. In the late 80's the second generation models were superseded by the present third generation wave models.

The improved understanding of the physical process responsible for wind wave evolution and the new computational methods brought by the third generation models added an increased computational expense, but with only marginal improvements in results. The second generation wave models had already been tuned to a considerable extent, and provided wave height forecasts comparable to those of the third generation wave models. Thus the benefits of the latter are mainly related to a more explicit formulation of the underlying physics of the wave evolution resulting in a better representation of the wave spectrum itself, rather than to the quality of wave height forecasts.

Even if there was to come a new generation of wave models with improved physics, better numerical schemes and higher resolution, the errors in wave predictions would still not fall within the error band of observations. This is because the errors due to the poor specification of the wind field are generally significantly greater than the wave model errors, so that better wave predictions are only possible with better driven wind fields. Since as yet there are no accurate wind fields, wave predictions can only be improved by 'improving the wind field', *i.e.*, tuning them to the observed wave predictions.

Wind fields and wave fields can be improved, to some extent, by assimilating wave observations. The essence of such assimilation is that wave observations just prior to the forecast are used to modify the wind fields and wave fields in such a way that the calculated waves are best-fit to the observed waves. Thus the forecast system of assimilated wave models adapts rapidly to the wave observations.

This thesis suggests BOWFOR (Onboard Wave Forecast methodology), a methodology that provides good wave forecasts onboard a ship by assimilating ship wave observations along the trip. This provides a versatile system capable of giving forecasts on any location of any chosen route, and which can also take into account external information (satellite, buoy or other ships' observations).

In the process of assimilating observations, the observations are given a coefficient of uncertainty, and visual wave observations are corrected by established empirical formulas.

The thesis is divided in seven chapters.

Chapters 2 and 3 describe the theory underlying the wave models.

Chapter 2 presents the linear wave theory and the representation of random sea waves by spectral analysis methods.

Chapter 3 outlines the history of wind waves theory along with physics behind the three generations of wave models.

Chapter 4 compares the performances of WAM, a third generation wave model developed by the WAMDI Group (1988), and of DOLPHIN, the second generation model developed by Holthuijsen and De Boer (1988). The comparison is made through hindcasts of storms that occurred in the Portuguese coast.

While the DOLPHIN model runs on a PC, the WAM model is currently run on CRAY computer, and its code had to be adapted so that both models could be run on a PC, thus providing a straightforward comparison.

The two models are assessed in terms of their adequacy for being used onboard ships. It is shown that WAM is to a certain extent more accurate than DOLPHIN, but that it cannot be efficiently run on board ships: it is computationally time- and space-consuming and not as user friendly as DOLPHIN. These conclusions justify using DOLPHIN for on board wave forecasts.

The wave forecasts of DOLPHIN can be improved by assimilating wave observations made by buoys, satellite or even ships. Chapter 5 presents an assimilation technique to be used with this wave model. The technique is tested with observations (measured and simulated) made by buoys in the forecast location and upwave of the forecast location, and by satellite. The continuous assimilation of significant wave height and mean wave period is shown to be very efficient, providing even better results than WAM.

Chapter 6 describes the BOWFOR methodology and its application to a ship journey from Europe to North America and return. Ship observations during the trip are used to assimilate DOLPHIN, providing forecasts for the next points in the route. This system enables the captain to know not only the expected wave conditions ahead in the route but also what those conditions would be if he wished to change the route.

Chapter 7 gathers achievements, conclusions and proposals of further work.

The final output of the thesis is the BOWFOR methodology, which is believed to be a contribution to the onboard route wave forecast.

The thesis has the following innovative aspects:

> Adaptation of the code of the most used third generation wave model WAM from its running in a main frame to a personal computer and comparison with the second generation wave model DOLPHIN. The results give a straightforward comparison between the two models;
>
> Setting up of continuous assimilations of significant wave and mean wave frequency. The examples suggest that the assimilation provides a very efficient forecast system;

Development of an easy, reliable and fast system of forecasting wave conditions onboard. The system is independent of land information after the departure of the ship, and therefore, even if communications are lost, good wave forecasts can be computed onboard the vessel.

CHAPTER 2

Description of Sea Waves

2.1 Linear Wave Theory

Ocean waves can be classified as sound, capillary, gravity, inertial and planetary waves. The wave period is of several months for planetary waves, half to one day for tidal waves, several hours for storm surges, dozens of minutes for tsunamis, a few seconds for wind-induced gravity waves, and fractions of a second for capillary waves.

This thesis will be mainly concerned with wind-induced gravity waves, because of their randomness and period, which greatly influence the response of a ship at sea. To start with, the basic dynamics of a sinusoidal motion on the free surface of a fluid are considered.

The simplest form of a surface wave is regular, long crested, sinusoidal, and with constant amplitude and period. The definition of the parameters of such a wave is as given below.

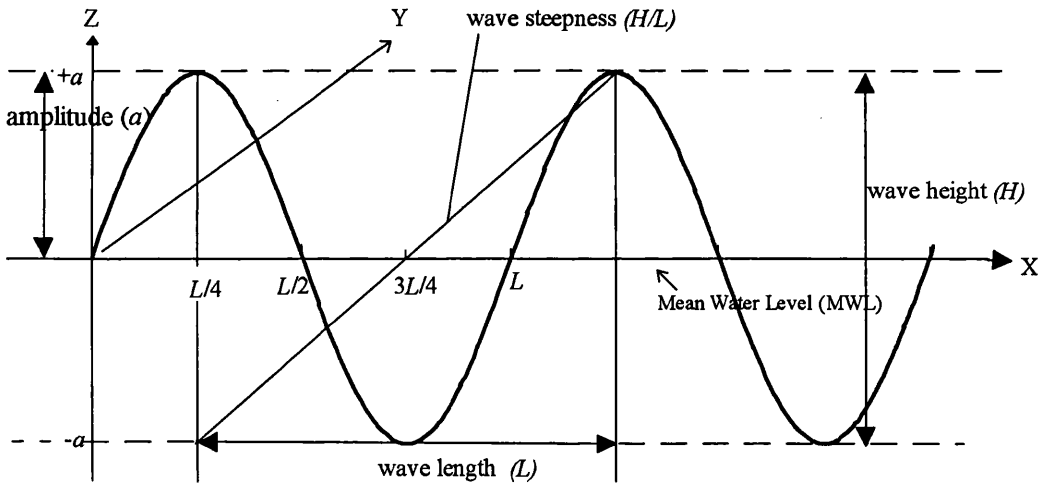

Figure 2.1 - Wave profile with various parameters.

The distance between the wave crest or trough and the mean water level is referred to as the wave amplitude, a, and twice this amplitude is the wave height, H, which is the distance between the wave crest and trough. The distance between two successive peaks or troughs is referred to as the wave length, L. These parameters are as seen in Figure *2.1*. The positive X-axis is in the direction of wave propagation, and the Y-axis is perpendicular to the X-axis and parallel to the wave crests. The Z-axis is perpendicular to the mean water surface defined by X-Y plane, and positive upwards.

Fixing a point in space and describing the sinusoidal motion as a function of time, *i.e.*, replacing the X-axis in Figure *2.1* by a time axis referred to as T-axis, leads to the definition of the time parameters. The time interval between two successive peaks or troughs passing a fixed point is referred to as the wave period, T. The number of peaks

or troughs which pass a fixed point per second is known as wave frequency, f, which is the inverse of the wave period.

From the above parameters we can further define the wave number k as $2\pi/L$, the wave angular frequency ω as $2\pi/T$, the wave steepness as H/L, and the wave phase speed c as L/T.

2.2 Mathematical formulation

Let us restrict ourselves to the case of constant water depth h and wave period T. For the sake of simplicity we will consider the case of two-dimensional motion. The wave height is assumed to be constant in the direction perpendicular to that of wave propagation, *i.e.*, along the crests. These assumptions of constant wave height and period exclude wind generated waves. In the simplest case one usually thinks of waves as an undulation over the water surface that propagates without change of form. Therefore we assume waves of constant form. This turns out to yield important mathematical simplifications because the motion appears to be steady.

We start by looking for the phase speed solution of an ocean surface wave described by

$$\eta(x,t) = a\cos(\omega t - kx), \tag{2.1}$$

in which η is the wave profile displacement from the mean water level (MWL), which is determined so that

$$\int_0^L \eta dx = 0. \tag{2.2}$$

The equations that describe the flow are obtained from the conservation of mass of the fluid, and from Newton's second law.

The flow is assumed to be incompressible, and the equation for the conservation of mass becomes the volume conservation or *continuity equation*

$$\frac{\partial u}{\partial x} + \frac{\partial w}{\partial z} = 0. \tag{2.3}$$

Applying Newton's second law the following equations are obtained:

$$\rho \frac{du}{dt} = \rho\left(\frac{\partial u}{\partial t} + u\frac{\partial u}{\partial x} + w\frac{\partial u}{\partial z}\right) = -\frac{\partial p}{\partial x} + \text{viscous forces}, \tag{2.4a}$$

$$\rho \frac{dw}{dt} = \rho\left(\frac{\partial w}{\partial t} + u\frac{\partial w}{\partial x} + w\frac{\partial w}{\partial z}\right) = -\frac{\partial p}{\partial z} - \rho g + \text{viscous forces}, \tag{2.4b}$$

where u, w are the velocity in the x and z directions respectively, p is the pressure, ρ is the water density and g is the acceleration of gravity. The terms $\partial u/\partial t$, $\partial w/\partial t$ are called local accelerations, and the rest of the acceleration terms like $u\partial u/\partial x$ and $u\partial w/\partial x$ are referred to as convective accelerations.

If the flow is laminar and the physical properties of the fluid satisfy certain conditions the viscous forces can be written in the x- and z-directions as

$$\mu\nabla^2 u \text{ and } \mu\nabla^2 w,$$

respectively, where μ is the kinematic viscosity and ∇ denotes Hamilton's differential operator,

$$\nabla = \left(\frac{\partial}{\partial x}, \frac{\partial}{\partial z}\right).$$

Substituting these viscosity forces into Equations *2.4a* and *b*, respectively, leads to the Navier-Stokes equations.

If the flow is turbulent, the instantaneous velocities can be regarded as a sum of a mean velocity and a velocity fluctuation. The velocity fluctuations will then represent additional (turbulent) stresses, called Reynolds stresses, and the resulting equations are called Reynolds equations.

The effects of viscosity and turbulence lead to the development of boundary layers at the bottom which affect the motion of the body of water outside the boundary layer. To be able to neglect the influence of this effect, upper bounds must be specified for *L/h* and *H/h*. An approximate criterion is $HL/h^2 < 20$ or *30*, depending on the bottom roughness. The waves obeying this criterion are referred to as short-period waves because the excluded waves are tidal waves and tsunamis near the coast.

The viscous forces will therefore be neglected, and the Eqs. *2.4* become the *Euler equations*

$$\frac{\partial u}{\partial t} + u\frac{\partial u}{\partial x} + w\frac{\partial u}{\partial z} = -\frac{1}{\rho}\frac{\partial p}{\partial x} \qquad \textbf{(2.5a)}$$

$$\frac{\partial w}{\partial t} + u\frac{\partial w}{\partial x} + w\frac{\partial w}{\partial z} = -\frac{1}{\rho}\frac{\partial p}{\partial z} - g. \qquad \textbf{(2.5b)}$$

The Euler equations, together with the equation of continuity, Eq. *2.3*, and suitable initial and boundary conditions, completely describe the flow of an inviscid fluid.

It can be shown that, if the fluid is really inviscid and the external forces are conservative, then the vorticity is constant for each fluid particle. This is Kelvin's theorem and one of its implications is that, if there is initially no vorticity at all, then the flow will remain without vorticity, or irrotational, in which case

$$\nabla \times \vec{V} = 0 \Leftrightarrow \frac{\partial u}{\partial z} = \frac{\partial w}{\partial x}. \qquad \textbf{(2.6)}$$

If the flow is irrotational, then a scalar φ can be defined at each point of the flow in such a way that

$$\vec{V} = grad\varphi \text{ or } (u, w) = \left(\frac{\partial \varphi}{\partial x}, \frac{\partial \varphi}{\partial z}\right). \qquad \textbf{(2.7)}$$

The scalar φ is called the *velocity potential.*

The irrotationality of the flow allows us to eliminate u and w from the equations and leave us with two unknowns, the velocity potential and the pressure.

The continuity equation expressed in terms of the velocity potential becomes the Laplace equation,

$$\frac{\partial^2 \varphi}{\partial x^2} + \frac{\partial^2 \varphi}{\partial z^2} = 0. \qquad \textbf{(2.8)}$$

Using the Equation *2.6* and substituting the fluid velocities by the velocity potential derivatives in Eqs. *2.5*, the Euler equations become

$$\frac{\partial}{\partial x}\left(\frac{\partial \varphi}{\partial t} + \frac{1}{2}\left(\left(\frac{\partial \varphi}{\partial x}\right)^2 + \left(\frac{\partial \varphi}{\partial z}\right)^2\right)\right) = -\frac{\partial}{\partial x}\left(\frac{p}{\rho} + gz\right), \qquad \textbf{(2.9a)}$$

$$\frac{\partial}{\partial z}\left(\frac{\partial \varphi}{\partial t} + \frac{1}{2}\left(\left(\frac{\partial \varphi}{\partial x}\right)^2 + \left(\frac{\partial \varphi}{\partial z}\right)^2\right)\right) = -\frac{\partial}{\partial z}\left(\frac{p}{\rho} + gz\right). \qquad \textbf{(2.9b)}$$

The gz term in the right hand side of Equation *2.9a* is introduced so that it has the same form of Equation *2.9b*.

Integration of the Eqs. *2.9* with respect to x and z, respectively, yields

$$\frac{\partial \varphi}{\partial t} + \frac{1}{2}\left(\left(\frac{\partial \varphi}{\partial x}\right)^2 + \left(\frac{\partial \varphi}{\partial z}\right)^2\right) = -\frac{p}{\rho} - gz + C_1(z,t), \qquad \textbf{(2.10a)}$$

$$\frac{\partial \varphi}{\partial t} + \frac{1}{2}\left(\left(\frac{\partial \varphi}{\partial x}\right)^2 + \left(\frac{\partial \varphi}{\partial z}\right)^2\right) = -\frac{p}{\rho} - gz + C_2(x,t), \qquad \textbf{(2.10b)}$$

where C_1, C_2 are arbitrary functions of integration. One can take $C_1(z,t) = C_2(x,t) = C(t)$, so that the equations of motion can be integrated once and combined to the equation

$$gz + \frac{p}{\rho} + \frac{1}{2}\left(\left(\frac{\partial \varphi}{\partial x}\right)^2 + \left(\frac{\partial \varphi}{\partial z}\right)^2\right) + \frac{\partial \varphi}{\partial t} = C(t). \qquad \textbf{(2.11)}$$

Equation *2.11* is referred to as the *Bernoulli equation*. It can be further simplified by recalling that φ and $\varphi + \int C(t)dt$ yield exactly the same flow:

$$gz + \frac{p}{\rho} + \frac{1}{2}\left(\left(\frac{\partial \varphi}{\partial x}\right)^2 + \left(\frac{\partial \varphi}{\partial z}\right)^2\right) + \frac{\partial \varphi}{\partial t} = 0. \qquad \textbf{(2.12)}$$

To solve Eqs. *2.8* and *2.12* some boundary conditions must be satisfied: a boundary condition at the bottom, two at the free surface, and a boundary condition at the ends of the horizontal direction in the region considered.

The boundary condition at the bottom is that there cannot be flow through the bottom boundary, or that the flow must be parallel to the bottom, *i.e.*,

$$w{=}0 \quad \text{or} \quad \frac{\partial \varphi}{\partial z} = 0 \qquad \text{at} \qquad z = -h. \qquad \textbf{(2.13)}$$

At the free surface it will be assumed that a fluid particle once on the free surface will remain there, therefore at the free surface $z=\eta(x,t)$, and

$$dz=\frac{\partial \eta}{\partial t}dt+\frac{\partial \eta}{\partial x}dx, \qquad \textbf{(2.14)}$$

where $dx=udt$ and $dz=wdt$.

Dividing Eq. *2.14* by *dt*, and using a subscript to indicate the partial derivative with respect to the subscript variable, yields

$$\varphi_z=\eta_t+\varphi_x\eta_x \qquad \text{at} \qquad z=\eta. \qquad \textbf{(2.15)}$$

Equation *2.15* is the kinematic boundary condition at the free surface, which relates the vertical component of water particle velocity at the surface with the surface position.

The second principle to be applied at the free surface refers to the pressure *p*. If we assume that the space above the water is the atmosphere and disregard the influence of the wind, then the pressure *p* can be considered constant along the surface, because the density of air is only about 1/800 times that of water. Taking *p* equal to zero in Bernoulli equation at the free surface, we get the dynamic boundary condition as

$$gz+\frac{1}{2}\left(\varphi_x^2+\varphi_z^2\right)+\varphi_t=0 \qquad \text{at} \qquad z=\eta. \qquad \textbf{(2.16)}$$

The conditions required at the ends of the region considered will actually determine the type of wave motion. The motion under study is a periodic, progressive wave of constant form. The condition in the *x*-direction is that the flow pattern at a given instant is the same at two points separated by an integer number of wave lengths. It can be shown that it is sufficient to impose this condition on the horizontal velocity, which yields the periodicity condition

$$\varphi_x(x,z,t)=\varphi_x(x+L,z,t). \qquad \textbf{(2.17)}$$

So far we have formulated the problem. Equations. *2.8* and *2.14* are to be solved with the boundary conditions given in Equations. *2.13*, *2.15*, *2.16* and *2.17*. Mathematically this system represents two important difficulties: both boundary conditions at the free surface are non-linear and the shape and position of the free surface boundary itself is one of the unknowns. These difficulties make it impossible to solve the problem analytically without further simplifications.

2.3 Small amplitude waves

In order to solve the above problem, the non-linear terms must be neglected, and to do that we should assess the order of magnitude of those terms. Let us first determine the order of magnitude of the non-linear terms in Eq. *2.16* - the squared fluid velocities at the free surface.

In a deep water wave at the free surface, the fluid particles move in circular paths, each orbit covering one wave period *T*. Since a fluid particle on the surface remains there, the diameter of the circular path must be the wave height *H*. The speed of such a particle can therefore be written as $\pi H/T$, which implies that

$$(\varphi_x)_{max} = (\varphi_z)_{max} = \frac{\pi H}{T} = O\left(\frac{H}{T}\right), \tag{2.18}$$

where $O()$ represents order of.

For η_t in Equation *2.15*, the maximum value occurs when the fluid particle is at the wave crest or trough,

$$\eta_t = \frac{H/2}{T} = O\left(\frac{H}{T}\right). \tag{2.19}$$

Similarly for η_x ,we have:

$$\eta_x = O\left(\frac{H}{L}\right). \tag{2.20}$$

The wave period is given by $T = L/c$. Substituting this in Equations *2.18* and *2.19* yields

$$\varphi_z = O\left(\frac{H}{T}\right) = O\left(c\frac{H}{L}\right) \tag{2.21a}$$

$$\eta_t = O\left(c\frac{H}{L}\right) = O(\varphi_z) \tag{2.21b}$$

Therefore the kinematic free surface condition the non-linear term is *H/L* times the order of magnitude of the linear terms

$$\varphi_x \eta_x = O\left(c\frac{H}{L}\right)O\left(\frac{H}{L}\right) = O\left(c\frac{H^2}{L^2}\right). \tag{2.22}$$

If we assume that the wave steepness is a small quantity, *i.e.*, *H/L<<1*, we can ignore the non-linear term. By analogous arguments the same will result in the dynamic boundary condition at the free surface, and the term $1/2g(\varphi_x^2 + \varphi_z^2)$can be ignored $(O(\varphi_x^2) = O(\varphi_z^2) = O(cH^2/L^2))$.

This leave us with the problem of the unknown position of the free surface.

Performing a Taylor expansion of the vertical velocity around $\eta = 0$, we have

$$\begin{aligned} \varphi_z(x,\eta,t) &= \varphi_z(x,0,t) + \eta\varphi_{zz}(x,0,t) + ... \\ &= \varphi_z(x,0,t) - \eta\varphi_{xx}(x,0,t) + ... \end{aligned} \tag{2.23}$$

The order of the second term on the right hand side is evaluated as

$$\eta = O(H) \text{ and } \varphi_{xx} = O\left(\frac{\varphi_x}{L}\right) = O\left(\frac{H}{L^2}\right). \tag{2.24}$$

Then

$$\varphi_z(x,\eta,t)=\varphi_z(x,0,t)+O\left(c\frac{H^2}{L^2}\right)$$
$$=\varphi_z(x,0,t)+O\left(\frac{H}{L}\varphi_z\right), \qquad \textbf{(2.25)}$$

which shows that if in the kinematic boundary condition, Eq. *2.15*, we evaluate φ_z at $z=0$ instead of at $z=\eta$ we are neglecting terms of the same order of magnitude as the non-linear terms. Similar result can of course be obtained for ϕ_t in the dynamic boundary condition at the free surface. Hence, it is assumed that the wave stepness is small.

All the assumptions made so far form the basis of the simplest mathematical model for the motion of free surface waves - the linear wave theory or small amplitude wave theory, first derived by Airy (1845) and Stokes (1847).

To recap: our aim is to find a solution for the two-dimensional Laplace equation,

$$\varphi_{xx}+\varphi_{zz}=\nabla^2\varphi=0, \qquad \textbf{(2.26)}$$

in the rectangular region $0\le x\le L$, $-h\le z\le 0$, with the following linearized boundary conditions:

kinematic bottom condition,

$$\varphi_z=0 \qquad \text{at} \qquad z=-h; \qquad \textbf{(2.27a)}$$

kinematic condition at the free surface

$$\varphi_z-\eta_t=0 \qquad \text{at} \qquad z=0; \qquad \textbf{(2.27b)}$$

dynamic condition at the free surface,

$$\eta+\frac{1}{g}\varphi_t=0 \qquad \text{at} \qquad z=0; \qquad \textbf{(2.27c)}$$

and the periodicity condition,

$$\varphi_x(0,z,t)=\varphi_x(L,z,t). \qquad \textbf{(2.27d)}$$

Since η does not appear in the differential equation of the above problem, it is convenient, for the time being, to eliminate η from the two surface conditions. For that purpose the dynamic condition at the free surface is differentiated with respect to t and the resulting expression for η_t substituted in the kinematic boundary condition at the free surface, becomes

$$\varphi_z+\frac{1}{g}\varphi_{tt}=0 \qquad \text{at} \qquad z=0. \qquad \textbf{(2.28)}$$

It follows from the constant form assumption that the surface elevation achieves the same value at several points (x,t) distanced in the direction of wave propagation: if one of these points is (x_0,t_0), then $\eta(x_0,t_0)=\eta(x,t)$ for all points (x,t) such that $x/t=x_0/t_0=c$.

Therefore the variation of η with x and t must be in the combination

$$\theta = 2\pi\left(\frac{t_0}{T} - \frac{x_0}{L}\right), \tag{2.29}$$

where the factor 2π is added to simplify the following derivations.

Using the above change in variables in the form,

$$\theta = \omega t - kx, \tag{2.30}$$

$\eta(x,t)$, $\varphi(x,t)$, etc. can be written as $\eta(\theta)$, $\varphi(\theta)$, *etc.* Changing variables from x, t to θ and noting that

$$\frac{\partial^2}{\partial x^2} = k^2 \frac{\partial^2}{\partial \theta^2}, \tag{2.31}$$

the Laplace equation becomes

$$k^2 \varphi_{\theta\theta} + \varphi_{zz} = 0. \tag{2.32}$$

Similarly the free surface boundary condition, Eq. *2.27*, is rewritten as

$$\varphi_z + \frac{\omega^2}{g}\varphi_{\theta\theta} = 0 \qquad \text{at} \qquad z=0, \tag{2.33}$$

the periodicity condition as

$$\varphi_\theta(0,z) = \varphi_\theta(2\pi,z), \tag{2.34}$$

and the bottom condition remains the same.

Now that both x and the time t have been removed from the formulation and the velocity potential is only a function of θ and z.

Equation *2.32* can now be solved by the method of separation of variables. Representing $\varphi(\theta,z)$ by the product of a function $f(\theta)$ depending on θ and a function $Z(z)$ depending on the vertical co-ordinate, Equation *2.32* becomes

$$k^2 \frac{\partial^2 f(\theta)}{\partial \theta^2} Z(z) + f(\theta)\frac{\partial^2 Z(z)}{\partial z^2} = 0. \tag{2.35}$$

Dividing this previous equation by $\phi(\theta,z)$, which is, $f(\theta)Z(z)$ and rearranging, we have

$$-k^2 \frac{f''}{f} = \frac{Z''}{Z}, \tag{2.36}$$

where ' represents ordinary differentiation.

The left hand side of Eq. *2.36* depends only on θ and the right hand side only on z. Hence they must be equal to the same constant, say $\lambda^2 > 0$. Equation *2.36* then splits up into two ordinary differential equations with constant coefficients:

$$f''+\frac{\lambda^2}{k^2}f=0, \tag{2.37a}$$

$$Z''-\lambda^2 Z=0. \tag{2.37b}$$

The solution of these equations can be written as

$$f=A\sin\left(\frac{\lambda}{k}\theta+\delta\right), \tag{2.38a}$$

$$Z=B\cosh\lambda z+C\sinh\lambda z. \tag{2.38b}$$

A, B and C are integration constants to be determined by the boundary conditions together with λ. The fourth integration constant has been transformed into the phase angle δ. However, we can always choose the origin of θ, so that $\delta=0$.

The value of λ can be found out applying the periodicity condition

$$f'(0)=f'(2\pi)\ , \tag{2.39}$$

which implies that λ/k must be equal to one, $k=\lambda$, since $\theta=2\pi$ corresponds by definition to one wave length and solutions with $\lambda/k=2,3,...$ must be discarded.

The constant B can be easily determined from the bottom boundary condition

$$Z'=0 \qquad \text{at} \qquad z=-h, \tag{2.40}$$

which gives

$$B=C\coth\ kh, \tag{2.41}$$

so that Equation *2.38b* becomes

$$Z=C\frac{\cosh k(z+h)}{\sinh kh}. \tag{2.42}$$

The velocity potential is then written as

$$\phi(\theta,z)=AC\frac{\cosh k(z+h)}{\sinh kh}\sin\theta. \tag{2.43}$$

Substituting the partial derivatives of the latter expression.

$$\phi_z=ACk\frac{\sinh k(z+h)}{\sinh kh}\sin\theta, \tag{2.44a}$$

$$\phi_{tt}=-AC\omega^2\frac{\cosh k(z+h)}{\sinh kh}\sin\theta, \tag{2.44b}$$

in the free surface condition, and after some algebra the following equation is obtained:

$$\omega^2=gk\tanh kh, \tag{2.45}$$

The free surface condition specifies this relation between ω and k, which can also be written as

$$c = \sqrt{\frac{gL}{2\pi} \tanh \frac{2\pi h}{L}} . \qquad \textbf{(2.46)}$$

This equation is known as the dispersion equation since from this it can be concluded that long waves travel faster than shorter waves.

The last unknown constants can obtained through the surface profile η. From the dynamic boundary condition at the free surface

$$\eta = -\frac{1}{g}\phi_t = -AC\frac{\omega}{g}\coth kh \cos\theta = -\frac{AC}{c}\cos\theta . \qquad \textbf{(2.47)}$$

Comparing Equation *2.47* with Equation *2.1*, we see that $-AC/c$ must equal the wave amplitude, or half wave height,

$$AC = -\frac{Hc}{2} . \qquad \textbf{(2.48)}$$

The final solution of the velocity potential for the linear wave theory is given as

$$\phi = -\frac{Hc}{2}\frac{\cosh k(z+h)}{\sinh kh}\sin(\omega t - kx), \qquad \textbf{(2.49)}$$

from which the wave velocity and pressure can be obtained.

Deep and shallow waters

The wave dispersion equation obtained above, Eq. *2.46*, allows the classification of the waves relative to the ratio *h/L*. For $h/L \geq 1/2$, $\tanh kh \to 1$, and the wave velocity is given as

$$c = \sqrt{g/k} . \qquad \textbf{(2.50)}$$

Since the water depth does not influence the wave speed, waves are said to be in deep waters.

For $h/L < 1/20$, $\tanh kh \to kh$, and c is given as

$$c = \sqrt{gh} . \qquad \textbf{(2.51)}$$

The wave speed only depends on the water depth, and the waves are said to be in shallow waters.

For $1/20 \leq h/L < 1/2$ the waves are said to be in intermediate depth, and the dispersion equation applies.

Equation *2.50* shows that waves disperse in deep waters, in such a way that the long waves travel faster and leave the short waves behind - that is why long waves are sometimes the forerunners of a storm. In shallow waters the wave speed does not depend

on the wave length, being only function of the water depth, and that is why near the coast long wave crests run parallel to the shore, following the depth gradient.

Wave group velocity

Wave groups are series of waves whose amplitudes vary smoothly between 0 and a maximum value. An infinite number of groups can be formed by superposing two small waves propagating in the same direction with the same amplitude but slightly different periods and wave lengths. The resulting displacement can be represented as the sum of the two individual displacements,

$$\eta = \eta_1 + \eta_2,$$

$$\begin{aligned} \eta(x,t) &= a\cos(\omega t - kx) + a\cos((\omega + \Delta\omega)t - (k + \Delta k)x) \\ &= 2a\cos(\omega t - kx)\cos(\Delta\omega t - \Delta kx)/2. \end{aligned} \tag{2.52}$$

The resulting disturbance appears as a series of successive groups of waves within which the amplitude varies from *0* to *2a*. The modulating wave or the amplitude envelope has length $L_{\text{mod}} = 2\pi/\Delta k$ and period $T_{\text{mod}} = 2\pi/\Delta\omega$. The speed of the disturbance as a wave group is then

$$c_g = \Delta\omega/\Delta k, \tag{2.53}$$

and from the dispersion equation one obtains

$$c_g = \frac{c}{2}\left(1 + \frac{2kh}{\sinh kh}\right). \tag{2.54}$$

We can now calculate the wave group velocity in terms of the criterion for deep and shallow waters. In deep waters the group velocity is

$$c_g = c/2, \tag{2.55a}$$

while in shallow waters the wave groups move at wave velocity

$$c_g = c. \tag{2.55b}$$

Wave energy

The energy contained in a wave propagates in the direction the wave propagates. The magnitude and the speed of this energy is derived as follows.

The sum E of the mean potential and kinetic energy of a wave is called the energy density. The instantaneous value of the potential energy per unit area is caused by the displacement of the water surface from the mean water level:

$$\int_0^{\eta} \rho g z dz = \frac{1}{2}\rho g \eta^2. \tag{2.56}$$

The energy of the wave motion is described well enough by its mean, and the mean value of the potential energy is

$$E_P = \frac{1}{16}\rho g H^2 . \tag{2.57}$$

The instantaneous value of the kinetic energy per unit volume equals

$$\frac{1}{2}\rho\left(u^2 + w^2\right) \tag{2.58}$$

Substituting the values of u and v and integrating from the bottom to the mean water level, we have, after some algebra, the instantaneous value of the kinetic energy per unit area,

$$\frac{1}{16}\rho g H^2 + \frac{1}{8}\rho g H^2 \frac{2kh}{\sinh 2kh}\left(\cos^2\theta - \frac{1}{2}\right) . \tag{2.59}$$

The mean value of the kinetic energy per unit area of the water surface, E_k, is then

$$E_k = \frac{1}{16}\rho g H^2 \tag{2.60}$$

The wave energy density is given as

$$E = E_p + E_k = \frac{1}{8}\rho g H^2 . \tag{2.61}$$

There exists a transport of energy over the depth of water in the direction of wave travel. The average value of this transport, per unit time and unit distance along the wave front, referred to as the energy flux, is the product of the energy density and the wave group velocity (Lighthill (1960)).

2.4 Description of Random Sea Waves

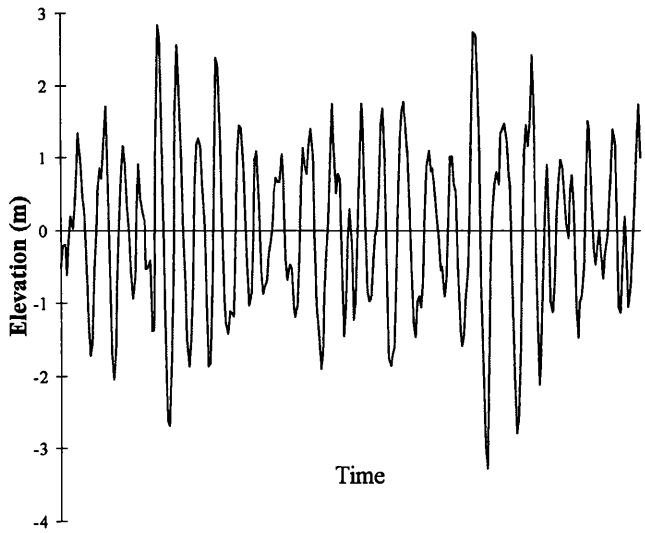

Figure 2.2 - Example of a wave record.

The previous sections presented the basic equations describing the sinusoidal motion of the free surface of a fluid from a deterministic point of view. However, the sea surface rarely ever exhibits a well behaved sinusoidal form; it has a random and confusing profile, and due to its complexity and irregularity can only be properly described through a representation based on stochastic processes.

If we measure the water surface elevation during a certain period of time at one location in the ocean we observe a random profile as the one shown in Figure *2.2*.

Such an irregular wave profile can be constructed by adding several sinusoidal waves of different wave heights, period and phase. Based on this observation, Pierson (1952) proposed describing the random ocean elevation as the superposition of an infinite number of regular waves, each obeying the linear wave theory, and having different frequencies, wave numbers and directions, and a randomly distributed phase angle.

The random wave profile is thus represented by a sum of wave trains or components with sinusoidal form, long-crested, and infinitesimally small amplitude:

$$\eta(x,y,t)=\sum_{n=1}^{\infty} a_n \cos\left(k_n x\cos\theta_n + k_n y\sin\theta_n - \omega_n t + \varepsilon_n\right), \qquad (2.62)$$

where θ_n is the angle formed by the x axis and the direction of propagation, as represented in Figure *2.3*. The quantities f_n and θ_n are densely distributed between 0 to ∞ and 0 to 2π respectively, and ε_n is a random variable uniformly distributed between 0 and 2π.

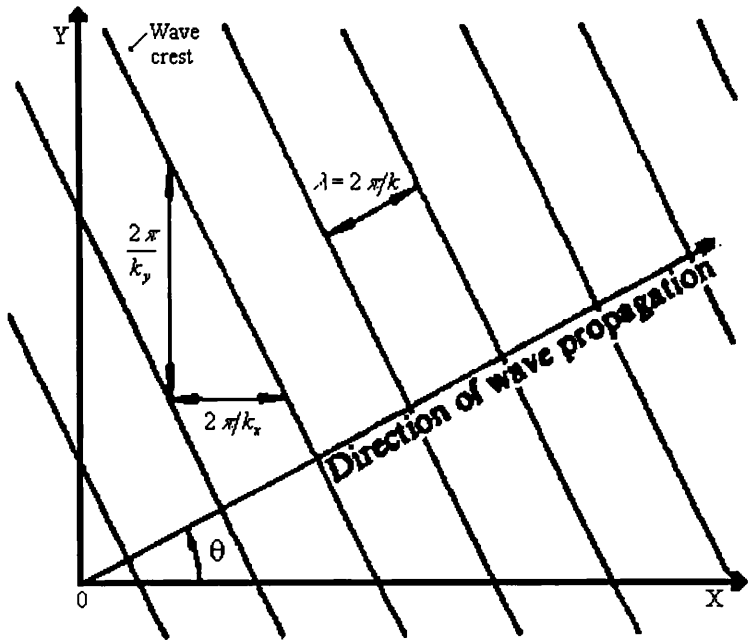

Figure 2.3 - Sinusoidal wave travelling at an angle θ with respect to the x-axis.

Since the wave phase is a random variable, each wave component in *2.62* is a realisation of a random process, so that the resulting wave profile is a stochastic process. This stochastic process is *ergodic*. A random process is said to be ergodic if it is stationary and if the expectations are equal to the corresponding temporal averages taken along a single realisation. The stationarity of a process can be defined in time or space. The process is stationary in time if it has the same statistics at any time. A stationary in space

or homogeneous process is a process whose characteristics are invariant to shifts in location.

Assuming the ocean surface elevation to be ergodic implies that the wave profile in any region of the ocean can be fully described by measuring the evolution of the sea surface elevation at a single point.

The ergodicity of the process results from the fact that the wave components in equation *2.62* are assumed to coexist and to be independent of each other and, as can be shown, that they are ergodic processes in the mean, mean square and auto-covariance statistics.

It can also be inferred that the resulting surface elevation has a normal or gaussian distribution, by virtue of the central limit theorem, because the surface elevation at each point is the sum of statistically independent random variables, *i.e.*, results from multiple independent causes. The gaussian property of wave records was first observed by Rudnick in 1951.

The ocean surface elevation is obviously not a stationary process, but a *sea state* is stationary. In fact a sea state is defined as the description of the sea-surface elevation during a relatively short-time period. It has been found in practice that the continuous monitoring of sea states is stationary during periods of approximately 3 hours, but in many cases truly stationary conditions are only observed in periods of about 20 minutes It has been empirically verified that with this definition a sea state can be represented by Equation *2.62*.

2.5 Spectra of Sea Waves

Equation *2.62* describes the time evolution of a sea state. It is more convenient to describe the sea state in the frequency domain. The frequency description of a sea state is obtained as follows.

If the sea surface elevation is a time-space stationary stochastic process, its *auto-covariance function* in the three-dimensional space is a function of space and time shifts only:

$$R(\vec{X},\tau) = \left\langle \eta(\vec{x},t)\cdot\eta(\vec{x}+\vec{X},t+\tau)\right\rangle, \tag{2.63}$$

where $\langle\ \rangle$ represents the ensemble average.

The direct Fourier transform of the auto-covariance function gives the *spectrum* of $\eta(x,y,t)$:

$$S(\vec{k},\omega) = \frac{1}{8\pi^3}\int_{-\infty}^{+\infty}\int_{-\infty}^{+\infty} R(\vec{X},\tau)\exp\left(-i\left(\vec{k}\cdot\vec{X}-\omega\tau\right)\right)d\vec{X}d\tau\,. \tag{2.64}$$

In turn, the inverse Fourier transform of this three-dimensional wave spectrum gives the auto-covariance function,

$$R(\vec{X},\tau) = \int_{-\infty}^{+\infty}\int_{-\infty}^{+\infty} S(\vec{k},\omega)\exp\left(i\left(\vec{k}\cdot\vec{X}-\omega\tau\right)\right)d\vec{k}d\omega\,. \tag{2.65}$$

Putting $\vec{X} = \vec{0}$, $\tau = 0$ in equations *2.63* or *2.65* gives the *variance* of the sea state

$$\sigma^2 = R(\vec{0},0) = \langle \eta^2(\vec{x},t) \rangle = \int_{-\infty}^{+\infty}\int_{-\infty}^{+\infty} S(\vec{k},\omega)\,d\vec{k}\,d\omega \,. \qquad (2.66)$$

Because this is the integral of the wave spectrum, the latter is also known as the *wave variance spectrum*.

The stationarity of a sea state can be tested in terms of a relation between the wave length and period with the wave spectrum. The stationarity is thought plausible when the time variability of the sea state is slow in the time scale, *i.e.*, when

$$\frac{T}{S}\frac{\partial S}{\partial t} \langle\langle 1 \,.$$

In the same way, the hypothesis of space stationarity or homogeneity is thought reasonable if the space variability of the sea state is small, *i.e.*, if the variations of S with x are small in the scale of the wave length:

$$\frac{L}{S}\frac{\partial S}{\partial x} \langle\langle 1 \,.$$

If, besides being stationary, the stochastic process is also gaussian, $R(\vec{X},\tau)$ as well as $S(\vec{k},\omega)$ determine its statistical characteristics completely. Thus under the gaussian assumption the variance spectrum completely specifies a sea state from a statistical point of view.

However, there are cases where there is no independence between the wave components and the linear wave theory hypothesis cannot be applied, resulting in the invalidity of the gaussian hypothesis. One of the ways of observing the departure from linearity and from the gaussian model is the asymmetry of $\eta(x,t)$ in relation to its mean level. The inclusion in the theory of non-linear developments along with experience have confirmed deviations from the gaussian hypothesis. Still, these deviations are generally not enough to abandon the description of the sea state by its variance spectrum, which allows a simple mathematical and physical description of a very complex phenomenon.

The variance of a sea state, as given in Equation *2.66*, can also be computed from

$$\langle \eta^2(\vec{x},t) \rangle = \sum_{i=1}^{\infty} \frac{a_i^2}{2} \,. \qquad (2.67)$$

The total energy per unit wave length of a simple sinusoidal wave, as given by linear wave theory, is proportional to the average of the square wave elevation $\rho g a^2/2$. The energy of a sea state is therefore the sum of the energy of all individual wave components. From Equations *2.66* and *2.67* it can be inferred that the sea state energy is proportional to the integral of the wave spectrum, its variance. The wave spectrum expresses the variance distribution of $\eta(x,y,t)$ over a continuous frequency domain of sinusoidal waves. The wave spectrum is also called the wave *energy spectrum* or *spectral density* and can be interpreted as physically expressing the energy distribution of the wave movement over a continuous domain of sinusoidal waves with infinitesimal energy, to which the linear wave theory is applied.

The dispersion equation establishes a biunivocal correspondence between the frequency and the wave number. This makes the information contained in $S(\vec{k},\omega)$ redundant and equivalent to the one given by the wave number spectrum F,

$$F(\vec{k}) = \int_{-\infty}^{+\infty} S(\vec{k},\omega)d\omega . \tag{2.68}$$

The wave number spectrum $F(\vec{k})$ could have also been obtained from the instantaneous elevations of the free surface in a homogeneous wave field $\eta(\vec{x})$. In that case, the auto-covariance function is given as

$$R(\vec{X}) = \langle \eta(\vec{x}) \cdot \eta(\vec{x}+\vec{X}) \rangle , \tag{2.69}$$

and the corresponding wave number spectrum is the direct Fourier transform of the previous auto-covariance function. The corresponding sea state energy can also be given as

$$\langle \eta^2(\vec{x}) \rangle = R(\vec{0}) = \int_{-\infty}^{+\infty} F(\vec{k})d\vec{k} = E . \tag{2.70}$$

In a similar way the wave frequency spectrum can be given as

$$S_\omega(\omega) = 2\int_0^{+\infty} S(\vec{k},\omega)d\vec{k} . \tag{2.71}$$

This could have also been obtained from the time surface elevation at a single point $\eta(t)$, and then computing the Fourier transform of its auto-covariance. The wave frequency spectrum of a sea state is easily computed from buoy measurements at a single location, but it does not provide information on the direction of the waves.

A description of the energy as a function of the wave angular frequency and wave direction is obtained from the three-dimensional wave spectrum in polar co-ordinates, $S(k,\theta,\omega)$, integrated in the wave number,

$$S_\omega(\omega,\theta) = 2\int_0^{+\infty} S(k,\theta,\omega)kdk , \tag{2.72}$$

where the following transformation is used:

$$k_x = k\cos\theta ,$$

$$k_y = k\sin\theta ,$$

and

$$d\vec{k} = kdkd\theta .$$

The directional wave spectrum in Equation *2.72* can also be given as a function of the frequency:

$$S(f,\theta) = 2\pi S_{\omega}(\omega,\theta). \tag{2.73}$$

The wave number spectrum and the directional wave spectrum give different descriptions of the same sea state, but they contain the same energy. This gives a relationship between the wave number spectrum and the directional spectrum:

$$S_{\omega} d\omega d\theta = F k dk d\theta \,. \tag{2.74}$$

Using the definition of group velocity of a progressive wave, Eq. *2.53*,

$$c_g = \frac{\partial \omega}{\partial k}, \tag{2.75}$$

the relationship between the directional wave spectrum and the wave number spectrum, Eq. *2.74*, becomes

$$S_{\omega}(\omega,\theta) = \frac{k}{c_g} F(k,\theta) = \frac{\omega}{c c_g} F(k,\theta). \tag{2.76}$$

Substituting the expressions *2.50* and *2.55a*, for deep waters wave velocity and wave group velocity respectively, Equation *2.76* becomes

$$S_{\omega}(\omega,\theta) = \frac{2\omega^3}{g^2} F(k,\theta). \tag{2.77}$$

The sea state is most of the time represented only as a function of the wave frequency, *i.e.*, in terms of the frequency wave spectrum along with the frequency mean wave direction and the frequency directional spreading. The one-dimensional wave spectrum $S(f)$ is the integral of $S(f,\theta)$ over the direction:

$$S(f) = \int_0^{2\pi} S(f,\theta) d\theta \,. \tag{2.78}$$

The mean wave direction $\theta(f)$ and directional spreading $\sigma(f)$ per frequency are given as

$$\theta(f) = \arctan\left(\frac{b(f)}{a(f)}\right), \tag{2.79}$$

$$\sigma(f) = \sqrt{2\left(1 - \sqrt{a^2 + b^2}\right)}, \tag{2.80}$$

where

$$a(f) = \frac{\int_0^{2\pi} S(f,\theta)\cos\theta d\theta}{S(f)}, \tag{2.81}$$

$$b(f) = \frac{\int_0^{2\pi} S(f,\theta)\sin\theta d\theta}{S(f)}. \tag{2.82}$$

3.2 Wave Spectral parameters

The description of a sea state by its directional spectrum or wave number spectrum in a discrete domain of directions and frequency or wave numbers involves a lot of information. Another way of describing the sea state is by using sea state medium parameters, which can also be used to define analytically the wave spectrum. Some of these parameters are equivalent to the ones used in the past to describe the sea state before spectral analysis was introduced.

One-dimensional wave profiles, such as the one shown in Figure *2.2*, can be recorded at a fixed location in the ocean. These time-history records of sea surface elevation exhibit a random form with many small maxima and minima superimposed on irregular undulations. To distinguish a single wave from local humps and hollows, the *zero-upcrossing method* is usually used - a wave sets in when the surface elevation crosses the mean water lever upward and is set down at the next zero-upcrossing. The wave height is defined as the vertical distance between the highest and lowest points between two successive upcrossings, and the zero upcrossing wave period as the time between the two zero upcrossing points.

After analysing a wave record by this method, the record is broken into a series of individual wave heights and periods, from which several height and period parameters can be calculated: the maximum wave height and period; the mean of the 1/10 highest wave heights and periods, the mean of the one-third highest wave heights and periods; and the mean wave height and mean zero upcrossing period of the record.

As we shall see below, these same parameters can also be obtained from the wave spectrum, calculated through the Fourier analysis of the wave record.

For historical reasons the sea state wave height parameter most commonly used is the mean height of the one-third highest waves, referred to as the *significant wave height.*

Longuet-Higgins (1952) verified that in a narrow band wave spectrum the wave height follows the Rayleigh distribution,

$$F(h) = 1 - \exp\left(-\frac{h^2}{8\sigma^2}\right), \quad h > 0, \tag{2.83}$$

with density function

$$f(h) = \frac{h}{4\sigma^2}\exp\left(-\frac{h^2}{8\sigma^2}\right), \quad h > 0. \tag{2.84}$$

Here, as usual, σ^2 is the variance of the sea-state.

This is used for calculating the average value of the one-*n*th highest wave height,

$$\overline{H}_{1/n} = n\int_{1/n}^{\infty} hf(h)dh. \tag{2.85}$$

When n equals 3, this gives the significant wave height as calculated from the wave spectrum,

$$H_S = 4\sqrt{m_0}, \tag{2.86}$$

where m_0 is the sea state variance, also known as the zero order spectral moment because it is the area under the spectrum (Figure *2.4*).

This significant wave height estimate has a small bias relative to the mean highest one-third wave heights as calculated directly from the wave record.

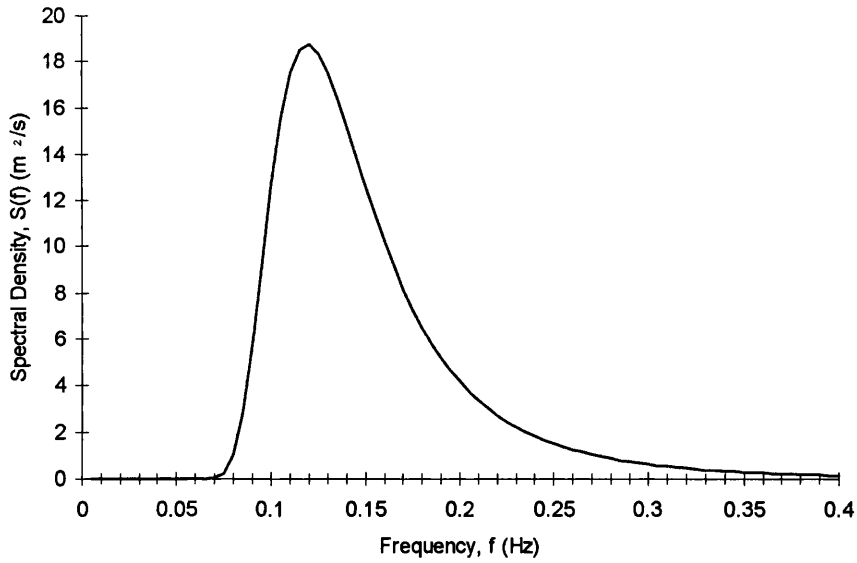

Figure 2.4 - Example of a spectral form - $H_S = 5$ m, $T_Z = 8$ s, $f_p = 0.12$ Hz.

There are several parameters for describing the sea state period or frequency.

One of these is the spectrum peak frequency, f_p, the frequency corresponding to the maximum of a spectral form like the one shown in Figure *2.4*.

Other is the mean zero-upcrossing period of waves,

$$T_Z = \sqrt{m_0 / m_2} \tag{2.87}$$

where m_n, the n order spectral moment, is

$$m_n = \int_0^\infty f^n S(f)\,df. \tag{2.88}$$

The zero-upcrossing period can have a large scatter when computed by different methods or estimation procedures from wave measurements. Because of this, the inverse of the *mean wave frequency*, f_m, the mean wave period parameter, is sometimes used instead:

$$T_m = \sqrt{m_0 / m_1}\,. \tag{2.89}$$

There are also several parameters for describing the mean wave direction: the *mean wave direction*,

$$\bar{\theta} = \frac{\int_0^\infty \int_0^{2\pi} \theta S(f,\theta)\,df\,d\theta}{\int_0^\infty \int_0^{2\pi} S(f,\theta)\,df\,d\theta}; \tag{2.90}$$

the vectorial mean wave spectral direction,

$$\theta_e = \arctan \frac{\int_0^{\infty} \int_0^{2\pi} S(f,\theta) \sin\theta \, df d\theta}{\int_0^{\infty} \int_0^{2\pi} S(f,\theta) \cos\theta \, df d\theta}; \tag{2.91}$$

and the mean vectorial wave power spectrum direction,

$$\theta_p = \arctan \frac{\int_0^{\infty} \int_0^{2\pi} S(f,\theta) c_g(f) \sin\theta \, df d\theta}{\int_0^{\infty} \int_0^{2\pi} S(f,\theta) c_g(f) \cos\theta \, df d\theta}. \tag{2.92}$$

If, as usual, the direction in the co-ordinates system is given relatively to the geographic North, then for a wave spectrum centred in the North direction (0 degrees) Equation *2.90* would give a mean wave direction of 180 degrees. This problem is overcome by the vectorial averages of Equations *2.91* and *2.92*, and using the sign of the sine term to solve the $\pm\pi$ ambiguity.

CHAPTER 3

Wave Models

It is known that Aristotle (384-322 BC) observed the existence of a relationship between wind and waves. The nature of this relationship, the description of wave generation, propagation and decay have now been the subject of investigation for a long time. As mentioned by Khandekar (1989), Leonardo da Vinci (1500), Euler (1755), and Benjamin Franklin (1872) also had an interest in wave phenomena.

The progressive knowledge in the field has led to the development of wave models, which enable the forecasting of sea states. The works of O. M. Phillips, J. W. Miles and K. Hasselmann are among the greatest contributions to wave modelling.

This chapter reviews the historical development of wave theories since the late 19th century, and describes the evolution of the first, second and third generation wave models.

A wind blowing over water will, by a variety of mechanisms, cause waves to grow. The spectral shape describing a sea state depends on the wind speed, the time for which the wind has blown, the fetch defining the length of water in line with the wind, and the water depth. The following are some facts and concepts about the behaviour of wind-waves needed for the exposition.

If the wind blows for a long time with a long fetch, the wave spectrum will reach an equilibrium in which the energy input to the waves by the wind equals the energy dissipated by wave breaking and other viscous effects. This type of sea state is termed fully developed.

Waves that are being locally generated by the wind are called wind sea. Their appearance is random, with sharp short crests and large directional dispersion. When these waves move out of the generating area they turn to swell. Then, with direction and frequency filtering in their propagation (long waves travelling faster, short waves staying behind), the wave pattern and form become more regular, with long round crests and a well defined propagation direction. Long period swell travels a very long distance without losing its identity.

For propagation over long distances waves obey the linear theory of wave propagation from a limited initial disturbance. Group velocity can be used to predict the arrival time of waves at a coastal location if the position of the storm over the ocean and the time of its occurrence are known.

3.1 Historical review

One of the earliest wave generation theories based on a mathematical argument is the Kelvin-Helmholtz instability theory (1868, 1871), in which air pressure was assumed to be 180 degrees out of phase with the surface elevation. For sufficiently large wind speed, the pressure over the surface, due to the Bernoulli effect, could cause an infinitesimal amplitude sinusoidal wave to grow against the restoring forces of gravity and surface tension.

Later on, Jeffreys (1924, 1925) assumed that the only important mechanism for transferring energy from wind to water was the difference of normal pressure between the windward and the leeward side of the wave crest. According to this, waves will continue to grow if the normal energy flux integrated over the water surface of the wave crest exceeds the rate at which the energy is dissipated by molecular viscosity. A limitation of Jeffreys' theory is that it does not allow the waves to grow when the wave phase speed is greater than the wind speed.

Sverdrup and Munk (1947) developed the first wave forecasting technique by introducing the concept of significant wave height. This is defined as the mean of the highest one third of the waves in the sea, and can be described as the height which an observer will propose to characterise the wave height of a sea state. Sverdrup and Munk incorporated the tangential wind stress in Jeffreys' theory and rewrote the wave growth expression.

The forecasting technique was based on the duration and fetch equations, which allow the growth of waves even when the phase speed is greater than the wind speed. This phenomenon was thought to be realistic and had been confirmed by observations.

The duration and fetch equations were written in a non-dimensional form using wave steepness and wave age parameters. From available data of different sources those authors developed a relationship between the two parameters, solved the equations and obtained duration and fetch charts from which wave height and speed could be obtained.

This technique was originally developed in 1943 during World War II to predict the sea state during landing operations. It could only be published in 1947 because of military secrecy. The technique was extensively modified by Bretschneider(1951,1952,1973), who obtained the SMB monogram-based wave forecast technique. In the 1950's several of these techniques were developed and reported.

The significant wave concept did not take into account the spectral character of the sea state. It was Pierson (1952) who recognised the statistical nature of the problem and developed a method in which the waves where modelled by a gaussian stochastic process.

The determination of completely developed spectra corresponding to different wind velocities allowed the development of wave forecast methods. The first completely developed spectra were proposed by Neumann (1952) from visual observations and led to the wave spectrum method of Pierson, Neumann and James (1955), which predicts the spectrum of a wave, allowing the significant wave height and other wave parameters to be derived.

The first attempt to develop a wave prediction model based on a differential wave transport equation, rather than on empirical integral relations between a few characteristic wave and wind field parameters, was made by Gelci *et al.* (1957).

The model source function has two components, a generation term and a dissipation term, empirically fitted to reproduce observed fetch and duration dependence.

In this context, the evolution of a surface wave field in space and time is governed by the basic transport or energy balance equation in Cartesian co-ordinates,

$$\frac{\partial S}{\partial t} + \vec{c}_g \cdot \nabla \mathrm{S} = \Phi, \qquad (3.1)$$

where $S(f,\theta,\vec{x},t)$ is the energy density of the wave field, dependent on frequency f, propagation direction θ, location $\vec{x}=(x_1,x_2)$, and time. $\vec{c}_g=\vec{c}_g(f,\theta)$ is the deep water group velocity, and the net function Φ represents the source functions.

The establishment of the energy balance equation by Gelci *et al.*, along with the theories of wave generation proposed by Phillips (1957) and Miles (1957), with Phillips'(1958) concept of a universal equilibrium range of the spectrum, and with Hasselmann's (1960, 1961, 1962, 1963) analysis of the non-linear energy transfer due to resonant wave-wave interactions, provided a theoretical framework which led to the development of first generation wave models, which took place in the 60s and with further modifications in the 1970s.

3.2 First generation wave models

The energy balance equation in a general form can be deduced by considering the energy flux through the boundary of a fluid volume element in a four-dimensional phase space of co-ordinates f, θ, $\vec{x}$. The equation represents the sum of the local variation of spectral wave density with the divergence of the spectral density flux in equilibrium with the sources of spectral density. The source term includes the wind generation, the resonant wave-wave interactions and the wave dissipation.

The first generation wave models, even though using not very realistic source functions, are able to compute the evolution of the wave spectrum. The spectrum is represented by a discrete set of spectral components which evolve independently, and these components are propagated along the modelling area according to the kinematic part of the energy balance equation.

Most models use the energy balance equation of conformal map projections. Each spectral component is propagated along great circle arcs at a deep water group velocity appropriate to its frequency. Grid paths on such projections are not in general along great circle arcs, although for distances less than a quarter of the earth's surface deviations from great circle paths are small and negligible. In these models each spectral component of the model evolves independently of the other components.

The following explains how wind input, resonant wave-wave interactions and wave dissipation were taken into account in the first generation wave models.

Wind Input

Phillips (1957) suggested that waves grow by a resonance mechanism when the speed and length of the atmospheric fluctuations match those of the water waves. Waves continue to grow by this mechanism until the wave slope becomes so large that non-linearities, which are neglected, become important.

In his theory, the energy grows linearly with time according to the equation

$$\frac{d}{dt}S(f,\theta)=\frac{2\pi^2\omega}{\rho^2c^3c_g}F_p(\vec{k},\omega)=A, \qquad (3.2)$$

where F_p is the three dimensional spectrum of pressure fluctuations. The latter can be specified based on correlation studies based on atmospheric pressure fluctuations and the turbulent boundary layer.

Phillips' resonance mechanism does not explain the major growth of wind waves because the observed pressure fluctuations are too small and the observed energy growth rates are more exponential than linear. The resonance mechanism is present during an initial generation phase, but only until the pressure and stress variations induced by the waves on the surface air flow induce further wave growth - an amplification mechanism established by Miles.

Miles (1957,1959) attempted to improve upon the classical Kelvin-Helmholtz instability theory by considering a wind profile continuously increasing with height and a pre-existing water wave which induces a disturbance in the shear flow; that part of the induced pressure disturbance which is in phase with the wave slope does the work and causes it to grow. There is a coupling between the air flow and the wave movement, and the wave energy growth is exponential:

$$\frac{d}{dt}S(f,\theta) = -\frac{\pi\omega}{k}\frac{\rho_a}{\rho}\left(\frac{d^2\overline{U}/dz^2}{d\overline{U}/dz}\frac{\langle w'^2\rangle}{\langle \eta_t^2\rangle}\right)_{cr} S(f,\theta) = B\cdot S(f,\theta) \quad (3.3)$$

Where ρ_a is the air density, w' is the waves induced fluctuation in the horizontal component of the mean wind velocity, $\overline{U}$ is the horizontal component of the mean wind velocity, and the subscript *cr* indicates that the values are to be evaluated at the critical layer, at which the wind speed equals the phase speed of the water waves.

The physical interpretation of Miles' mechanism is not straightforward. Lighthill (1962) presents a coherent interpretation, saying that Miles' mechanism is associated with the action of the vortex forces in the air flow in the neighbourhood of the critical layer.

Miles' mechanism is particularly effective for waves with phase velocities appreciably lower than the wind speeds. For waves with phase velocity greater than the maximum wind speed or for waves travelling at angles greater than 90° to the wind direction, Miles' theory does not provide any growth nor any decay.

Since in Miles theory the only role of the turbulence is to maintain the shear flow, it is called a quasi-laminar approach.

Snyder and Cox (1966) combined the two wave energy growth expressions above to get Miles-Phillips growth formula,

$$\Phi = A + B\cdot S(f,\theta). \quad (3.4)$$

These authors tested Phillips' and Miles' proposals by analysing wave growth data from observations made in the Bahamas, assuming constant values of A and B. The conclusion was that the growth curve is almost an order of magnitude smaller when compared with the observed growth rates. Another data set comparison made by Barnett and Wilkerson (1967) showed again that Miles' theory underpredicted the wave growth by almost an order of magnitude.

Wave Dissipation

Waves in deep waters may lose energy by viscous dissipation and by wave breaking. The

continuous dissipation by viscosity is understood and easily calculated, but it is only important to capillary or very short gravity waves, and is therefore usually ignored. Dissipation by wave breaking is the most important dissipation process in deep waters, which can be observed in the form of whitecaps.

Whitecapping is a very localised phenomena in time and space, highly non-linear and very complex. Hasselmann (1974) showed that wave breaking by whitecapping, and in general any process which is weak-in-the-mean, even if it is highly non-linear locally, will give rise to a source function which to the lowest order is proportional to the energy density spectrum. However, the proportionality constant may still depend non-linearly on integral properties of the spectrum. The source term is said to have a *quasi-linear* form.

In order to derive a whitecap dissipation term Hasselmann further assumed that whitecaps can be treated as random distributed perturbation forces, which are formally equivalent to pressure pulses, and that the scales of the whitecaps in space and time are small compared to the wavelength and period of the associated wave.

To derive the dissipation term he took three process into account. The first two were the pressure induced decay and the attenuation of short waves by the passage of large whitecaps. Both these processes are sensitive to the coverage of breaking, which depends on the overall steepness of the wave field - the third process. The dissipation term obtained is proportional to the square of the frequency and includes a constant to be determined from the energy balance equation if the other terms are known,

$$\Phi_{ds}(\vec{k}) = -C\omega^2 F(\vec{k}). \tag{3.5}$$

Nevertheless, most of the first generation wave models do not take this expression into account. The dissipation source function was generally treated in the wind-sea region of the spectrum as a device for preventing the spectrum from exceeding a prescribed universal saturation level (Phillips, 1958), which becomes effective only when this level is approached.

Phillips suggested that in a well developed deep-water wind sea spectrum there exist space and time scales within which the energy distribution depends only on physical parameters, characterising the formation of sharp crests in breaking waves. He postulated that for a range of frequencies greater than the spectral peak frequency the only significant parameter is the acceleration of gravity. Phillips' formulation for this saturation or equilibrium range in frequency domain, obtained in dimensional grounds, is

$$S_{P0}(f) = \alpha g^2 (2\pi)^{-4} f^{-5}, \tag{3.6}$$

were α is called Phillips' constant.

Pierson and Moskowitz (1964) considered only fully developed seas and modified Phillips spectrum to specify the spectrum for frequencies lower than the spectral peak,

$$S_{PM} = S_{Po} \cdot \phi_{PM}. \tag{3.7}$$

Their shape function, ϕ_{PM}, which can be thought of as a high-pass filter acting on Philips spectrum, is

$$\phi_{PM} = \exp\left\{-(5/4)(f/f_P)^{-4}\right\}, \tag{3.7a}$$

where the subscript p means peak and *PM* Pierson Moskowitz. This shape function extends Phillips spectrum over the whole frequency range.

Wave-Wave Interactions

The wind input source term does not allow the growth of waves with velocity higher than the wind velocity. The growth of the part of the spectrum corresponding to wave velocities higher than the wind velocities is induced by the non-linear resonant interactions between the spectral components.

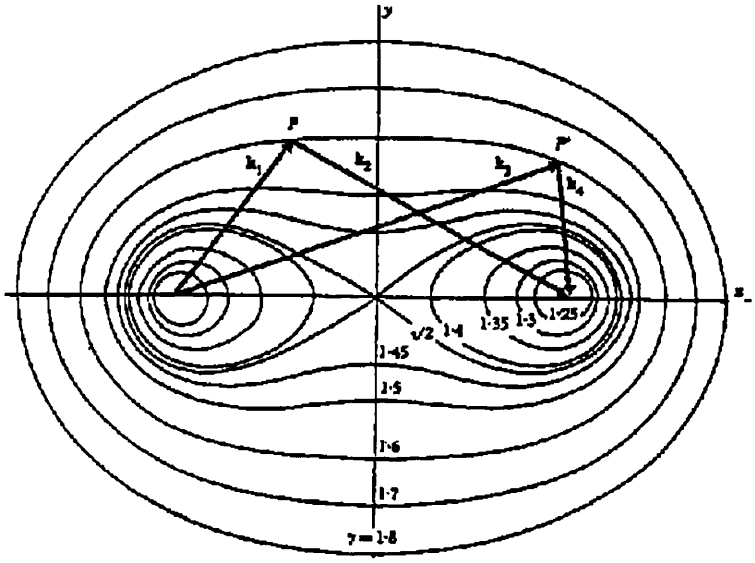

Figure 3.1 - Non-linear resonance interactions configurations (figure taken from *Hasselmann 1963b*).

Research and developmental work on wave-wave interactions expanded after an important paper by Phillips (1960), which used a deterministic approach to face the problem. Phillips showed that, under certain conditions, the third-order perturbations can become large and unsteady. He showed that there exists a configuration of three wave numbers, $\vec{k}_1$, $\vec{k}_2$ and $\vec{k}_3$, which interact to give a continuous transfer of energy to a distinct fourth wave with wave number, $\vec{k}_4$, whose amplitude grows linearly with time. The conditions for the existence of unstable perturbations are called resonance conditions and are defined by the equations

$$\vec{k}_1 + \vec{k}_2 = \vec{k}_3 + \vec{k}_4 = \vec{k}\,, \tag{3.8a}$$

$$\omega_1 + \omega_2 = \omega_3 + \omega_4\,. \tag{3.8b}$$

The wave number and frequency pairs are those of free primary waves which individually satisfy the dispersion equation (for deep waters $\omega = \sqrt{gk}$), leading to

$$\sqrt{k_1} + \sqrt{k_2} = \sqrt{k_3} + \sqrt{k_4} = \gamma\sqrt{k} \tag{3.9}$$

where

$$\gamma = \frac{\sqrt{k_1} + \sqrt{k_2}}{\sqrt{k}} = \frac{\sqrt{k_3} + \sqrt{k_4}}{\sqrt{k}}. \tag{3.10}$$

From Equations *3.9* and *3.10*, the angle between $\vec{k}_1$ and $\vec{k}$ with $|\vec{k}| = 1$, $\hat{\alpha}_1$, is seen to be such that

$$\cos\hat{\alpha}_1 = \frac{1 + k_1^2 - \left(\gamma - \sqrt{k_1}\right)^4}{2k_1}. \tag{3.11}$$

In Figure *3.1* the vectors that satisfy the resonance conditions are graphically presented for constant values of γ.

Phillips' work was further extended theoretically by Longuet-Higgins (1962), Benney (1962) and others. Longuet-Higgins calculated the interactions for the simplest possible case, namely when two of the three primary wave numbers are equal (i.e. $k_1 = k_2$), while Benny derived the complete set of interaction equations governing the time dependence of the resonant modes. The effect of resonant interactions on the entire energy spectrum of the wind waves was derived by Hasselmann (1962, 1963), who carried out perturbation analysis of fifth order using a generalised technique applicable to any system involving weak interactions between ocean wave fields or other random fields. Hasselmann developed the energy transfer in terms of coupling coefficients characterising the interactions between the wave field and its physical environment. The interaction integral, Φ_{nl}, can be written in the compact form:

$$\begin{aligned}\Phi_{nl}(\vec{k}_4) = \omega_4 \int \sigma \cdot \delta(\vec{k}_1 + \vec{k}_2 - \vec{k}_3 - \vec{k}_4) \cdot \delta(\omega_1 + \omega_2 - \omega_3 - \omega_4) \cdot \\ \left[N(\vec{k}_1)N(\vec{k}_2)\left(N(\vec{k}_3) + N(\vec{k}_4)\right) - N(\vec{k}_3)N(\vec{k}_4)\left(N(\vec{k}_1) + N(\vec{k}_2)\right)\right] d\vec{k}_1 d\vec{k}_2 d\vec{k}_3,\end{aligned} \tag{3.12}$$

where σ is proportional to the square of an interaction coefficient, with a very complicated expression (Hasselmann (1962, 1963)), δ is the Dirac function, and N is the action spectral density obtained by dividing the wave number spectrum by the angular frequency,

$$N(\vec{k}_i) = \frac{F(\vec{k}_i)}{\omega_i}. \tag{3.13}$$

These transfer equations are derived assuming the Boltzmann hypothesis of statistical independence of interacting particles. They conserve energy over the entire spectrum.

The resonant interactions by themselves cannot be considered as a source for wave generation or wave dissipation, since they do not change the total wave energy. However, these resonant interactions may play an important role in wave growth by transferring the wind energy input at high frequencies to the low frequencies of the spectrum, which in turn permit further wind input at high frequencies.

It was only after the source function of non-linear transfer had been derived that it was possible to write down the general expression for the source functions of the energy balance equation (Hasselmann (1962)), consisting of three terms representing the input

from the wind, the non-linear transfer and the dissipation by whitecapping, in a form which is still used today.

The computation of the non-linear interactions, Eq. *3.12*, requires an enormous amount of impracticable calculations, and some form of parameterization was needed. Because the importance of non-linear interactions was not recognised in first generation models, the non-linear transfer was either neglected entirely or was incorporated as a relatively simple parameterization, obtained by Hasselmann (1963b), for a fully developed Neumann spectrum.

The first generation wave models were applied successfully for many years. However, they did not represent the physics of wave generation correctly. They overestimated wind input and disregarded non-linear transfer.

To reproduce the observed wave growth Phillips' A term had to be chosen to be several orders of magnitude greater than estimates of the term based on turbulent pressure measurements, just as the term B had to be increased almost an order of magnitude beyond the theoretical estimates of Miles or Jeffreys.

The A and B terms were usually chosen to be those obtained by Barnett and Wilkerson (1967). These terms were set to fit the measurements of wave growth, without removing the effect of dissipation, so that dissipation was, most of the times, not considered in the source functions.

The models were also unable to explain the overshoot phenomenon of a growing wind sea, first observed by Barnett and Wilkerson (1967) and subsequently confirmed by other workers. The growth of a particular spectral component when traced along the fetch in a generating area shows a rapid increase, overshooting the equilibrium value and then dropping sharply, undershooting to a minimum value. The overshoot phenomenon forms an integral part of the wave generation process and is caused by non-linear energy transfer.

3.3 Second generation wave models

The analysis of extensive field measurements of wave growth under carefully selected, uniform fetch-limited wind conditions (Mitsuyasu *et al.* (1971); Hasselmann *et al.* (1973)), corroborated by wind-wave tank experiments by Mitsuyasu, led to a completely different view of the spectral energy balance of a growing wind-sea. This interpretation of the spectral energy balance in the 70's required a restructuring of wave models, which led to the second generation wave models.

As already mentioned, the principal source of energy during the main growth phase of the waves on the low frequency part of the spectrum is the non-linear energy transfer from higher frequency components to the right of the spectral peak, rather than direct wind forcing. The estimated residual wind input on the forward face of the spectrum is nearly an order of magnitude smaller than that assumed by first generation models, and was therefore consistent with earlier theoretical estimates and with later direct measurements.

The spectral peak of a growing wind-sea was observed to be enhanced by a factor of approximately three relative to the peak of a fully developed spectrum. This explained the unexpectedly high non-linear transfer rate, which was computed to be an order of magnitude greater than that originally evaluated by Hasselmann (1963b) for a fully developed spectrum.

The non-linear transfer was also found to control the shape of the spectrum, including the development of the peak itself. The overshoot phenomenon was explained naturally by the existence of this very sharp peak, significantly more pronounced than that of a fully developed spectrum, which migrated toward lower frequencies as the wave spectrum developed.

At higher frequencies, a universal equilibrium range was not confirmed. Although the frequency spectrum followed Phillips' f^{-5} power law approximately, the level of the spectrum (Phillips' constant α) decreased with increasing fetch.

Hasselmann *et al.* (1973) indicated that the energy balance in the f^{-5} region of the spectrum between f_p and $3f_p$ is not governed by whitecapping, as thought by Phillips, but primarily by the energy input from the atmosphere and the non-linear energy transfer by wave-wave interactions toward lower and higher frequencies. These authors derived the JONSWAP spectrum,

$$S_J(f) = \alpha g^2 (2\pi)^{-4} f^{-5} \phi_{PM}(f, f_p) \cdot \phi_J(f, f_p, \gamma, \omega), \qquad (3.14)$$

where

$$\phi_J = \exp\left\{\ln \gamma \exp\left[-(1/2)(f/f_P - 1)^2 / \sigma^2\right]\right\}, \qquad (3.15)$$

σ is the peak width parameter and γ is the peak enhancement factor, that is equal to the ratio of the maximal spectral density to the maximum of the corresponding Pierson-Moskowitz spectrum with the same values of α and peak frequency. The JONSWAP shape function, ϕ_J, gives the change in the spectral shape when waves are not fully developed.

Several authors have demonstrated from experimental studies that there is a range of frequencies above the frequency of the wind-wave spectral peak where the spectrum is saturated and in equilibrium with the local wind. However, there has been some controversy concerning the precise form of the spectrum in the equilibrium conditions and the dynamic process that is responsible for the equilibrium. Prevosto *et al.* (1995) review the relevant literature about the power law of the high frequency tail of the spectrum, presenting recent evidence that it may be closer to -4 than to -5, as originally suggested by Phillips.

Whereas the first-generation wave models had been based on primarily decoupled wave dynamics, the second generation wave models had to cope with a dominantly non-linear, coupled set of wave propagation equations. In the revised energy balance of the second generation wave models the independent evolution of individual wave components is effectively prevented by the coupling through the non-linear energy transfer.

In most of the second generation models, Miles mechanism is considered using the empirical expression provided by Snyder *et al.* (1981). These authors used wave growth measurements obtained in the Bright of Abaco, together with a re-examination of earlier results, to derive a growth factor

$$B = [0.2 \text{ to } 0.3]\frac{\rho_a}{\rho}\omega\left(\frac{U_5 \cos(\phi - \theta)}{c} - 1\right), \qquad (3.16)$$

Where ϕ is the wind direction, and U_5 is the mean wind speed at a height of five meters above the water surface.

This gives growth rates proportional to the wind velocity, while in Miles' theory the growth rate is proportional to the square of the wind velocity; in other studies the square proportionality is maintained (*e.g.* Steward (1974), Plant (1982)).

In most of the second generation wave models Phillips mechanism is not taken into account, since it is only important for the start of wave growth. For that reason those models cannot be initialised from zero energy.

As the surface gravity waves grow in an active wind field, the average wave slope increases. As the waves continue to grow, the non-linear terms of the governing equations become important enough that the linear theories of Miles and Phillips no longer apply. The growth of the spectrum for velocities higher than the wind velocity is not directly induced by the wind, but by the non linear resonant interactions between the spectral components.

The second generation spectral wave models include a parameterized version of the wave-wave interaction process, that is essentially absent in the first generation spectral wave models. Restrictions resulting from the non-linear parameterization require the spectral shape of the wind sea spectrum to be prescribed.

The first parameterized model was developed by Hasselmann *et al.* (1976). They used the JONSWAP spectrum with fixed peak width and peakness parameters. The peak frequency and Phillips constant were given by prognostic equations that took into account advection, non linear interactions, wind input and dissipation.

This parametric model was not applicable when the wind field was rapidly changing or when the sea state was transitional. It was also limited to growing wind seas and hence could not be applied in situations of swell dominated sea. The limited applicability of this model led to the development of models which combine the parametric wave representation with a discrete representation, which were classified as *coupled hybrid* models by the SWAMP Group (1985).

In the coupled hybrid models the wind-sea spectrum is treated parameterically and the discrete representation is limited to swell. The source function used for the wind sea part of the spectrum is obtained from an empirical growth curve.

These models use a finite difference scheme for the propagation of the parameteric wind sea and a spectral ray technique for the propagation of swell. A major inadequacy in the formulation of hybrid models has been the treatment of wind-sea swell transition regime, where the non linear energy distribution is neither negligible nor dominant.

Coupled discrete wave models were designed to overcome this short-coming. The discrete representation normally includes both swell and wind-sea, while the tail-end of the spectrum beyond the peak is treated parameterically. There is a wind input source function and usually an exponential type term to represent wave dissipation. The non-linear interactions are taken into account in the wind sea part of the spectrum by adjusting to an empirical form, or by the use of parameterizations with a small number of degrees of freedom.

Still, in both second generation wave models, hybrid and discrete, there is a separation between the wind-sea and the swell parts of the spectrum. The non-linear interactions are represented in the wind-sea part, and in the swell part the components develop

independently. The separation schemes are very simplified and artificial, exhibiting difficulties in the transition zone between the wind sea and swell for asymmetric or complex spectral forms, like those resulting from rapid variations in wind direction, where the propagation term in the transport equation can compete with the source terms. The defective parameterization of the non-linear source term gives wrong results and can also give non numerical instabilities associated with the incapacity to smoothen secondary peaks.

3.4 Third generation wave models

The third generation wave models incorporate the essentials of the presently known physics. Their development was due to a paper by Hasselmann and Hasselmann (1985), where a discrete operator of non-linear interactions providing a new method for efficient computations of the non linear transfer integral was proposed.

The first third generation wave model, WAM (WAMDI group,1988), was developed by an international group of wave modellers, after the shortcomings of the previous models were presented in SWAMP (1985). Some of the WAMDI group leading experts published a book (Komen *et al.*,1994) where the presently known dynamics of ocean waves is discussed, along with the scientific basis, actual implementation and applications of the WAM model.

WAM was the first third generation wave model, and it is probably the most used wave model in operation today. It is one of the models used in this work so it will be convenient to summarise here the scientific basis of WAM in its present version - cycle 4.

Contrary to the second generation models, the third generation wave models include no prescribed spectral form; the wave spectrum results from the integration of the energy balance equation. The WAM model solves the energy balance equation in spherical coordinates, in deep waters and without the presence of currents,

$$\frac{\partial}{\partial t}S+(\cos\phi)^{-1}\frac{\partial}{\partial\phi}\left(\dot{\phi}\cos\phi S\right)+\frac{\partial}{\partial\lambda}\left(\dot{\lambda}S\right)+\frac{\partial}{\partial\theta}\left(\dot{\theta}S\right)=\Phi, \qquad (3.17)$$

where

$$\dot{\phi}=\left(c_g\cos\theta\right)R^{-1},$$
$$\dot{\lambda}=\left(c_g\sin\theta\right)\left(R\cos\phi\right)^{-1},$$
$$\dot{\theta}=c_g\sin\theta\tan\phi R^{-1},$$

ϕ is the longitude, λ is the latitude and S represents the spectral density with respect to (f,θ,ϕ,λ).

The net source function Φ is given by three source terms: wind input Φ_{in}, wave-wave interactions Φ_{nl}, and dissipation due to whitecapping Φ_{ds}. The parameterizations of the three source terms and the reasons that led to the choice of those parameterizations will be given below. The propagation of wave energy for different wave numbers is taken along great circle arcs along which the potential energy is conserved.

Miles (1967) attempted to modify his theory to include interaction between waves and the air turbulence. Davies (1969, 1972) investigated the nature of turbulent air flow over a wavy boundary and how the air flow could produce work on the waves. Subsequent studies have considered the impact of turbulence using eddy viscosity models of varying degrees of complexity. Jacobs (1987) reviews some of the earlier studies and presents an asymptotic theory for turbulent flow over water waves. The eddy viscosity is assumed to vary linearly with distance from the water surface, and the direct effect of small-scale turbulence on wave growth is considered.

Jacobs obtains growth rates which compare favourably with observations for the most rapidly amplifying waves; his study further demonstrates that waves travelling against the wind, or more rapidly than the wind, transfer energy and momentum from water to air. However, Jacobs' model and other turbulence models yield growth rates which are not very different from those obtained by the quasi-laminar approach.

Janssen (1982) presents an extension of Miles' quasi-laminar theory. He considers that, as a consequence of the alterations induced by the waves in the airflow, the wind velocity profile is function of time. Further Janssen (1989a), Janssen *et al.* (1989) and Janssen (1991) conclude that the growth rate of waves depends additionally on three other factors: the effects of stratification in the air, gustiness and wave age.

Janssen *et al.* (1989) make a first attempt to parameterize the interactions between wind and waves and a more realistic one is given by Janssen (1991). A similar parameterization is used in WAM and is presented below.

According to Miles (1957), the growth rate of gravity waves due to wind depends on two parameters, namely

$$\chi = \frac{u_*}{c}\cos(\theta - \phi) \tag{3.18a}$$

and

$$\Omega_m = \frac{\kappa^2 g z_0}{u_*}, \tag{3.18b}$$

where κ^2 is the von Kármán constant and u_* the wind friction velocity.

The effect of stratification is partly accounted by scaling with the friction velocity, and the profile parameter Ω_m characterises the state of the mean air flow through its dependence on the roughness length z_0 which, in turn, depends on the sea state.

The roughness length is given by the Charnock relation,

$$z_0 = \alpha_c \tau / g, \tag{3.19}$$

where α_c is the dimensionless Charnock parameter, and τ is the kinematic stress given as

$$\tau = \left(\kappa \vec{U}(z_{obs})/\ln(z_{obs}/z_0)\right)^2, \tag{3.20}$$

z_{obs} being the mean height above the waves.

In this case the dimensionless Charnock parameter is not constant but dependent on the sea state due to its dependence on the wave induced stress,

$$\alpha_c = \hat{\alpha} \Big/ \sqrt{1 - \frac{\tau_w}{\tau}} \,. \tag{3.21}$$

In the latter equation $\hat{\alpha}$ is a constant and τ_w is the wave stress, *i.e.*, the stress induced by gravity waves:

$$\vec{\tau}_w = \frac{\rho}{\rho_a} g \int d\omega d\theta \gamma N \vec{k} \,. \tag{3.22}$$

A simple parameterization of the growth rate was obtained by Komen *et al.* (1994), from the fit of numerical results using the previous parameters, Eq. *3.18*,

$$\gamma_{in} = \frac{\rho_a}{\rho} \omega B \chi^2 \,. \tag{3.23}$$

Miles' parameter is given as

$$B = \frac{\beta_m}{\kappa^2} \mu \ln^4(\mu), \quad \mu \le 1, \tag{3.24}$$

where β_m is a constant, $\mu = kz_c$ is the dimensionless critical height (z_c is the critical height where the wind velocity equals the wave velocity), and in terms of wave and wind quantities μ is given as

$$\mu = \left(\frac{u_*}{\kappa c} \right)^2 \Omega_m \exp\left(\frac{\kappa}{x} \right). \tag{3.25}$$

From these results the wind input source term in WAM is

$$\Phi_{in} = \gamma_{in} N \,. \tag{3.26}$$

The constant $\hat{\alpha}$ has the value of 0.01, which is chosen so that for old wind sea the Charnock parameter α_c has the value of 0.0185 (Wu (1982)). β_m is chosen in such a way that the growth rate, γ_{in}, is in agreement with numerical results obtained from Miles growth rate, $\beta_m = 1.2$.

Non-linear Energy Transfer

The expression of the non-linear energy transfer source term is obtained theoretically without the use of poor fundamental hypotheses or approximations. This makes the non-linear source term the best known today. However, the numerical implementation of the term is still not feasible.

In the second generation models an attempt was made to address the problem by giving a parameterization of the non linear transfer for a given wave spectrum. A more powerful approach is used in third generation wave models, where the above mentioned discrete operator introduced by Hasselmann and Hasselmann (1985) is used to take into account

the non-linear energy transfer. The usefulness of the discrete interaction approximation follows from its correct reproduction of the growth curves for growing wind sea.

The discrete operator of non-linear interactions follows from the result of numerical experimentation. It was also concluded that the non-linear interactions can by modelled by one pair of symmetrical interactions where two of the wave numbers are equal, *i.e.*,

$$\vec{k}_1 = \vec{k}_2 = \vec{k}\,. \tag{3.27}$$

The two used configurations are symmetrical in $\vec{k}$ with

$$\omega_1 = \omega_2 = \omega\,, \tag{3.28a}$$

$$\omega_3 = 1.25\omega = \omega_+ \qquad \text{and,} \tag{3.28b}$$

$$\omega_4 = 0.75\omega = \omega_-\,, \tag{3.28c}$$

which correspond to the two wave numbers $\vec{k}_3 = \vec{k}_+$ and $\vec{k}_4 = \vec{k}_-$. These wave numbers have an angle with $\vec{k}$ of 11.5 and -33.6 degrees respectively

The discrete interactions for the rate of change in time of the action density in wave number space is given by

$$\frac{\partial}{\partial t}\begin{pmatrix} N \\ N_+ \\ N_- \end{pmatrix} = \begin{pmatrix} -2 \\ +1 \\ +1 \end{pmatrix} C g^{-8} f^{19}\left[N^2\left(N_+ + N_-\right) - 2NN_+N_-\right]\Delta\vec{k}\,, \tag{3.29}$$

where $\partial N/\partial t$, $\partial N_+/\partial t$ and $\partial N_-/\partial t$ are the rates of change in time of the action density at the wave numbers $\vec{k}$, $\vec{k}_+$ and $\vec{k}_-$ due to the discrete interactions within the infinitesimal interaction phase-space element $\Delta\vec{k}$, and C is a numerical constant.

The net source function in the WAM model is obtained by summing the previous rates of change in action over all wave numbers, directions and interaction configurations.

Wave dissipation

The wave dissipation term is still the worst known. Three approaches have been used to formulate the dissipation source function (Komen *et al.* (1994)). The probability model, the 'whitecap' model and the 'quasi saturated' model, have until now been unable to close the problem theoretically.

In the probability model the existence of a limiting amplitude is accepted on the grounds of Stokes' limiting criterion that wave will break when the downward acceleration at the crest exceeds half of the acceleration of gravity. In this model, proposed initially by Longuet-Higgins (1969), the probability of a given steepness being exceeded is obtained from the bivariate probability distribution of wave height-period. This approach was also used later by Yuan *et al.* (1986). This is a very simple approach but the applicability of a rigid limit of wave amplitude, derived deterministically for periodic wave to a wave spectrum, is not forthright.

Komen *et al.* (1984) used the whitecap model approach (Hasselmann (1974)), Eq. *3.5*, to obtain a dissipation source term numerically, for an asymptotic sea state, where the sum of the three source functions is zero in all the domains,

$$\Phi_{ds} = C\left(\frac{\hat{\alpha}}{\hat{\alpha}_{PM}}\right)^{m}\left(\frac{\omega}{\bar{\omega}}\right)^{n}\omega F(\vec{k}), \tag{3.30}$$

where C, m and n are fitting parameters.

$\hat{\alpha}$ is an integral parameter of the wave steepness

$$\hat{\alpha} = m_0 \bar{\omega}^4 / g^2 , \tag{3.31}$$

and $\hat{\alpha}_{PM}$ is the corresponding value for the Pierson-Moskowitz spectrum, and $\hat{\alpha}/\hat{\alpha}_{PM}$ is therefore a measure of the overall steepness of the wave field.

Equation *3.30* for $n = 1$ corresponds to the result of Hasselmann (1974).

In the 'quasi saturated' model, introduced by Phillips (1985), and by Donelan and Pierson (1987), a complementary assumption has been added to those of the whitecap model: that whitecapping is essentially local in wave number space.

Phillips (1985) has argued that, in the equilibrium range wind input, wave-wave interactions and dissipation are all of roughly equal importance, and the ratios of the three terms must be constant taking into account that there is no internal wave number scale.

He obtained a dissipation term that can be written in a quasi-linear form, as in the whitecap model,

$$\Phi_{ds} = -\gamma_{ds} F(\vec{k}), \tag{3.32}$$

but in this case

$$\gamma_{ds} = C\omega k^8 F^2(\vec{k}), \tag{3.33}$$

where C is a constant.

The contrast in the factor γ_{ds} is determined by the integral proprieties of the wave field in the whitecap model and by the local spectrum itself in the 'quasi-linear' model.

It is interesting to note that in Komen *et al.* the dissipation source function also includes the concept of saturation, since the factor $(\hat{\alpha}/\hat{\alpha}_{PM})^m$ depends on the degree of saturation.

It is still not clear as to whether whitecapping should be considered to first order local in space and time (Haselmann, 1974) or local in wave number (Phillips, 1985). It is also unclear whether either could be accepted as first approximation. However the expression of Komen *et al.* can accommodate either hypotheses.

The dissipation source function used in WAM is in accordance with an integral form for γ_{ds}. However, the expression for γ_{ds} was determined empirically and differs in detail from the integral form originally proposed by Hasselmann.

At high frequencies the growth rate of waves, given by the wind input source term, scales with the wave number as $\gamma_{in} \propto k^{3/2}$ and the whitecapping dissipation scales as $\gamma_{ds} \propto k$, such that an imbalance in the high-frequency wave spectrum is anticipated.

Janssen *et al.* (1989b) realised that the wave dissipation source function has to be adjusted in order to obtain a proper balance at high frequencies. Assuming that there is a large separation between the length scale of the waves and the whitecaps, the power of the wave number in the dissipation term is found to be equal to one. For the high-frequency part of the spectrum, such a large separation may not exist, allowing the possibility of a different dependence of the dissipation on the wave number.

To overcome the imbalance, the dissipation source term in WAM - cycle 4 is

$$\Phi_{ds} = -4.5\langle\omega\rangle\left(\langle k\rangle^2 m_0\right)^2\left[\frac{0.5k}{\langle k\rangle} + 0.5\left(\frac{k}{\langle k\rangle}\right)^2\right]N . \qquad (3.34)$$

The constant values of *4.5* and *0.5* were obtained in such a way that the energy balance equation produces results which are in good agreement with data on fetch-limited growth and with data on the dependence of the surface stress on wave age.

Typical results are shown in Figure *3.2* for a young wind sea and an old wind sea. These were obtained using the three parameterizations 4.26, 4.29 and 4.34 of the physics source terms, and by numerically solving the energy balance equation for deep waters and a constant wind velocity of *18 m/s*, neglecting currents and advection.

The directional averages of Φ_{in}, Φ_{nl} and Φ_{ds} are shown as functions of frequency, as well as the net Φ_{tot}.

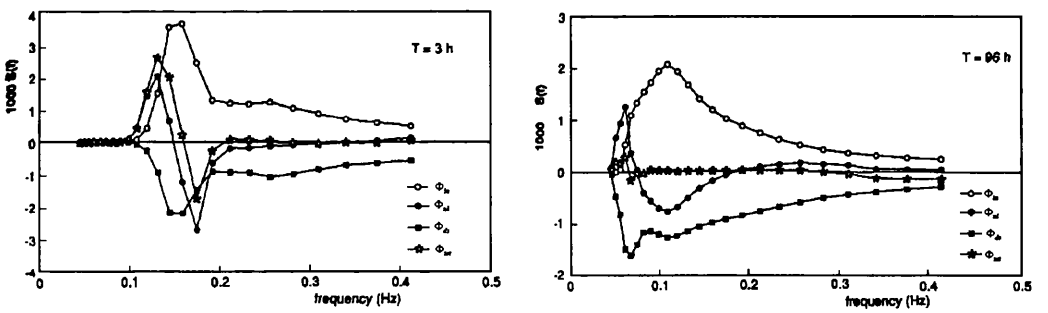

Figure 3.2-Left: Energy balance for a young duration-limited wind sea (T=3 h). Right: Energy balance for an old wind sea (T=96 h) (figures taken from *Komen et al., 1994*).

As expected, the wind input is always positive and the dissipation always negative.

The non-linear interactions show a three lobe structure of different signs (plus-minus-plus). They transport energy, input by the wind, in intermediate frequencies towards low and high frequencies.

For a young sea the non-linear interactions transfer energy from the region just beyond the location of the spectral peak to the region just below the spectral peak, thereby shifting the peak towards lower frequencies.

This shift of energy will continue until in an old wind sea the peak of the spectrum no longer receives input from the wind, because the waves are running faster than the wind.

In this case the waves around the spectral peak are subjected to a considerable dissipation, so that their wave steepness becomes reduced. Consequently the non-linear transfer is reduced as well, due to its dependence on wave steepness.

CHAPTER 4

Application of the Wave Models

4.1 Introduction

The objective of this thesis is to give an easy, fast and reliable way of forecasting the wave conditions on board of a ship once the wind fields are provided.

In the previous chapter it was said that the most used third generation wave model is WAM. This chapter provides an assessment of the results and of the feasibility of running WAM on board of ships. In addition, the second generation wave model DOLPHIN is assessed, and at the end of the chapter the two models are compared.

The WAM model is continuously updated. Cycle 4 is the most recent version. It has several programs for the various stages of pre-processing, processing and post-processing.

WAM was developed to run on a CRAY computer, but all the programs are coded in FORTRAN, and the code is provided, so that it is possible to adjust the model to different computer systems. Since it is more likely for a ship to have a personal computer (PC), we have decided to change the WAM code in order to run it on a PC (Pentium 133 MHz, 16 MB RAM). This is thought to be a reasonable and practical machine.

The DOLPHIN model runs on a PC, and so the comparison of the two models is straightforward.

Although the third generation wave models represent better the physics behind the wind waves, in most cases the results, mainly the significant wave height, do not differ much from those obtained by using second generation wave models. The latter use less adequate physics, but have been tuned to a considerable extent.

The models results will be compared with sea state measurements obtained during a measurement campaign that took place off the coast of Figueira da Foz in Portugal (*9.24 W, 42.26 N*).

Although both models compute the two dimensional wave spectrum, comparisons will be made only with the measured significant wave height, mean wave frequency and mean wave direction. This is because graphical comparison between measured and computed two dimensional wave spectra is not as clear as the comparison between the corresponding spectral integral properties, and also because most of the ship response models need as input the spectral integral properties rather than the full two dimensional wave spectrum. The latter, in turn, is obtained inside the ship response model by adjusting a prescribed spectral form to the spectral integral properties. The use of the mean wave frequency instead of the mean zero-upcrossing period was already justified in Chapter 2.

4.2 Directional Waverider

The sea state measurements used here were performed by a directional Waverider buoy at a deep water location. A brief explanation on how the buoy measures the sea state is given below.

Measuring the pitch, roll and heave motions of a surface following buoy is the most widely used method of directional wave measurement. It gives a robust measure of the mean wave direction, but a less robust measure of directional spread.

Directional Waverider buoys (see Tucker (1991)) are commercial buoys manufactured by Datawell in the Netherlands. The Directional Waverider measures the three components of acceleration of a particle following buoy giving the same information of pitch, roll and heave measurement buoys.

At wave frequencies the Waverider follows the motion of the water it displaces, and it is stopped from following slow drift by the mooring. A sensor inside the buoy contains an inertia stabilised platform that carries a vertical accelerometer which measures the vertical true acceleration. The pitch and roll of the buoy hull along two axes fixed in the buoy are also measured relatively to the stable platform.

A three component fluxgate compass is fixed to the buoy hull, using the same axes. The compass can be rotated mathematically by the pitch and roll angles to give the true horizontal magnetic components, and hence the correct direction of the magnetic north.

A two axis horizontal accelerometer is also fixed to the buoy hull along the same axis, and again, using the pitch and roll angles and the measured vertical acceleration, the true horizontal accelerations are calculated. These are rotated about a vertical axis to give the N-S and E-W components of acceleration.

These three acceleration signals are processed aboard. Each signal is double integrated and high-pass filtered, using a moving average filter. These raw and processed data are then transmitted over an HF radio link or recorded on board the buoy. From these data the two dimensional wave spectrum is estimated.

4.3 Description of the storms

The buoy measurements cover the Winter of 93-94. Figure *4.1* presents the significant wave height and peak period measurements from October 1993 until the beginning of March 1994. The wave measurements are available every three hours. During this period there are some missing measurements, in particular all the November measurements. The missing data are due for example to the deterioration of radio conditions in severe storms, or to complete breakdown. Severe wave conditions can be observed at the beginning of January and February.

The corresponding measured mean wave direction measurements are shown in Figure *4.2*.

The mean wave direction is given according to the Nautical convention. The direction of the x-axis is towards North, and the angles are measured clockwise from the geographic North, as shown in Figure *4.3*.

In the location of the buoy the sea state usually has a strong component of swell coming from Northwest. This can be concluded from the measured high peak periods (over 10s) in Figure *4.1*, and from the mean wave direction measurements in Figure *4.2*.

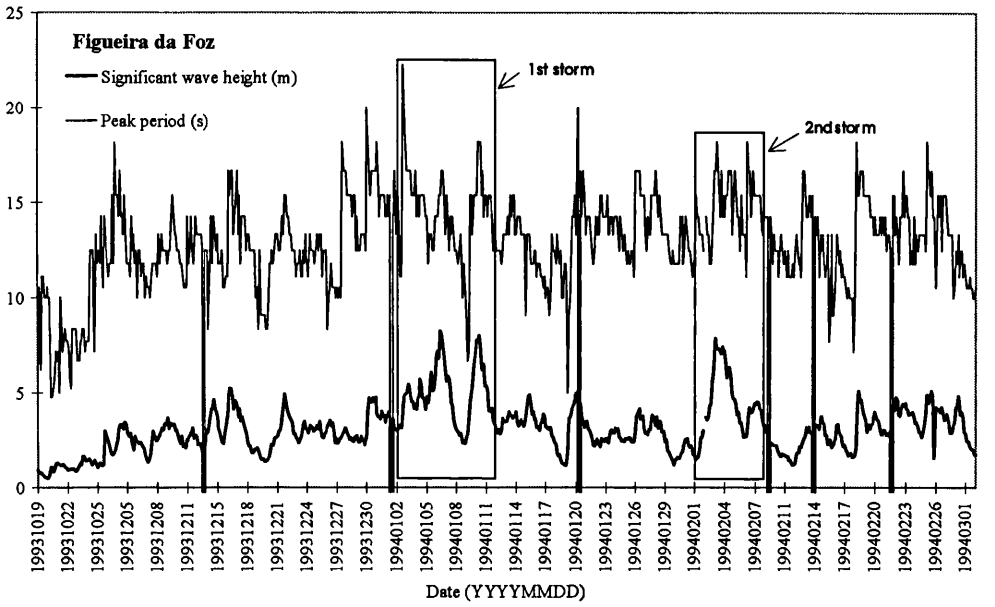

Figure 4.1 - *Three hourly measurements of a directional Waverider at a deep water location (9.24 W, 42.26 N) off-shore of Figueira da Foz.*

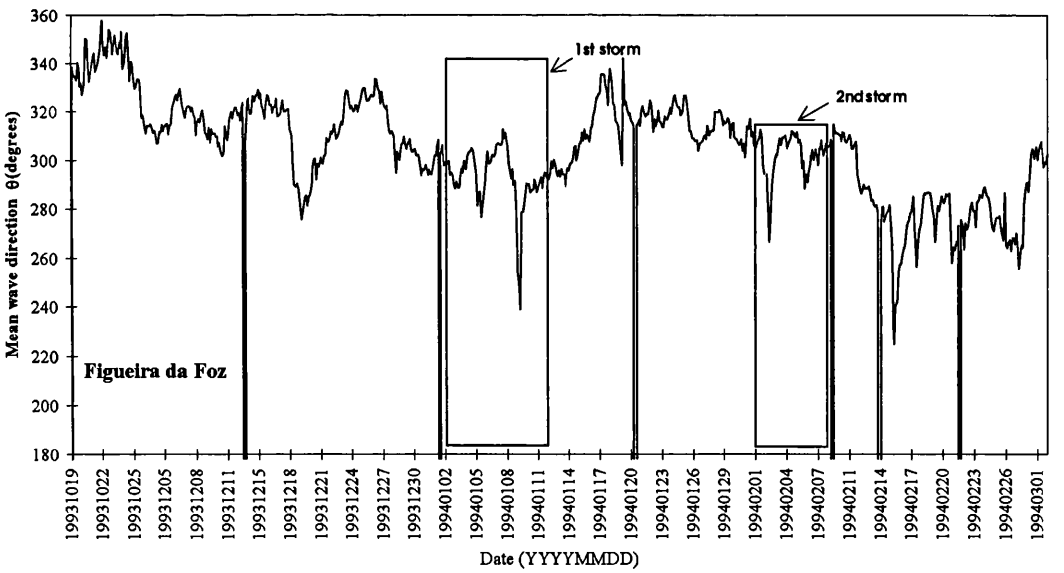

Figure 4.2 - *Three hourly measurements of a directional Waverider at a deep water location (9.24 W, 42.26 N) off-shore of Figueira da Foz.*

Among these measurements, significant storms were chosen for assessing and comparing the hindcasting performance of the WAM and DOLPHIN models.

Two periods were considered. First, the period from 11 a.m. on the 2nd of January until 2 a.m. on the 12th. Two high peaks of significant wave height, of 8.24m and 8m, occurred during this period.

The second period covers a storm that occurred in the beginning of February, where the significant wave height reached 7.9 m. The period starts at 2 a.m. on the 1st of February

and goes until 11 p.m. on the 8th. There is a missing measurement at 8 p.m. on the 2nd of February.

The two periods are marked in Figures *4.1* and *4.2* as '1st storm' and '2nd storm'. The terms are between quotation marks because the first period actually contains two consecutive storms.

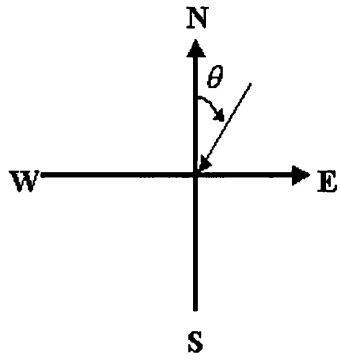

Figure 4.3 - Wave propagation sign convention.

The wave models require input wind velocity fields at 10 m height from the sea surface. The wind fields were provided by the European Centre for Medium-Range Weather Forecast (ECMRWF).

The ECMRWF runs a global spectral wind model with an horizontal resolution of 213[1] and a vertical resolution of 31 levels. The wind fields are provided every 6 hours.

For the storm periods now chosen, the available wind fields are provided on a grid. The grid covers a North Atlantic area, from -80 to 20 degrees of longitude and from 15 to 75 degrees North. The grid spacing is of 4 degrees in longitude and 3 degrees in latitude.

The wind field has to cover such a large area on the North Atlantic because swell generated further West in the North Atlantic arrives at the buoy location.

In order to analyse the wave conditions at a given time, the wind field must be provided days before on an oceanic scale. This swell can travel for days from the generated area until it reaches the actual location.

The wind fields and the measured wave conditions in the two chosen periods will be now described.

The velocities in the wind fields during the first storm are presented in Appendix A. In order to initiate the sea state a spin up period of approximately 6 days was used. This spin up period was obtained by identifying in which day the computations should start in order that there were no alterations on the model results for the hindcast period if the computations started sooner. The computations, and therefore the required wind velocity fields, start on the 27th of December.

On the 28th and 29th of December high winds can be observed from the North of USA towards the North of Europe.

---

[1] A model with spectral resolution n can distribute $2n$ independent bits of information over the circumference of the earth, the associated resolution being $40000/2n$ Km.

On the 31st of December a cyclone with wind velocities up to 28 m/s appears on the Northeast of New York moving further East.

On the 3rd of January at 6 a.m. and 6 p.m. winds of 24m/s were blowing from the Northwest toward the North coast of Portugal. On the same day around 4 p.m. the significant wave height was over 5 m, a limit also crossed on the 4th.

On the 6th there are high winds (26 m/s) at 20°W and from 45° to 48°N on the Northwest of the Iberian Peninsula.

On the 8th there is a cyclone moving from east of Montreal towards England, which on the 9th was blowing in the central and North coast of Portugal. These winds caused the appearance of the wind sea on the 9th in Figueira da Foz. This is seen by the sudden drop of the peak period on that day. The cyclone is also responsible for the severe wave conditions on the 10th of January.

The velocities in the wind fields during the second storm can be observed in Appendix B. In order to initiate the sea state a spin up period of 6 days was used. The computations, and therefore the required wind velocity fields, start on the 26th of January 1994.

From 6 p.m. on the 2nd until the 4th of February a cyclone located at Northwest of the Iberian Peninsula caused the severe wave conditions of the 4th of February.

On the 5th a cyclone starts moving from the North coast of the USA towards the North of Europe.

4.3 WAM model

The physics of the WAM model has already been presented in Chapter 3. Here we only give a brief account of how the model numerically solves the energy balance equation and of how the code was adjusted to a PC.

The model solves numerically the energy balance equation with the source functions given in Chapter 3. It uses the directional frequency wave spectrum discretised over frequency-directional bins.

The spectrum has a prognostic and a diagnostic part. The prognostic part has ND directional bands and NF frequency bands. These frequency bands are given on a logarithmic scale, with $\Delta f/f = 0.1$, spanning a frequency range of $f_{\max}/f_{\min} = 1.1^{NF-1}$.

The logarithmic scale is used in order to achieve a uniform relative resolution, and also because the non-linear transfers scale with frequency. The starting frequency $f_{\min}$ may be selected arbitrarily.

Beyond the high-frequency limit f_{hf} of the prognostic region of the spectrum,

$$f_{hf} = \min\left(f_{\max}, \max\left(2.5\langle f\rangle, 4f_{PM}\right)\right) \qquad 4.1$$

an f^{-5} tail is added, with the same directional distribution as the last band of the prognostic region.

The diagnostic part of the spectrum is therefore given as

$$S(f,\theta)=S(f_{hf},\theta)\left(\frac{f}{f_{hf}}\right)^{-5} \quad \text{for } f>f_{hf}. \qquad 4.2$$

The prognostic part of the spectrum is obtained by numerically solving the energy balance equation.

The energy balance of the spectrum is evaluated in detail up to a high cut-off frequency. For the integration of the source function, a time-centred implicit integration scheme is used whose time step is matched to the evolution of lower frequency waves This scheme allows a time step of 20 minutes, established by the numerical stability of the advection procedure. For propagation, a first order upwind scheme is used. The propagation time step can be chosen to be equal or larger than the source term time step. For more details about these schemes see WAMDI(1988).

WAM was compiled with FORTRAN 90 for Windows 95. Extensive work was performed in order to be able to compile it. All the files had to open at the right time, and common blocks and parameters had to be defined for each subroutine. Several minor changes in the code also had to be performed in order to adjust the code to the present system.

A subroutine to read the input wind fields was also coded.

WAM results

The WAM model runs on a latitudinal-longitudinal grid with arbitrary resolution and a prescribed topographic data set. The grid, identifying the sea and land points, is set up by the user. Land grid points are not computational grid points.

The program can be run with depth refraction and currents, but these options are not used here since we consider only deep waters without the presence of currents. The program can also be run with nested grids. The boundary conditions of a fine grid of limited extension are given by the results of a run of a coarser grid on which the finer grid is embedded; this option is also not used.

The model was run on a grid covering most of the North Atlantic. Two grids with different resolution were considered. One with 2 by 2 degrees spacing, shown in Figure *4.4*, and the other with 1 by 1 degree spacing, shown in Figure *4.9*. These grids do not cover all the extension of the wind field grid. Unnecessary computations are avoided since the wind grid points ignored have no influence on the wave conditions at the output location.

The coarser grid covers the region between 16° to 74° North in latitude, and from 80° West to the Meridian of Greenwich. The 1° by 1° grid goes from 15° to 70° North and covers the same longitudes as the coarser grid.

For practical reasons, large scale models have a fairly coarse resolution, but they are nevertheless well suited to deal with large-scale phenomena, such as the present large extra tropical Winter storms of the North Atlantic Ocean, originating at high latitudes on the American Coast and gradually moving East towards Europe.

Using a large scale model is necessary for the computations of the sea state in limited regions that require a proper assessment of what is happening elsewhere in the basin, as is the case of the Portuguese Coast, where the sea state has a high component of swell

generated far away. This large scale model can also be applied to ship routing in the North Atlantic, a type of application aimed at in this thesis.

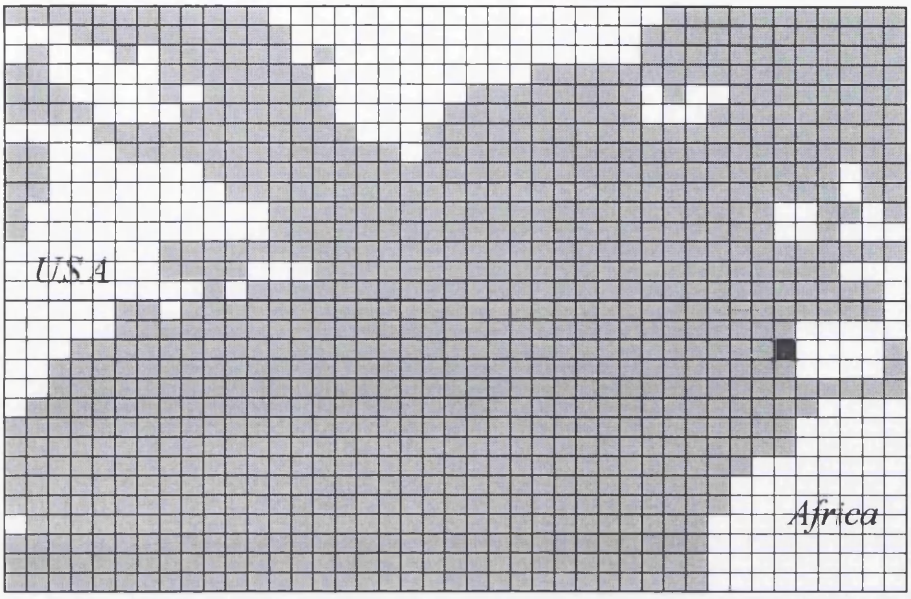

Figure 4.4 - 2°x2° grid, from 16° N to 74° N in latitude and from 80° W to 0° in longitude.

The number of direction and frequencies is a user option. A compromise must be established between the number of directions and frequencies and the computer time and space. We next analyse the effect of varying these parameters on the model results.

The starting frequency was chosen to be 0.025 Hz since, as seen from the peak period measurements (Figure *4.1*), the wave conditions on the Portuguese Coast have a high component of swell.

In all computations the source term time step and the propagation time step are both of 20 minutes. The latter could have been chosen larger than the former, but in this way the propagation computational effort is less.

The model wind input source function does not account for Phillips' term. Therefore, the computations can not have a 'cold' start. In one of the pre-processing programs, an initial JONSWAP spectrum is computed at all computational grid points from local initial winds according to fetch laws with a square cosine directional distribution.

Several runs were performed with WAM with different frequency, direction and grid resolutions. The results were compared with the measurements in terms of the root-mean-square error, *r.m.s.*, and the scatter-index, *S.I.*.

The root-mean square error is

$$rms = \sqrt{\frac{1}{n-1}\sum_{i=1}^{n}\left(\chi_i^{obs} - \chi_i\right)^2} \qquad 4.3$$

where χ^{obs} is the measured or observed parameter and χ the model-computed parameter. The scatter-index is obtained by normalising the root-mean-square-error by the average of the measured parameter,

$$S.I. = 100 \cdot \frac{\sqrt{\frac{1}{n-1}\sum_{i=1}^{n}(\chi_i^{obs} - \chi_i)^2}}{average(\chi)}. \qquad 4.4$$

The WAM model includes test cases with directional resolutions of 12 and frequency resolutions of 25. A test using 18 directions and 25 frequencies was compared with another test using 40 frequencies. Although the number of frequencies does not have a high influence on the sea state results, a higher number of frequencies is expected to better represent the discretization of the spectrum, but it is clear that the number of frequencies does not have to be much higher than 40.

The significant wave height resulting from the two tests is compared with the wave measurements in Figure *4.5*. The two runs give very similar results. They overestimate the first two peaks of the significant wave height on 3rd and 4th of January, and underestimate the two high storm peaks on the 6th and 10th of January.

Figure *4.6* compares the results for mean wave frequency. The computations show a good agreement with the measured mean wave frequency. The run with *NF=25* has a scatter-index almost 1% higher than the run with *NF=40*. The scatter-index in the first run is of *12%* and in the second of *11%*.

In order to proceed, we have adopted a resolution of 40 frequencies and changed the directional resolution. The justification for this choice is that 40 frequencies provide a better discretization of the wave spectrum, and a slightly better hindcast of the mean wave frequency.

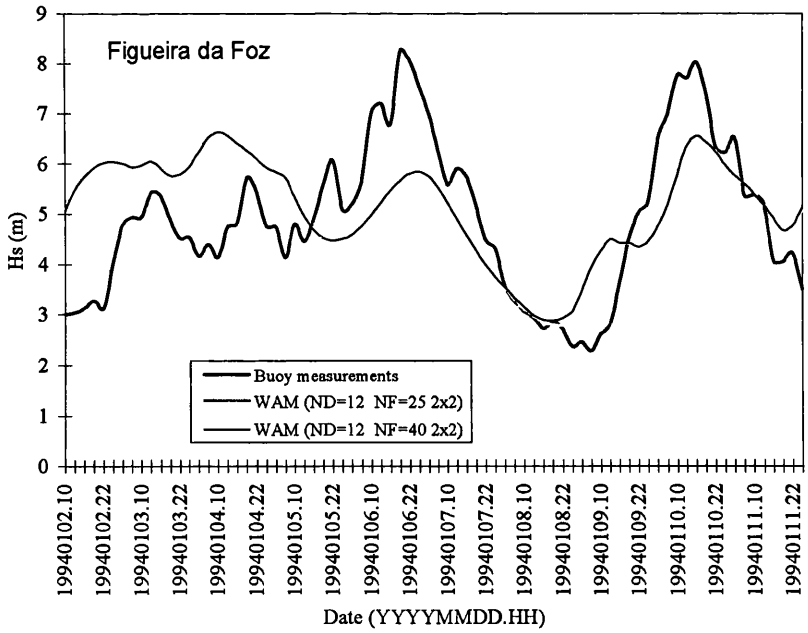

Figure 4.5 - *Comparison of the significant wave height obtained by WAM using a frequency resolution of 25 and 40 on a 2°x2° grid with a directional resolution of 12.*

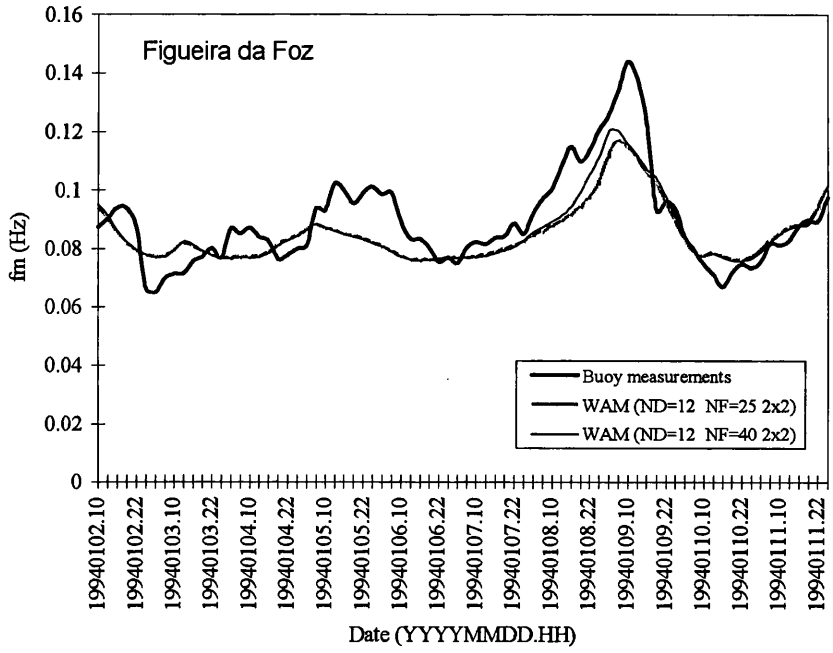

Figure 4.6 - *Comparison of the mean wave frequency obtained by WAM using a frequency resolution of 25 and 40 on a 2°x2° grid with a directional resolution of 12.*

The results of fixing the resolution in 40 frequencies and varying the direction are shown in Figures *4.7* and *4.8*. The figures compare the buoy measurements of significant wave height and mean wave frequency with the model results, and are based on three different tests with directional resolutions of 12, 18 and 72. The significant wave height time series exhibits the same behaviour in all runs, but the results obtained with 18 directions are closer to the measurements.

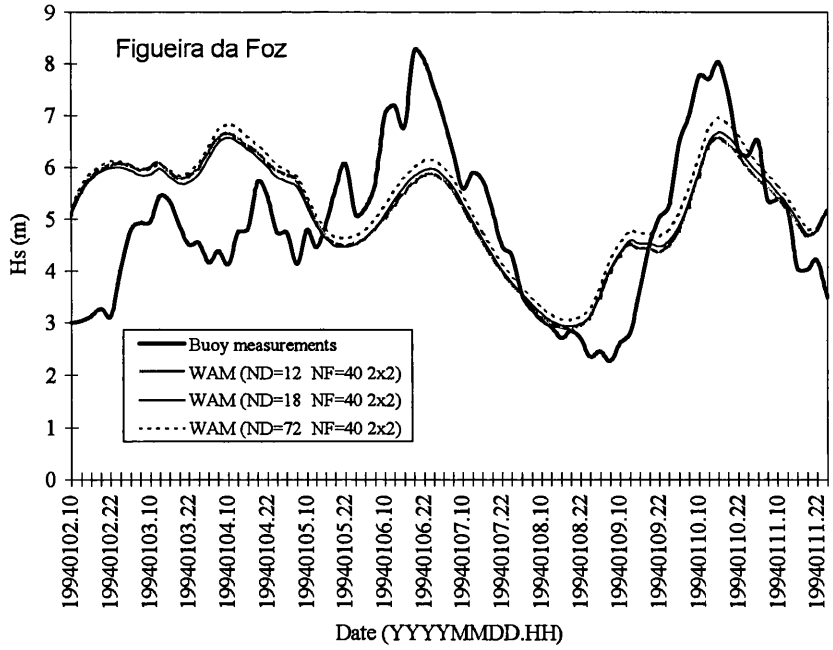

Figure 4.7 - Comparison of significant wave height obtained by WAM using a directional resolution of 12, 18 and 72 on a 2°x2° grid with frequency resolution of 25.

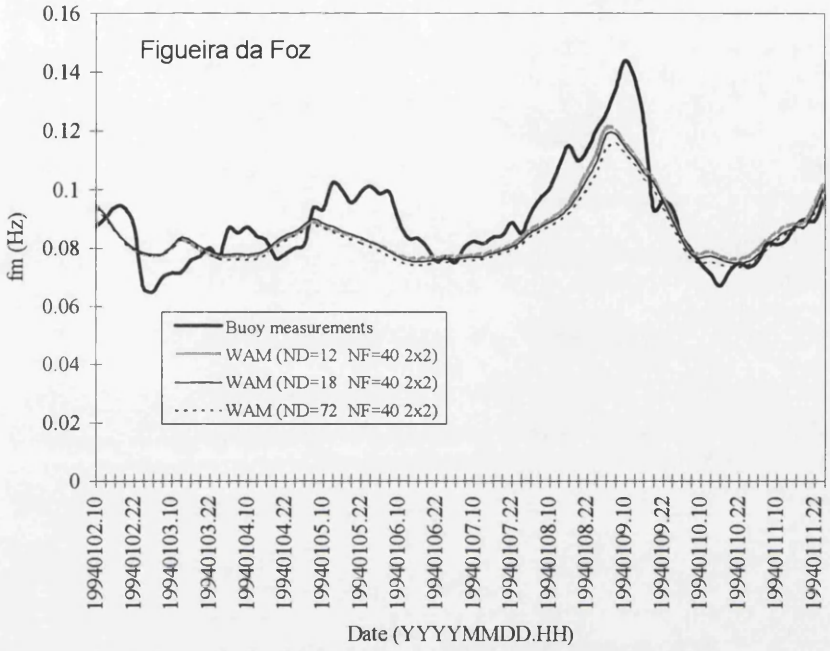

Figure 4.8 - Comparison of the mean wave frequency obtained by WAM using a directional resolution of 12, 18 and 72 on a 2°x2° grid with frequency resolution of 25.

The model run with 5 degrees resolution (72 directions) does not improve the results, while the computational space and time increase significantly - for example, while for the 20 degrees resolution (18 directions) it takes 50 minutes to compute a day hindcast, with 5 degrees resolution it takes 12 hours and 4 times as much disk space.

There is only a small difference in the mean wave frequency time series obtained in the three runs, and the results are in good agreement with the buoy measurements.

Figure 4.9 - 1°x1° grid from 15° N to 70° N in latitude and from 80° W to 0° in longitude.

All these runs were performed in the 2° by 2° grid. In order to examine the effect of the grid resolution, the results of the run using 40 frequencies and 18 directions were compared with a run with the same directional and frequency resolution in a 1° by 1° grid.

The 1° by 1° grid is presented in Figure *4.9*. It provides a better description of the coast line, but the computational grid points are almost quadruple. The output location - which is the computational grid point closer to the buoy location (9.24 W, 42.26 N) - differs in the two grids. For the 2° by 2° grid it is 40°N 10°W, and in the 1° by 1° grid 40°N 9°W.

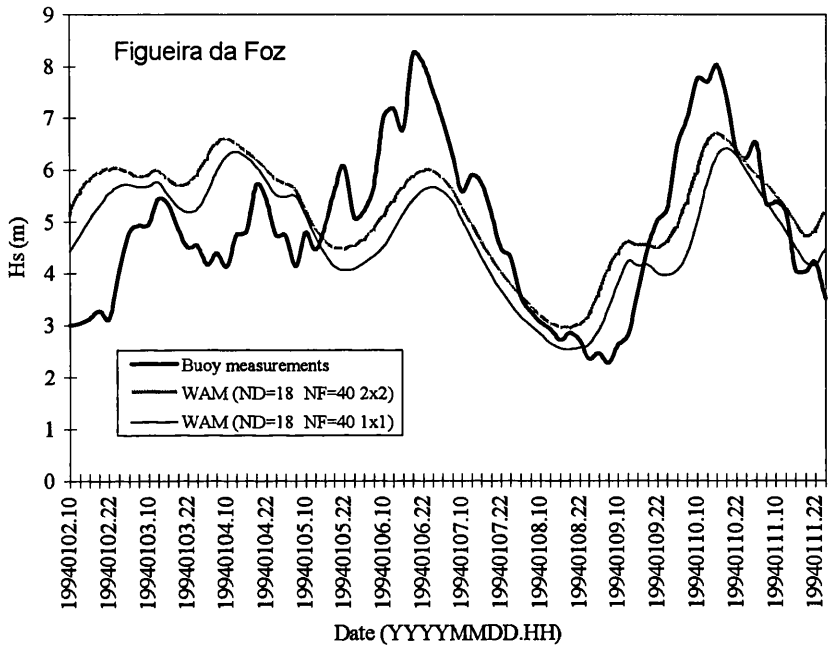

Figure 4.10 - Comparison of the significant wave height obtained by WAM on a 2°x2° grid and a 1°x1° grid using a directional resolution of 18 and a frequency resolution of 40.

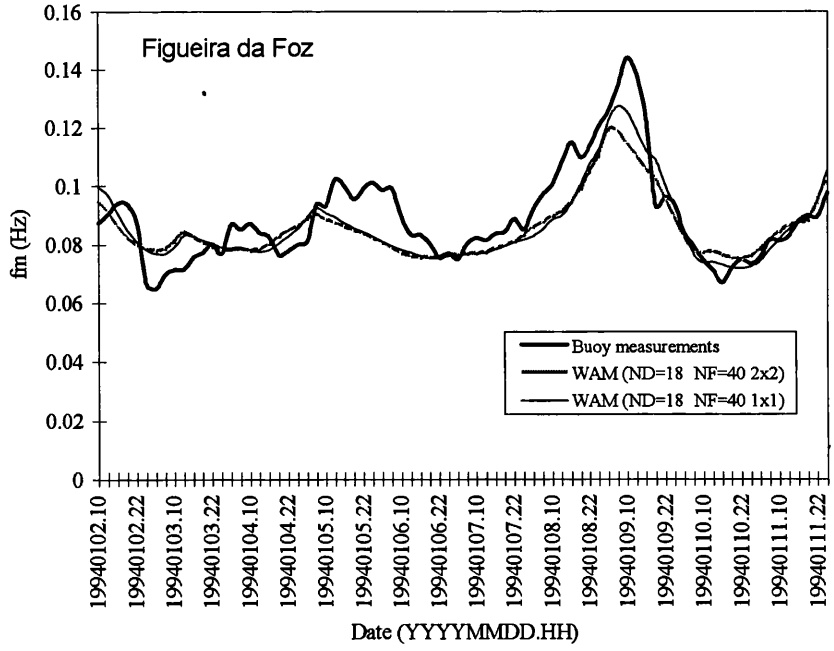

Figure 4.11 - Comparison of the mean wave frequency obtained by WAM on a 2°x2° grid and a 1°x1° grid using a directional resolution of 18 and a frequency resolution of 40.

The comparison of results using the different resolution grids with the buoy measurements is presented in Figure *4.10* for the significant wave height, and in Figure *4.11* for the mean wave frequency.

The mean wave direction shows a difference of only 1 cm in the root mean square error between the two grids. The finer grid run gives a significantly better hindcast of the mean wave frequency. The scatter-index drooped from 11.15% in the coarser grid to 9.89% in the finer grid.

Table *4.1* gathers the root-mean-square error and scatter-index of all the previous tests. In the computations of the mean wave direction, in all trials, the root-mean-square error is of about 8°. This is considered to be a reasonable error for computation of ship response at sea, since the directional resolution in the computation of ship responses is usually higher than 15°.

			H_s		f_m	
Number of directions	Number of frequencies	Grid	*r.m.s (m)*	*S.I.(%)*	*r.m.s (Hz)*	*S.I.(%)*
12	25	2x2	1.33	26.97	0.011	11.89
12	40	2x2	1.34	27.27	0.010	10.93
18	40	2x2	1.30	26.43	0.010	11.15
72	40	2x2	1.34	27.11	0.011	12.24
18	40	1x1	1.31	26.51	0.009	9.89

Table 4.1 - Root-mean-square error and scatter-index for the several tests performed with WAM in the 1st storm.

Number of directions	Number of frequencies	Grid	Precision	Computing time per 24 h hindcast	Disk Space
12	25	2x2	Single	16 min	1.3 MB
12	40	2x2	Single	26 min	2 MB
72	40	2x2	Single	12 h	12 MB
18	40	2x2	Single	50 min.	3 MB
18	40	1x1	Single	2 h 48 m	15 MB
18	40	1x1	Double	15h 15m	30 MB

Table 4.2 - Computing time and disk space need for each of the tests performed with WAM.

Table *4.2* presents the disk space and computing time required for performing each of the tests. In one of the tests all the real variables in the programs were defined with

double precision; the test was revealed to be very time- and space-consuming, and gave no significant improvement in the results.

In Table *4.1* the best results for significant wave height were obtained with 18 directions and 40 frequencies in a 2°x2° grid. The best results for the mean wave frequency period were obtained for this same frequency-direction resolution on a 1°x1° grid. Although the significant wave height hindcast does not differ much in the two runs (1 cm), there is a difference of 1.26% in the scatter-index of the mean wave frequency. So a 1°x1° grid with 18 directions and 40 frequencies should be used to produce a better hindcast. However, a run with this grid resolution needs 5 times more space than the 2°x2°, and is more than 3 times slower.

The results also show that the coarser grid with 25 frequencies and 12 directions gives a good first estimate of the sea state conditions with less computational time and disk space.

For the second storm, the WAM results were obtained on a 1°x1° grid using a direction resolution of 18 and a frequency resolution of 40. The model hindcasts are compared with the buoy measurements of significant wave height in Figure *4.12*, and with the mean wave frequency measurements in Figure *4.13*. The lines in these pictures and in all the pictures referring to this storm show a discontinuity due to a gap in the measurements.

The numerical results generally overestimate the significant wave height measurements. Nevertheless, during the peak of the storm the computations show a reasonable agreement with the buoy measurements. The model results have a root-mean square error of 1.5 m. In this case, the computations of the mean wave frequency show a less good agreement than in the first storm, the scatter index being of 12%.

The deterioration of the model results is believed to be a consequence of errors in the wind fields, and not in the wave model itself.

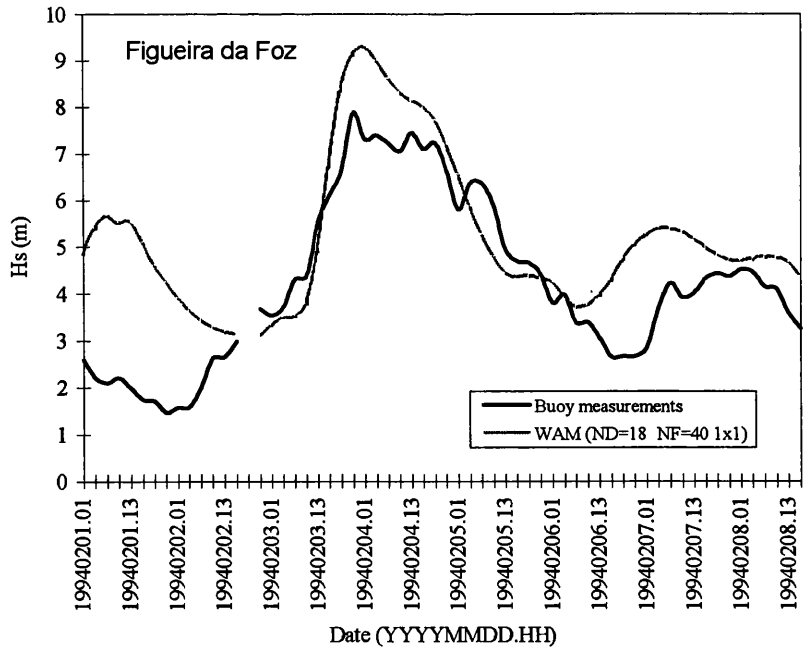

Figure 4.12 - Comparison of the significant wave height measured and obtained by WAM on a 1°x1° grid using a directional resolution of 18 and a frequency resolution of 40.

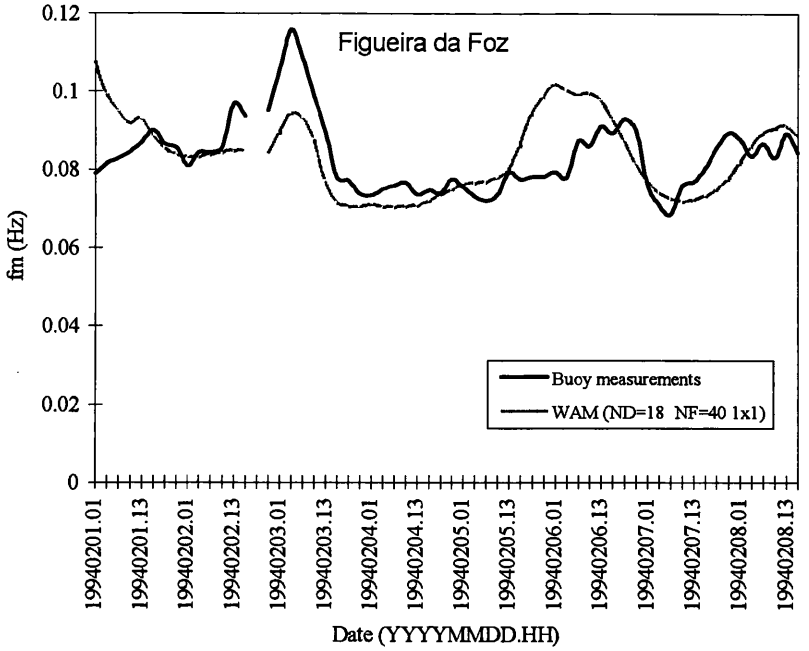

Figure 4.13 - Comparison of the mean wave frequency measured and obtained by WAM on a 1°x1° grid using a directional resolution of 18 and a frequency resolution of 40.

4.4 DOLPHIN model

DOLPHIN-B (Holthuijsen and de Boer (1988)) is a discrete spectral wave model. It computes the two-dimensional wave energy spectrum at a given location (x,y,t) in the ocean by integrating the lagrangian spectral energy balance of the wave components present at that location.

In DOLPHIN, the integration of the energy balance equation is carried out along the characteristics of the equation radiating from the forecast point. These characteristics are obtained by back tracing all wave components of the discretised two-dimensional target spectrum. Since the model considers only wave components arriving simultaneously at one forecast location, all components can be traced by simply determining, for each frequency and direction, the distance of the wave component to the forecast location.

The generation and dissipation of the waves is modelled with first generation source functions in the far field (far from the target point) and with second generation source functions in the near field. These source functions, which simulate atmospheric input, non-linear wave-wave interactions and white-capping, are

$$\Phi = (A + B \cdot S) \qquad S < S_{PM} \qquad 4.5a$$

$$\Phi = \frac{1}{\tau}(S - S_{PM}) \qquad S > S_{PM} \text{ and } |\theta - \phi| < 90° \qquad 4.5b$$

$$\Phi = 0 \qquad S > S_{PM} \text{ and } |\theta - \phi| > 90° \qquad 4.5c$$

where S_{PM} is given by Equation *4.7*.

The expressions for A and B, which represent the linear growth proposed by Phillips (1957) and the exponential growth proposed by Miles (1957), are taken from Cavaleri and Malanotte (1981), and Snyder *et al.* (1981) respectively, with coefficients tuned to fit the growth curves of SPM (1973):

$$A = 188\left(\frac{\rho_a}{\rho}\frac{\pi}{g}c_{drag}\right)^2\left(U_{10}\cos(\theta-\phi)\right)^4, \qquad 4.6$$

$$B = 0.59\frac{\rho_a}{\rho}f\left(\frac{U_{10}\cos(\theta-\phi)}{c}\right). \qquad 4.7$$

Here, c_{drag} is the drag coefficient, which equals 0.0012.

The decay time scale τ has been tuned to the dissipation of a decaying swell in the WAM model. The expression thus obtained is

$$\tau = c_{diss}f^{-1}\left(\frac{g}{fU_{10}}\right)^3\cos^{-1}(\theta-\phi), \qquad 4.8$$

where c_{diss} is a dissipation coefficient taken equal to 2.

In the near field the value of the energy scale parameter α of the Pierson-Moskowitz spectrum depends on the local wind sea in the direction of propagation:

$$\alpha = \min\left\{0.0081, 0.0023\tilde{S}_\theta^{-0.223}\right\}, \qquad 4.9$$

where $\tilde{S}$ is the dimensionless wave energy of the wind sea part of the spectrum, estimated from the transect $\tilde{S}_\theta(f)$ of $S(f,\theta)$ in the direction θ by assuming a $\cos^2(\theta)$ directional distribution:

$$\tilde{S}_\theta = \frac{\pi}{2}\frac{g^2}{U_{10}^4}\cos^{-2}(\theta-\phi)\int_{0.7PM}^{\infty}S_\theta(f)df, \qquad 4.10$$

where the Pierson-Moskowitz frequency $f_{PM} = 0.13g/U_{10}$. This dependency of α on $\tilde{S}_\theta$ allows the spectral density to overshoot the Pierson-Moskowitz limit, which is a non-linear (second-generation) characteristic of the model. In the far field the wave components are decoupled in the model, and the value of α is 0.0081. This makes the model a first-generation model in the far field.

By specifying a string of forecast times and locations, the wave conditions are forecast for targets that may be stationary or moving. Such a string can be located along the projected track of a ship.

DOLPHIN results

This model has already been calibrated in previous works (Guedes Soares *et al.* (1994), and Guedes Soares and Caires (1995)), and the variables have to a certain extent been tuned to the conditions in the Portuguese Coast. Therefore, no sensitivity analyses will be made to the choice of those variables.

DOLPHIN uses a ray technique to compute the two-dimensional wave spectrum at a given location by integrating along radiating curves the spectral energy balance of the wave components. With this ray technique, DOLPHIN does not require an input computational grid.

The wave computations are executed over the geographic region covered by the wind field. No waves enter across the boundary of the wind grid; waves start to grow on that boundary.

In place of the input grid representing sea and land points, DOLPHIN requires the description of the coast line of the region covered by the wind grid. Like WAM, the model can run in cartesian or spherical co-ordinates. Since we are considering a large area, the use of spherical co-ordinates is preferred, as it takes into account the curvature of the earth. The coast lines are described by the longitude and latitude of coastal points, on a latitude-longitude resolution of 5 minutes.

The frequency distribution is logarithmic. The number of frequencies, and the highest and lowest frequencies are user inputs. We have taken a lower frequency of 0.025 (as in WAM), the highest frequency as 0.6, and 40 frequencies.

The directional resolution must be such that the directional spacing is small compared to the directional spreading. For wind sea, a directional step of 10 degrees is enough, but since in this case we are in the presence of swell generated far away, a directional step of 2 degrees was taken.

The rays generated by DOLPHIN for the computations in Figueira da Foz are shown in Figure *4.14*. The wind field area ignored in the WAM grids is also not taken into account in this model, since no rays are shot into that area.

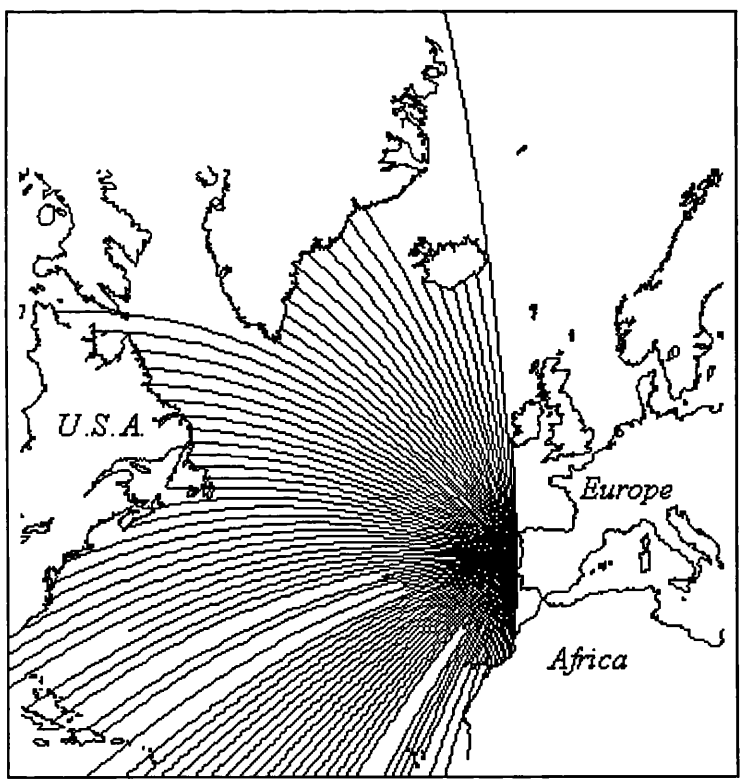

Figure 4.14 - Rays generated by DOLPHIN from Figueira da Foz.

The computational time step to numerically integrate wave growth and dissipation must be equal or smaller than the wind time step, and can not be larger than the wind grid spacing divided by the wave group velocity. Its value must be such that the waves do not travel a distance higher than the spatial time step of the wind. In the present case,

because the grid resolution of the wind field is coarse (4°x3°), an integration time step of 6 hours was chosen.

The time span over which non-linear interactions are taken into account was chosen to be 6 hours.

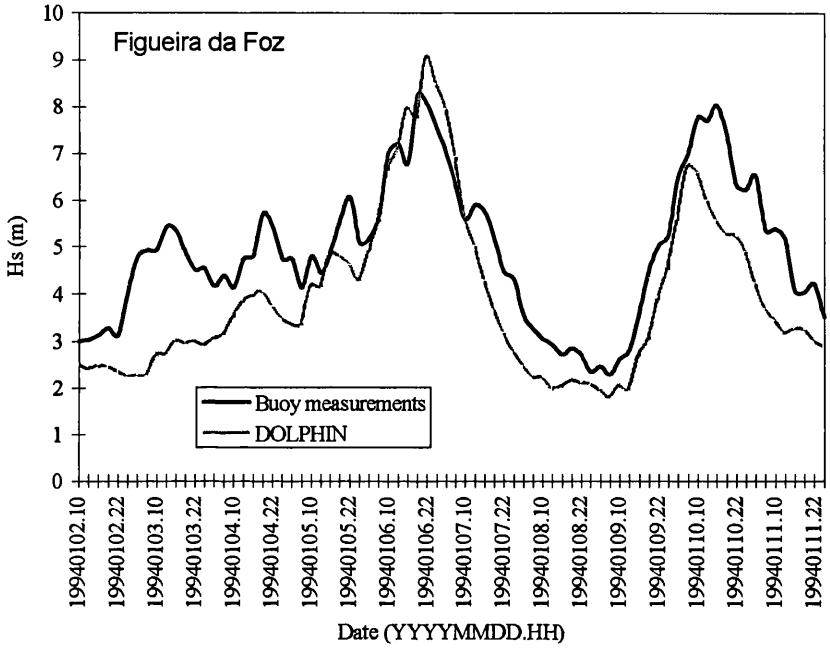

Figure 4.15 - Comparison of significant wave height measurements with DOLPHIN results.

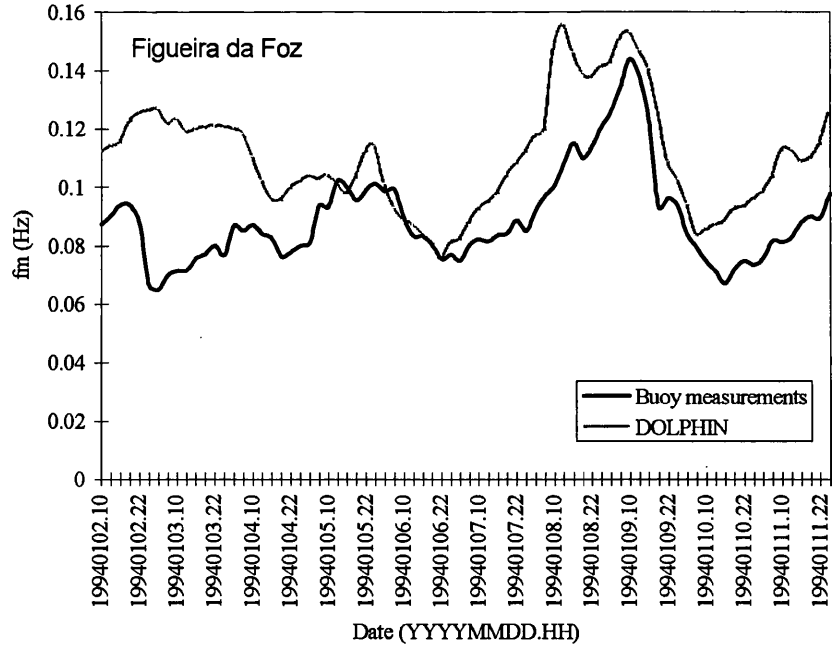

Figure 4.16 - Comparison of mean wave frequency measurements with DOLPHIN results.

For the 1st storm, the model results for significant wave height, mean wave frequency and mean wave direction are compared with the corresponding measurements in figures *4.15*, *4.16* and *4.17* respectively.

The computed significant wave height shows a good agreement with the measurements from 6th of January onwards. During the previous period, significant wave height is underestimated, and the peak on the 3rd of January was unnoticed by the model.

The hindcasts of the mean wave frequency are not very good until the 6th of January, as was the case with the significant wave height. The high frequency waves measured in the 8th of January were not computed by the model.

The model computed mean wave direction shows a very good agreement with the measurements.

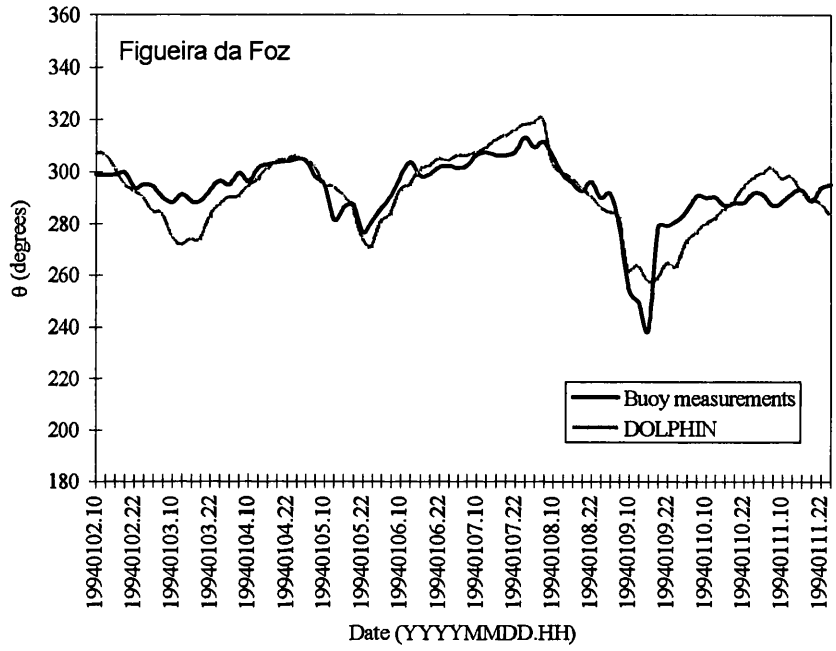

Figure 4.17 - Comparison of mean wave direction measurements with DOLPHIN results.

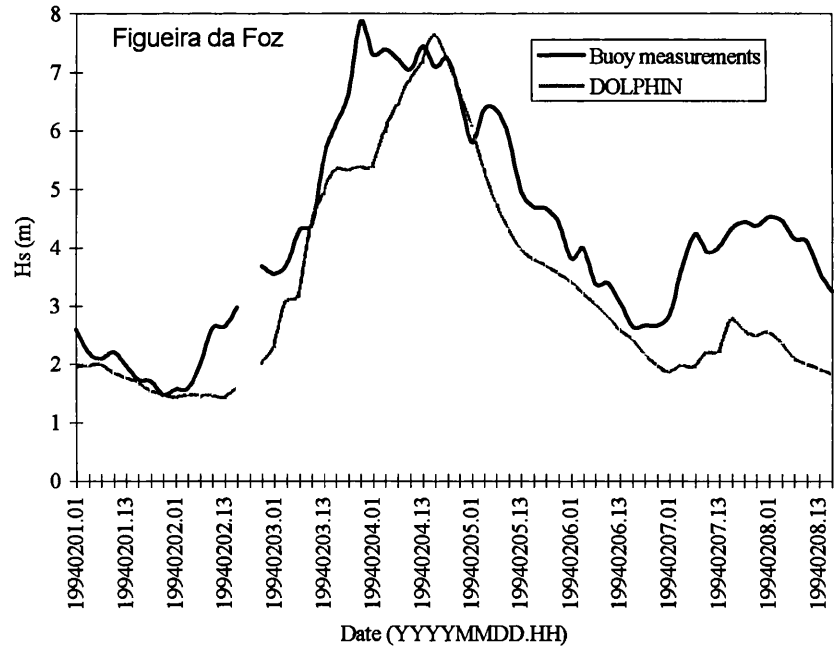

Figure 4.18 - Comparison of significant wave height measurements with DOLPHIN results.

Figures *4.18*, *4.19* and *4.20* compare the hindcast of significant wave height, mean frequency and mean wave direction for the 2nd storm with the corresponding measurements.

It can be seen in Figure *4.18* that the model results follow the significant wave height measurements until the 7th of February, and that from then on the results deteriorated considerably.

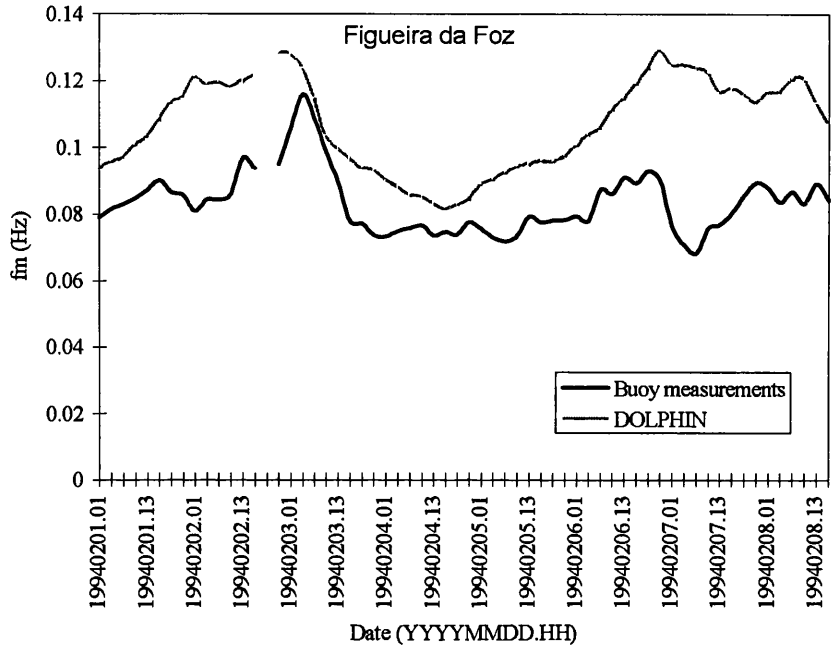

Figure 4.19 - Comparison of mean wave frequency measurements with DOLPHIN results.

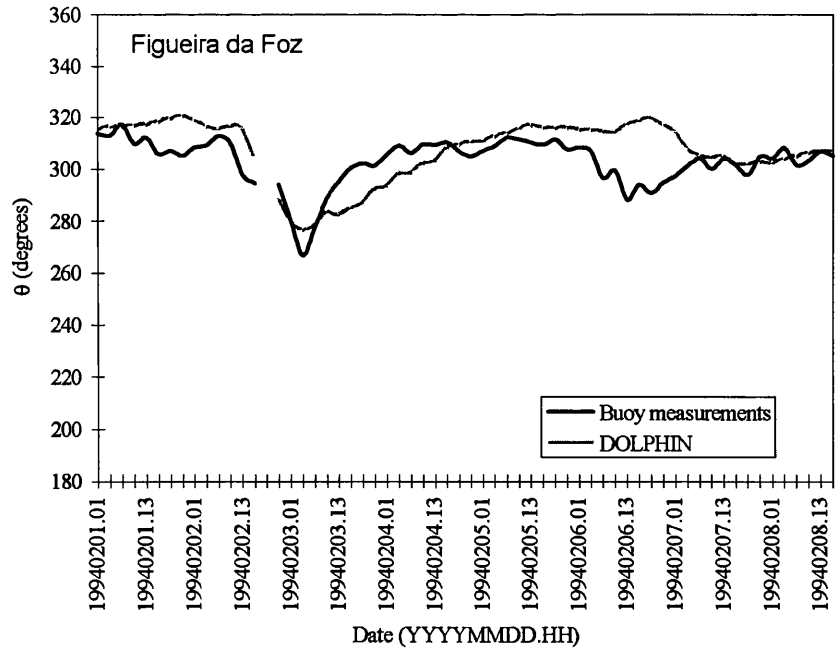

Figure 4.20 - Comparison of mean wave direction measurements with DOLPHIN results.

The DOLPHIN computations of the mean wave frequency reveal a large bias, overestimating the buoy measurements.

The mean wave direction computations show a good agreement with the measurements, except for the large bias on the 6th of February.

The root-mean square error and the scatter-index of the model computations for the two storms is summarized in Table *4.3*.

	H_S		f_m		θ	
	r.m.s. (m)	*S.I. (%)*	*r.m.s. (Hz)*	*S.I. (%)*	*r.m.s.(°)*	*S.I. (%)*
1st storm	1.3	26.32	0.026	28.94	8.46	2.89
2nd storm	1.21	26.61	0.026	31.48	10.46	3.41

Table 4.3 Root-mean-square error and scatter-index of DOLPHIN computations for both storms.

DOLPHIN gave worst results in the 2nd storm, just as WAM. This reinforces the conclusion that the deterioration of the results in the 2nd storm is due to higher errors in the input wind velocity fields.

The model runs were very fast, each storm taking around 11 minutes to perform all computations. The required disk space is less than 1 MB.

4.5 Comparison of the two models

The wave parameters obtained by WAM and DOLPHIN are compared with each other and the buoy measurements.

Figure *4.21* presents the comparison of results of significant wave height for the 1st storm. DOLPHIN shows better agreement than WAM.

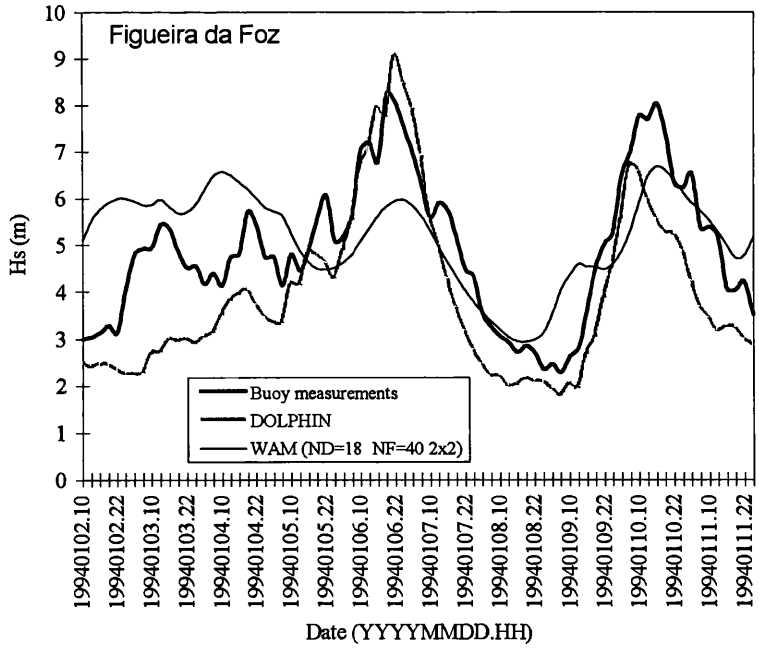

Figure 4.21 - Comparison of significant wave height measurements, DOLPHIN results and WAM results.

Figure 4.*22* gives the results for the mean wave frequency. DOLPHIN has a scatter-index twice as high that of WAM.

Both models show a good agreement with the measured mean wave direction, as shown in Figure *4.23*.

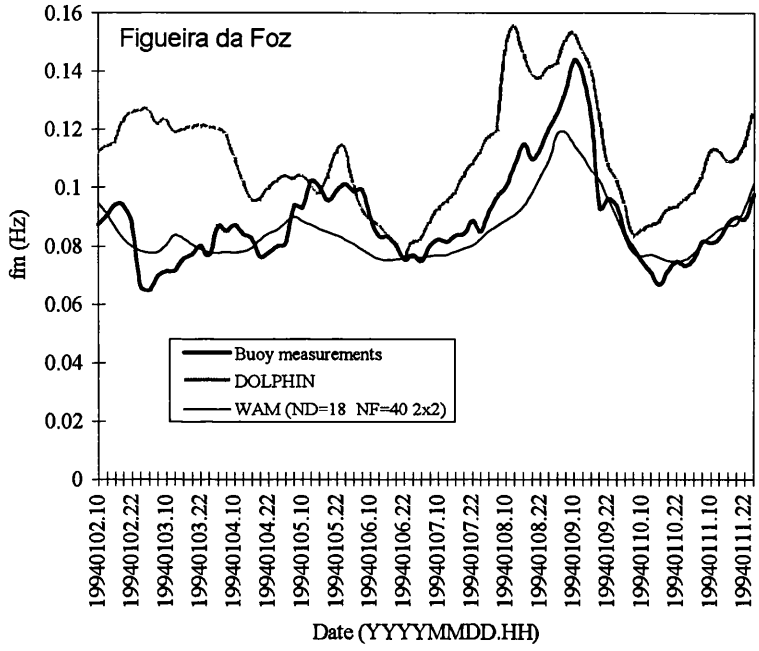

Figure 4.22 - Comparison of mean wave frequency measurements, DOLPHIN results and WAM results.

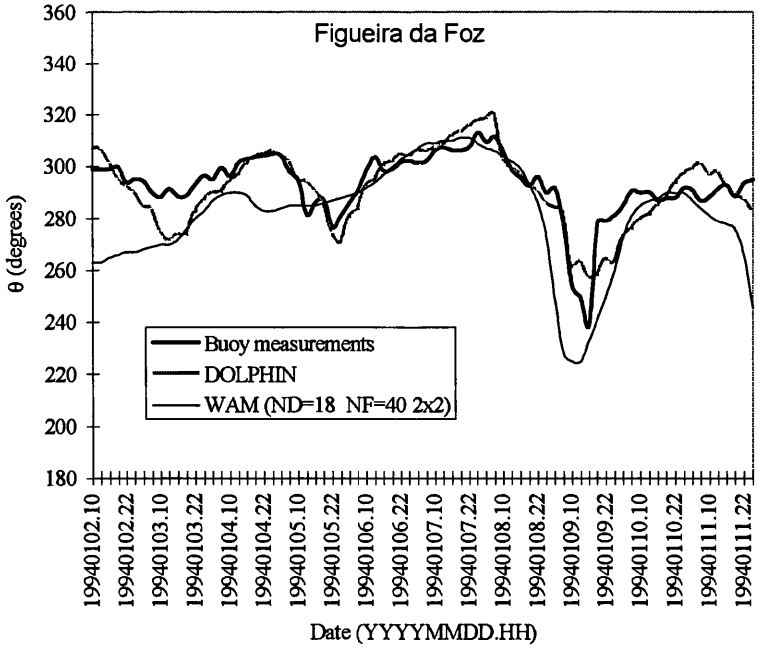

Figure 4.23 - Comparison of mean wave direction measurements, DOLPHIN results and WAM results.

For the 2nd storm, the comparison of model results and buoy measurements is given in figures *4.24*, *4.25* and *4.26*.

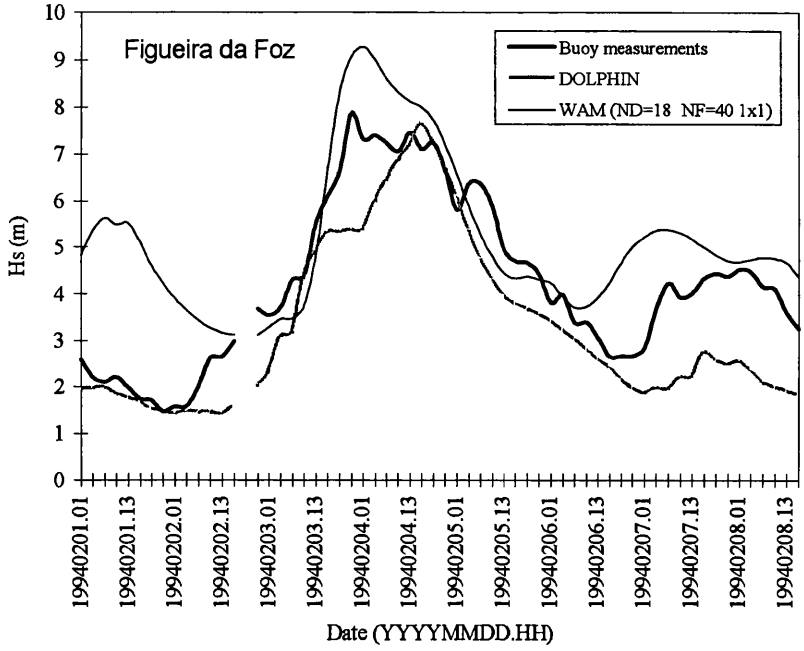

Figure 4.24 - Comparison of significant wave height measurements, DOLPHIN results and WAM results.

Both models show a relatively good agreement with the significant wave height observations. WAM underestimates the time series while DOLPHIN overestimates it.

The mean wave frequency time series computed by DOLPHIN is again worse than the WAM hindcast.

The DOLPHIN mean wave direction hindcasts show better agreement with measurements than those of WAM.

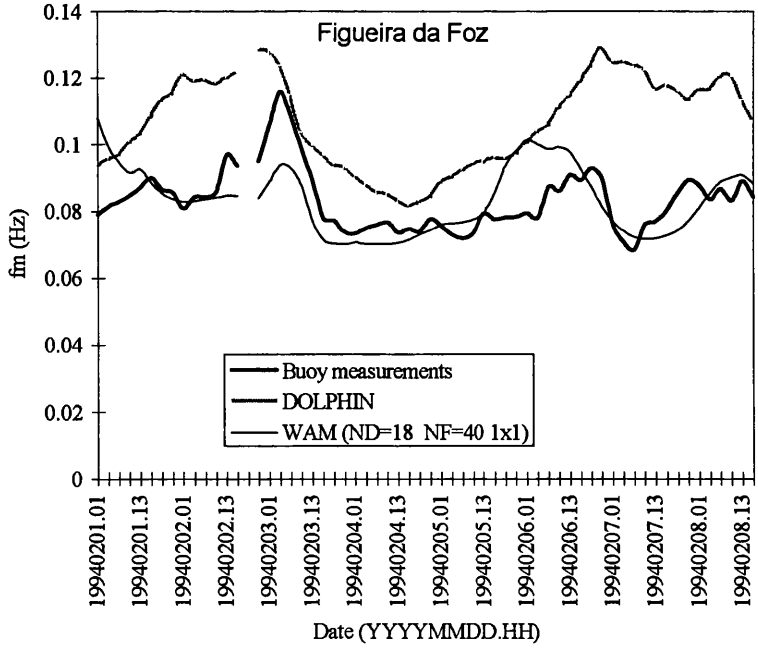

Figure 4.25 - Comparison of mean wave frequency measurements, DOLPHIN results and WAM results.

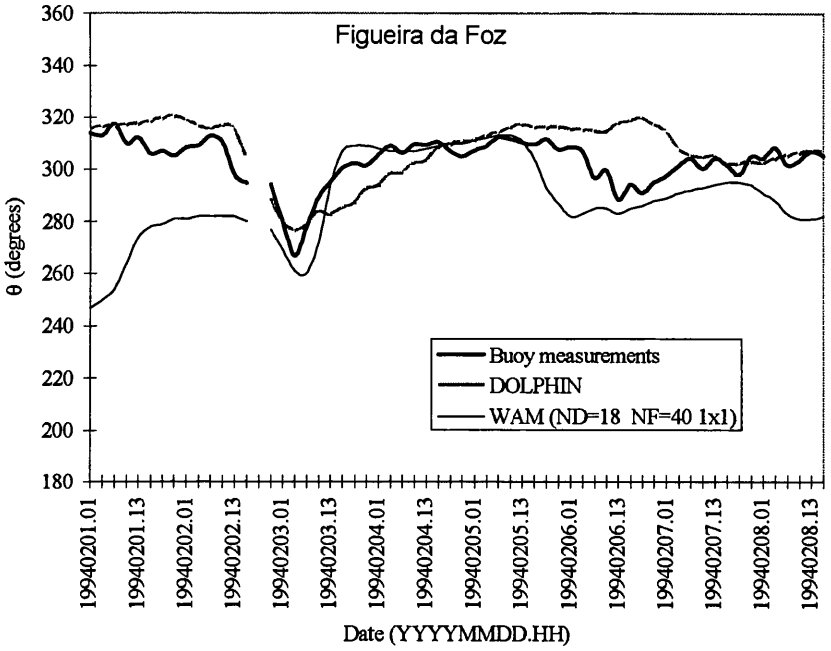

Figure 4.26 - Comparison of mean wave direction measurements, DOLPHIN results and WAM results.

As a conclusion, it may be said that DOLPHIN matches WAM as regards significant wave height hindcasts; that the mean wave frequency estimates obtained by DOLPHIN are by far worse than those of WAM; and that both models perform good mean wave direction computations.

Although the results of WAM are overall better, the required computing time is not feasible on a ship journey. As said at the beginning, sea state hindcasts onboard should be provided by a fast tool. This requirement is fulfilled by DOLPHIN.

Another advantage of DOLPHIN is the ray technique, which enables hindcasts at the required ship route locations, and not in the nearest grid point.

CHAPTER 5

Assimilation of Wave Observations

5.1 Introduction

The improved understanding of the physical process responsible for wind wave evolution has been incorporated in progressively more sophisticated models, thus improving model performance. However, the added computational expense of the more sophisticated models yields only a marginal increase in model performance. There are external parameters influencing model performance which will not be affected by refined physics. An example of this is the quality of the wind fields used to drive the wave model.

The model estimations can be improved using observations. The combination of using model results and observations to create an optimal estimate of the sea state is called data assimilation.

The previous chapter compared numerical results of DOLPHIN and WAM. It was concluded that although DOLPHIN results do not match WAM results, the lower computer effort leads us to choose DOLPHIN as the forecasting wave model onboard a ship.

This chapter explores the potentialities of assimilating DOLPHIN. The assimilated results will be shown to be more accurate than the WAM results, and still require less computational effort. These features indicate that the assimilation of DOLPHIN is feasible and effective.

5.2 Assimilation techniques

There are several data assimilation methods. All methods involve finding a solution that minimises some prescribed cost function, and differ mainly in their definition of the cost function, *i.e.*, the definition of the best, and in the different mathematical techniques used to determine the minimum of the cost function.

The cost functions are generally constructed from a subset of the following five basic penalty terms:

the misfit between observed and modelled data;

the deviation between the model data and some first-guess model values;

the difference between the optimally fitted control variables and some first-guess expectations of the most likely set of control variables;

a possible error incurred in satisfying the dynamical model equations with the chosen set of control variables and model state variables;

the difference between the modelled system state and the true state of the system.

The methods have been classified relatively to the cost function as

optimal interpolations;

direct least squares fitting;

adjoint model technique;

Green function method.

These assimilation techniques can be more generally divided into sequential techniques and *variational* techniques.

Sequential techniques use wave observations to correct the wind and waves at each time level of the model without regard for the previous states of the model, an example being the optimal interpolations technique.

Variational techniques take the dynamics of the model into account, and for that reason their effects are expected to be more persistent. The most advanced among them is the *adjoint technique*. This technique determines a very large number of local corrections: every single wind velocity vector in space and time is corrected (*e.g.* las Heras (1994)). The method requires a considerable computer capacity, and such detailed corrections in the wind fields are not very effective and sometimes redundant, because of the loss of wind details in the integrating effect of propagation, generation and dissipation, and also because the wind errors affecting the wave fields are highly correlated in time and space. A common error is in the time and space location of a storm, which affects several wind vectors.

In the following, we present a variational technique of wave assimilation which is consistent with the model dynamics, corrects the time-space wind fields and uses a relatively small number of corrections compared with conventional adjoint techniques.

In this method, the observed wave field is represented by a set of observed wave parameters, such as the significant wave height and the mean wave frequency. More parameters can be used without increasing the number of model runs, and therefore having negligible effect in the required computing time.

The assimilation technique minimises the difference between the modelled waves and the observed waves under certain constraints. The constraints express the confidence in the wave observations and the confidence in the control variables, which are quantified in a cost function J given by the sum of the misfit between the observed waves and the modelled waves, J^{χ}, and the difference between the best-fit control variables and their first-guess value, J^{Ψ}:

$$J = J^{\chi} + J^{\Psi} \tag{5.1}$$

The misfit J^{Y} between an optimal quantity Y^{o} and the computed or initial quantity Y is defined as

$$J^{Y} = \sum_{i,j} \left(Y_i^o - Y_i\right) M_{i,j}^{Y} \left(Y_j^o - Y_j\right), \tag{5.2}$$

or, in matrix notation,

$$J^{Y} = \left(\vec{Y}^0 - \vec{Y}\right)^T M^{Y} \left(\vec{Y}^0 - \vec{Y}\right) \tag{5.3}$$

where $M^{Y} = \left[M_{i,j}^{\chi}\right]$ is some suitably defined positive definite metric matrix; for a gaussian process it is equal to the inverse of the error covariance matrix.

The misfit between the observed wave parameters, χ_i^{obs}, and the modelled waves, χ_i, is given by

$$J^{\chi} = \sum_i \sigma_{\chi_i}^{-2} \left(\chi_i^{obs} - \chi_i\right)^2, \qquad 5.4$$

where $\sigma_{\chi_i}^2$ is the variance of the observed wave parameter χ_i. Comparing Equation *5.4* with Equation *5.3* we see that in the former only the main diagonal of the inverse error covariance matrix is considered.

The other term in Equation *5.1*, the difference between the best-fit control variables $\vec{\psi}$ and their first-guess value $\vec{\psi}^{fg}$, is

$$J^{\psi} = \sum_j \sigma_{\chi_i}^{-2} \left(\psi_j - \psi_j^{fg}\right)^2, \qquad 5.5$$

where $\sigma_{\psi_j}^2$ is the variance of the control variable ψ_j. Here, again only the main diagonal of the inverse covariance matrix is considered.

The cost function is minimised by finding the partial derivatives of the cost function relative to the control variables and setting them to zero,

$$\frac{\partial J}{\partial \psi_j} = 2\sum_i \sigma_{\chi_i}^{-2} \left(\chi_i^{obs} - \chi_i\right) \frac{\partial \chi_i}{\partial \psi_j} + 2\sum_j \sigma_{\psi_j}^{-2} \left(\psi_j - \psi_j^{fg}\right) = 0. \qquad 5.6$$

The following estimates are calculated on the basis of the first-guess wave field χ_i^{fg}:

$$\chi_i = \sum_j \left(\chi_i^{fg} + \frac{\partial \chi_i}{\partial \psi_j} \left(\psi_j - \psi_j^{fg}\right) \right), \qquad 5.7$$

with

$$\frac{\partial \chi_i}{\partial \psi_j} = \frac{\partial \chi_i^{fg}}{\partial \psi_j}. \qquad 5.8$$

The wave field is computed with the first guess wind field and the first-guess wave model, and once for each control variable with a perturbed value of 10% of its standard deviation.

The derivatives in Equation *5.6* are estimated using finite difference and the resulting system of linear equations is solved with a conventional matrix solver to obtain the optimum values of the control variables.

The control variables thus obtained are then used to correct the wind field and wave model. They are taken to be constant in time and space during the assimilation period and, contrary to other assimilation techniques, are extrapolated into the forecast.

The number of model runs with the wave model is equal to the number of control variables plus one (first guess plus each control variable variation). Therefore, the computing time is proportional to the number of control variables, and the technique is consequently efficient only when a limited number of control variables is considered. This

leads to the choice of integral control variables, which need only be in a small number because their optimisation improves the results to a large extent.

The above assimilation technique was developed by Holthujsen *et al.* (1996), who used significant wave height observations (made by the altimeter of the ERS-1 satellite and two Waverider buoys in the North Sea) to assimilate two storms that occurred in rapid succession in the Norwegian Sea. In this study, the control variables were chosen to be a N-S and a W-E shift in the location of the wind fields, a variation in the magnitude of all wind vectors, a common directional rotation of all wind vectors, and an increase in the dissipation coefficient. The assimilation period of five days provided a two days forecast. It was concluded that the buoy data and the satellite data are equally effective in improving the wave field at their respective locations, and that supplementing one data set with the other was not very effective.

The authors also speculated that satellite data tend to optimise the wind field and the resulting wave field on a large scale, although the buoy optimises the wave field and forecasts locally. For forecasting at a single space location, it was found better to assimilate buoy data at the forecasting point than satellite data, because the use of the latter along with buoy data did not improved the buoy forecasts relatively to the use of buoy data alone.

5.3 Assimilation in the Indian Ocean

This section presents an example of swell wave height[1] assimilation at a near-shore location (10 Km offshore) in Kerala, southern India.

A situation is considered in which some swell-sensitive field operations are being carried out at a point located some distance off the SW coast of India (near Kerala). In particular, predicting the crossing of the threshold level of 1 metre swell wave height is considered to be important. This is essentially swell forecasting at one point in the ocean. The purpose is to see to what extent the assimilation of buoy and/or satellite (SAR) data may improve the forecast. Additionally, we will also investigate whether the assimilation of a buoy located some distance upwave from the forecast point improves the forecast on the forecast point; this may be expected since the information of the upwave buoy precedes the waves that arrive at the forecast point. To investigate this, the buoy is moved 200 km upwave (*i.e.*, in the direction of Cape Town in South-Africa).

The forecast period in this case was extended to three days. This increase in one day relatively to the referred example in the North Sea makes sense, since swell comes from far away and an assimilating technique can improve its forecasts during longer periods than wind sea forecasts (wind sea was mainly the case in the above mentioned assimilated North Sea storm).

---

[1] Although the term 'swell' appears in this section, what is being assimilated is not exactly swell wave height but low frequency significant wave height. This is given by four times the square root of the integral of directional wave spectrum calculated only up to the frequency of 0.1 Hz. This 'low frequency significant wave height', is here called *swell wave height*, and we write it as

$$H_{swell} = 4\sqrt{m_{0.1}},$$

where $m_{0.1}$ is the variance of the wave components with frequencies below 0.1 Hz.

The 'measurements' used are simulated using DOLPHIN hindcasts with analysed wind fields from the European Centre of Medium Range Weather Forecast (ECMWF, Reading, England).

Three types of measurements are considered: simulated measurements in the near-shore buoy, simulated measurements in the off-shore buoy (200 Km Southwest of Kerala), and simulated satellite measurements.

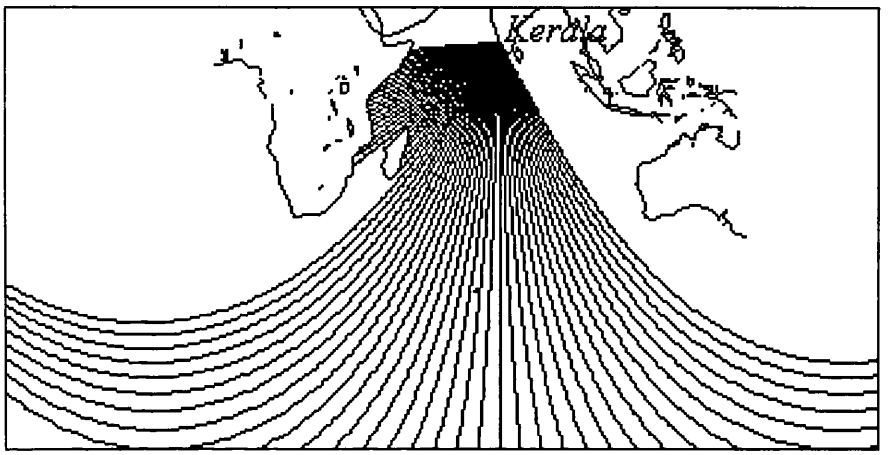

Figure 5.1 - Wave rays indicating great circles along which swell can propagate towards the near-shore buoy.

The buoy measurements were simulated every 6 hours for 5 days. The satellite measurements were simulated every 30 min for 15 days. There are approximately 6 satellite measurements a day, 88 for the 15 days. Only points of the satellite track that would influence the buoy forecasts were chosen. Points that were not covered by the rays leaving the near-shore buoy (Figure *5.1*) were not considered. The locations of the buoys and satellite points can be observed in Figure *5.2*. It should be noted that although all satellite points are represented the observations do not occur all in the same day (only 6 a day).

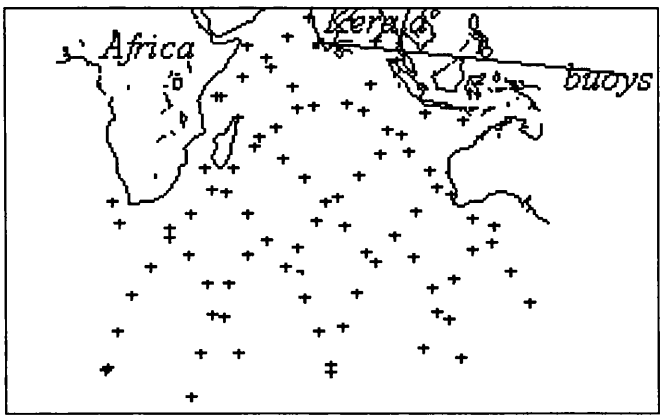

Figure 5.2 - Buoys(■) and satellite (+) locations.

The satellite simulated data is filtered because the assimilation of a large set of satellite data is not very effective with a wave ray model like DOLPHIN. The model computes forecasts at one time-space location each time. For a very large number of spatial points

sequentially distributed in time, the computations are less time consuming in a grid model.

It is standard in assimilation techniques to assume a 10% error in the buoy measurements and a 20% error in the satellite measurements. The same values were assume here.

The spin up period in this case is 15 days. This is because of the geometry of the problem: the wave rays for swell cover extremely long distances (Fig. *5.1*), and the swell arriving at the forecast point can be generated as far away as South-America, even though storms off South-Africa are more relevant.

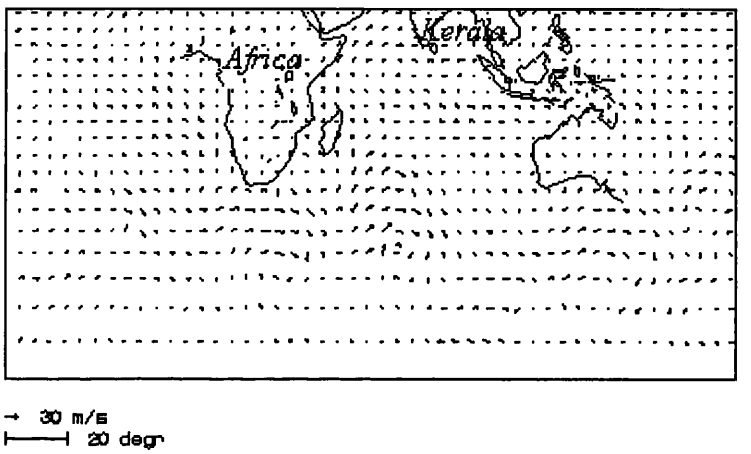

Figure 5.3 - Wind velocity fields on the 2-jul '95 at 12 a.m.

The period selected for hindcast comprises a storm that occurred near South-Africa in June 1995 producing high swell conditions off Kerala. Figure *5.3* shows the wind fields on the 2nd of July 1995 at 12 a.m., the date of the peak of the wind conditions, with wind velocities reaching 30 m/s. Looking at the rays shot from the buoy location (shown in Figure *5.1*), we see that such winds will influence the wave conditions in the forecast location.

The simulated inshore buoy measurements are shown in Figure *5.4*. The driven wind fields caused an increase in the swell wave height on the 7th of July, culminating in a peak of 1.1 m at 0 a.m. on the 9th.

The DOLPHIN computations were performed with the 12 and 24 hour forecast wind fields of ECMWF (*i.e.* the forecasts corresponding to 00:00 and 12:00, produced at 12:00 of the previous day). This is a relatively crude procedure, in that the 6, 12, 18 and 24 hour wind forecasts are normally available. But since the DOLPHIN forecasts with these wind fields turned out to be close to the simulated measurements, there was no point in including all the four in the calculations, so that only the 12 and 24 wind fields were chosen.

Five control variables were chosen for the assimilation: space and time shifts in the location of the wind field, a common correction on the magnitude, and a common rotation of all wind vectors. The space shift of the wind fields in the N-S and W-E direction had a standard deviation of two degrees, the time shift a standard deviation of 6 hours, the magnitude of the wind vectors of 100%, and the wind vectors clockwise

rotation of 10 degrees. No model control variables were included, since in this situation only the wind field is assimilated, and not the wave model.

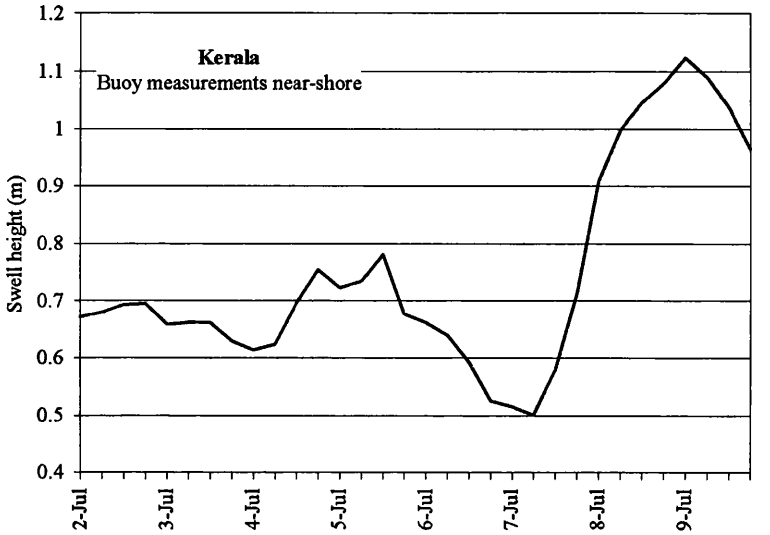

Figure 5.4 - Simulated buoy measurements in the near-shore buoy.

The effects of assimilating near-shore buoy measurements, offshore buoy measurements, or satellite measurements in the near-shore buoy hindcasts and forecasts are shown in Figure *5.5*. The crossing of the 1 m level was best forecast by the assimilation using the offshore buoy measurements.

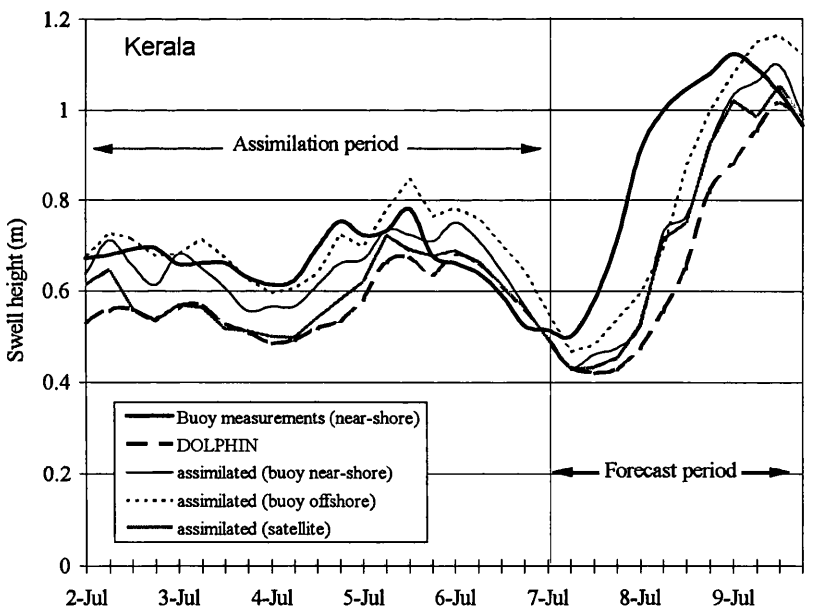

Figure 5.5 - Comparison of the assimilated DOLPHIN model, and DOLPHIN results with the buoy inshore measurements.

Table *5.1* gathers the scatter-index of the above assimilations, and also of an assimilation of satellite data along with near-shore buoy measurements.

During the hindcast period, DOLPHIN hindcasts in the near-shore buoy had a low scatter-index, which was improved with the assimilation of each of the measurements, in particular with near-shore buoy measurement.

The best forecasts in terms of scatter-index are those obtained by assimilating the offshore buoy. The assimilation of satellite measurements is not very efficient, even though the predictions improve if combined with the near-shore buoy measurements.

Buoy inshore scatter-index	Assimilation period	Forecast period
DOLPHIN	18.43	30.94
Assimilated (buoy near-shore)	8.77	21.99
Assimilated (buoy offshore)	9.89	19.25
Assimilated (satellite)	15.39	23.09
Assimilated (satellite+buoy near-shore)	14.12	21.47

Table 5.1 - Scatter-index of the DOLPHIN and assimilated results in Kerala.

5.4 Continuous assimilation in Figueira da Foz

Houlthuijsen *et. al.* (1996) show that the assimilation forecasts are effective in the case of two North Sea storms. According to the above example, assimilated swell forecasts using an upwave buoy are also effective. This section assesses the effectiveness of a *continuous* assimilation technique.

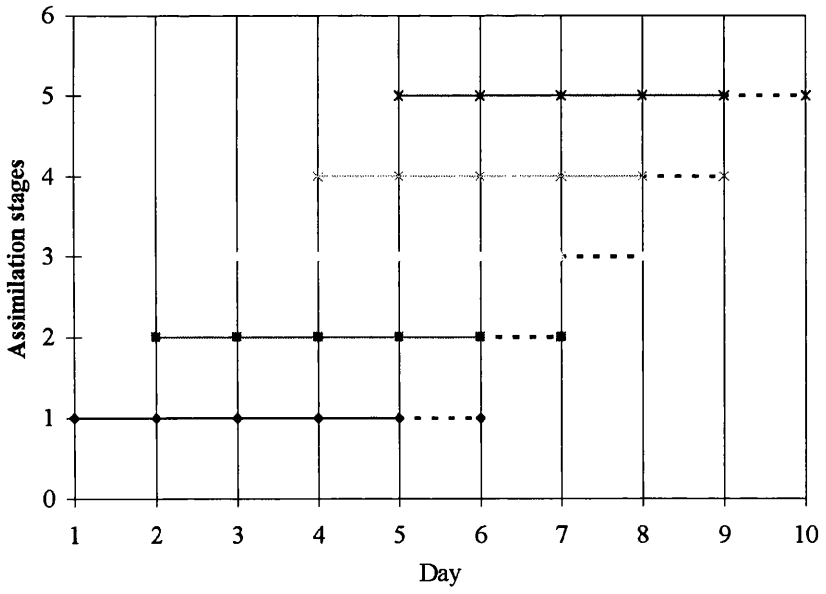

Figure 5.6 - Scheme of the continuous assimilation procedure.

When wave observations are provided daily, it is possible to daily feed the assimilation scheme, and only one day forecast is necessary. This is a context of continuous

assimilation which fits the problem of forecasting on board a ship. The following is an example of application of this method to the two storms considered in Chapter 5.

The significant wave height measurements are first assimilated during five days and forecasts are provided for the sixth day. When the observations of the sixth day become available, the first day is discarded and the hindcast frame is shifted forward. This is then repeated. The scheme of the assimilation stages are presented in Figure *5.6*.

The forecasts consist of 8 observations (daily measurements are taken three-hourly) and the quality of the forecasts is expected to decrease in later forecasts, but even these are suppose to be good in view of the good results achieved with the longer period forecasts of 2 and 3 days.

After some sensitivity analyses, the control variables were chosen to be two shifts in the wind fields (S-N, W-E), a common rotation to all wind vectors, a proportional variation of magnitude common to all wind vectors, and the wave model dissipation coefficient (Equation *5.8*).

The choice of these wind field control variables are justified by the fact that bad wave forecasts are mainly due to bad driven wind fields, in which these control variables represent common errors. The fifth control variable is included because dissipation is the less known term in the energy balance equation.

The standard deviations of the control variables are of one degree in the shift of locations, of 100% in the wind vectors magnitude and dissipation coefficient, and of 10 degrees in the rotation of the wind vectors.

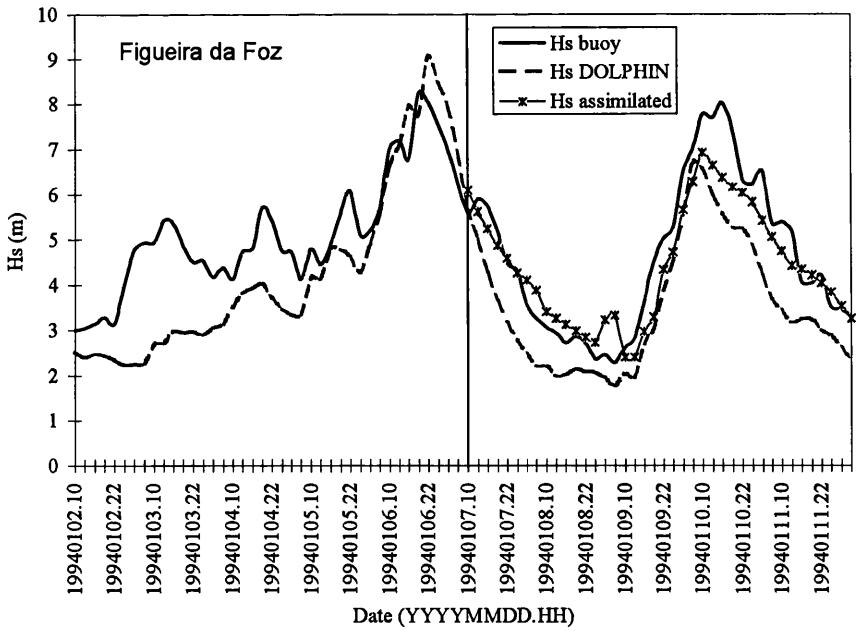

Figure 5.7 - Significant wave height measurements on the '1st storm' compared with DOLPHIN and assimilated DOLPHIN using H_S measurements.

For the '1st storm' presented in Section 4.3 the results are shown in Figure *5.7*. The period chosen in Chapter 5 for the hindcast of the storm covered almost 10 days. This period was now extended (with three extra observations) so that 10 full days could be considered.

The five initial days are used for the first assimilation period and therefore the assimilated forecasts are only provided from the 7th to the 12th of January.

The significant wave height forecast was highly improved, and the assimilated forecast shows a very small bias relatively to the observations (Figure *5.7*).

Recall that the DOLPHIN hindcasts of the mean wave frequency are not as good as the significant wave height ones relatively to the WAM results (presented in Chapter 4). We will now find out if assimilating the significant wave height improves the mean wave frequency forecasts. The results are presented in Figure *5.8*. It is seen that the improvements are not as substantial as in the case of significant wave height.

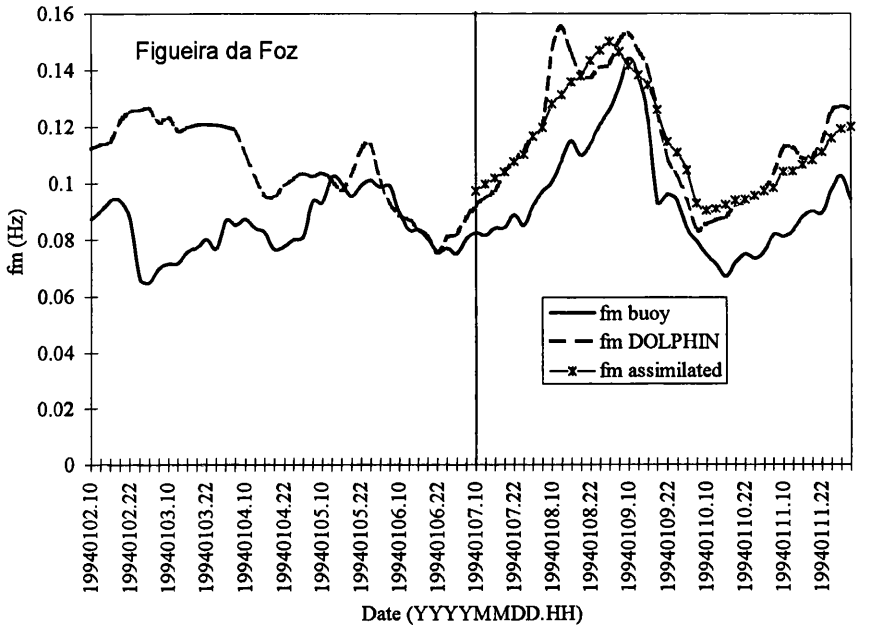

Figure 5.8 - Mean wave frequency measurements on the '1st storm' compared with DOLPHIN and assimilated DOLPHIN using H_S measurements.

The same scheme of assimilation was carried out for the '2nd storm'. In this case eight full days were considered which, because of the necessary initial five days, provide only three days of assimilation forecasts.

In this particular storm the significant wave height resulting from DOLPHIN computations alone had a high error, and as in the '1st storm' the assimilated forecast is much improved, as seen in Figure *5.9*.

For the mean wave frequency the results are shown in Figure *5.10*. The assimilation forecast improves DOLPHIN results only in the first two days; on the 8th of February the assimilated forecasts are almost coincident with the DOLPHIN forecasts.

The effect of assimilating the significant wave height on the mean wave frequency is in this case of dropping the scatter-index from 25% to 22%. Although the results improve, the improvement is not significant, and the quality of the results is below the WAM mean wave frequency hindcasts.

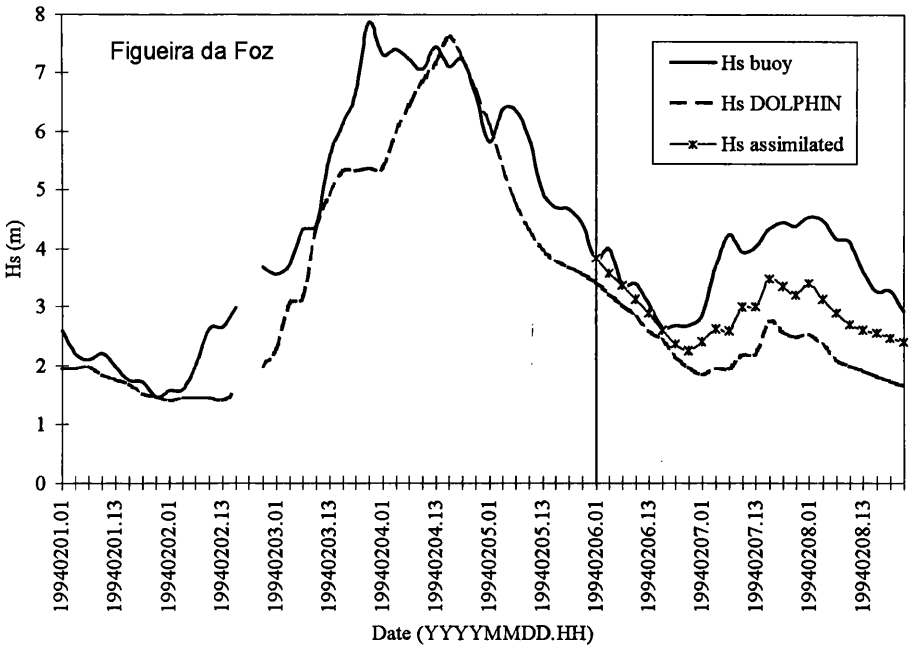

Figure 5.9 - Significant wave height measurements on the '2nd storm' compared with DOLPHIN and assimilated DOLPHIN using H_S measurements.

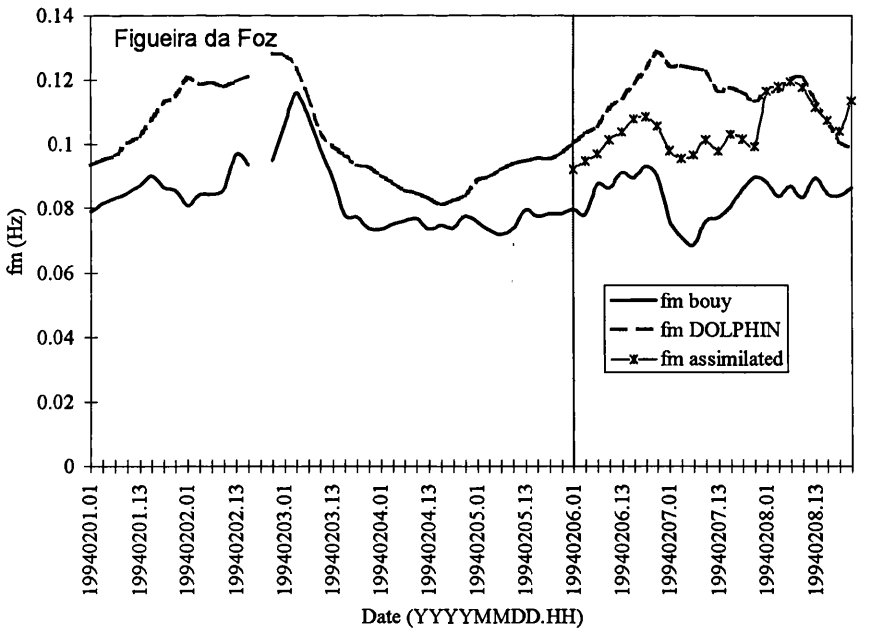

Figure 5.10 - Mean wave frequency measurements on the '2nd storm' compared with DOLPHIN and assimilated DOLPHIN using H_S measurements.

This led to the set up of an assimilation example where not only the significant wave height time series but also the mean wave frequency time series is assimilated. The results are shown for the '1st storm' in Figure *5.11* for the significant wave height, and in Figure *5.12* for the mean wave frequency. Figures *5.13* and *5.14* give the results for the '2nd storm'.

The results show significant improvements in the mean wave frequency forecasts. The forecast of the significant wave height was also significantly improved, with less than 1% increase in the scatter-index as compared with the case of assimilating the significant wave height alone.

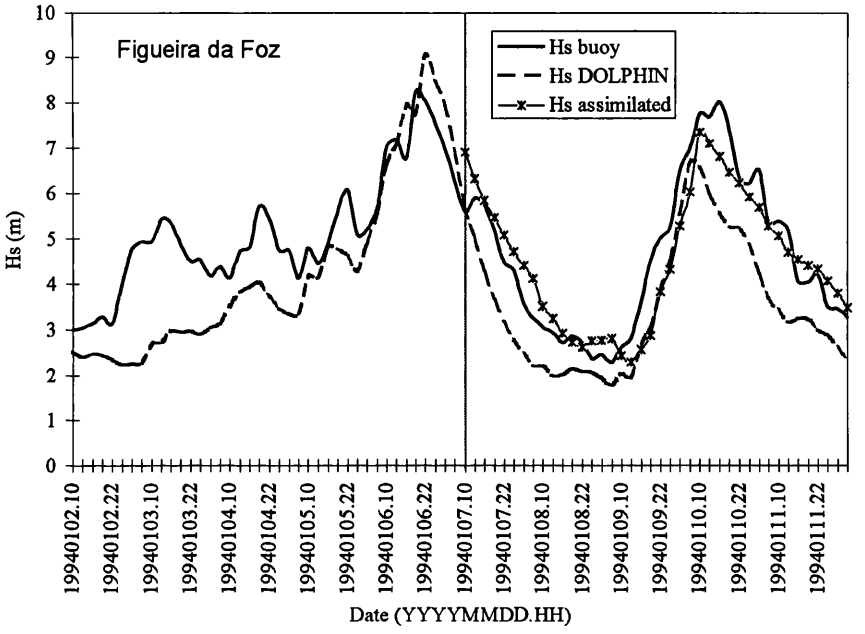

Figure 5.11 - Significant wave height measurements on the '1st storm' compared with DOLPHIN and assimilated DOLPHIN using ($H_S + f_m$) measurements.

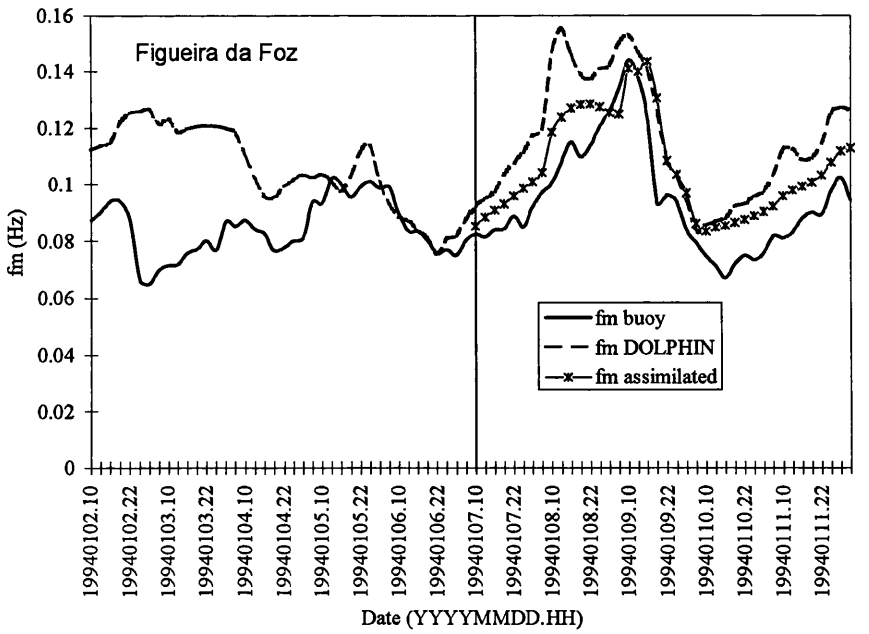

Figure 5.12 - Mean wave frequency measurements on the '1st storm' compared with DOLPHIN and assimilated DOLPHIN using ($H_S + f_m$) measurements.

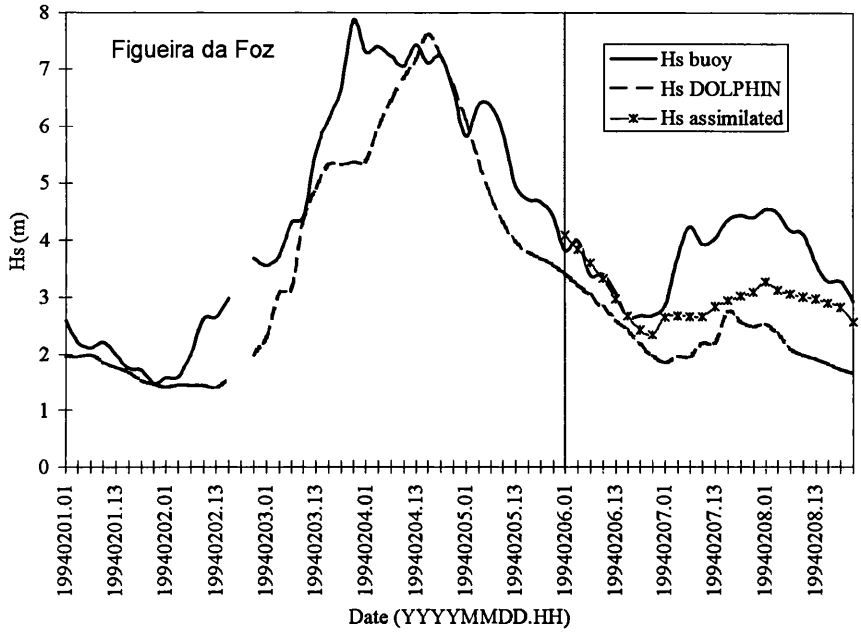

Figure 5.13 - Significant wave height measurements on the '2nd storm' compared with DOLPHIN and assimilated DOLPHIN using ($H_S + f_m$) measurements.

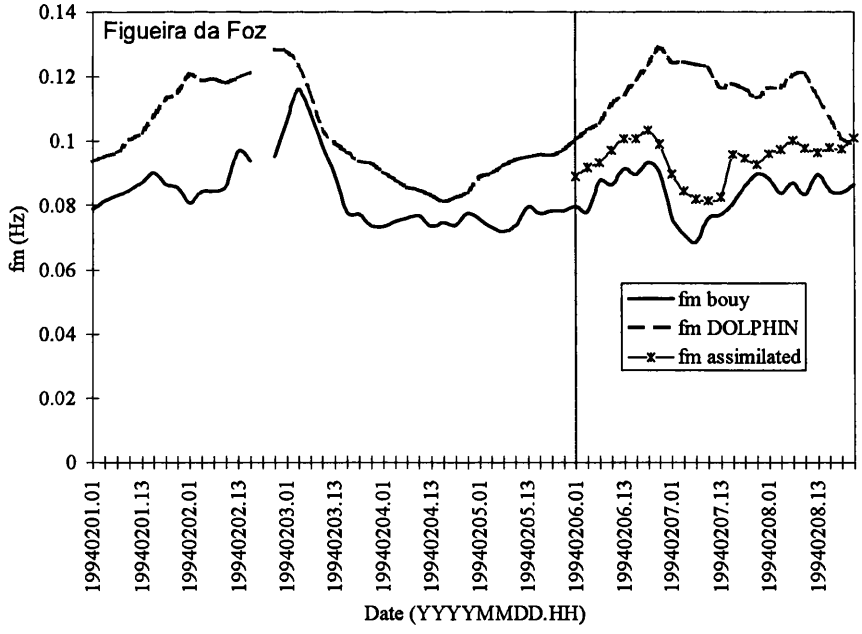

Figure 5.14 - Mean wave frequency measurements on the '2nd storm' compared with DOLPHIN and assimilated DOLPHIN using ($H_S + f_m$) measurements.

The scatter index of all these continuous assimilation examples are presented in Table *5.2*. The assimilation of the buoy measurements was more efficient on the '2nd storm' than on the '1st storm' (higher decrease on the scatter-index). This can be used to confirm the speculation of Chapter 5 that the worst model hindcasts in the '2nd storm' were due to higher errors in the driving wind field.

The assimilation of significant wave height with mean wave frequency measurements is efficient and the addition of mean wave frequency measurements in the assimilation did not increase the computational time.

	1st storm 7-12 Jan '94		2nd storm 6-8 Feb '94	
	H_S	f_m	H_S	f_m
DOLPHIN	27.08	24.64	41.77	40.66
assimilated (using H_S)	14.11	22.29	24.82	27.18
assimilated (using H_S and f_m)	14.94	14.30	25.11	13.54

Table 5.2 - Scatter-index for the continuous assimilation examples.

5.5 Conclusions

The results of this study indicate that an assimilation based only on a few integral control variables is effective. It is possible that a few more integral control variables could somewhat improve the results. But further increasing the number of control variables would make the finite difference technique of the assimilation process inefficient.

The data used in the present study were observations (real or simulated) of significant wave height, swell wave height and mean wave frequency. Since the technique is independent of the type of observation, other wave parameters, such as the mean wave direction, could have been used. In fact, the entire observed spectrum (one-dimensional or two-dimensional) can be used.

In agreement with the already mentioned published example of assimilation of satellite and buoy measurements of significant wave height in the North Sea, the swell assimilation example in the Indian Ocean (Section 5.3) suggests that satellite measurements are not effectively assimilated. On the other hand, the same example has shown that the assimilation upwave of the desired location is efficient.

Finally, the example of operational (continuous) assimilation scheme in Section 5.4 revealed an overall improvement in the forecasts, and the assimilation of mean wave frequency measurements together with significant wave height measurements was shown to improve significantly the forecast of the two parameters.

Regarding our final objective, the BOWFOR methodology, the conclusions of this section are twofold.

Firstly, the effectiveness of assimilating upwave measurements anticipates an efficient wave assimilated forecast at least for ship routes where the assimilated locations are upwave of the forecasting ones.

Secondly, the assimilated forecasts can be carried out easily and rapidly on a personal computer, and are shown to be even more accurate than those provided by WAM, being thus ideal for onboard forecasting.

CHAPTER 6

The BOWFOR Methodology

6.1 Introduction

The Onboard Wave Forecast BOWFOR methodology is presented and tested with two practical applications in this chapter.

The BOWFOR methodology provides wave forecasts along a ship route using the assimilated DOLPHIN wave model. The methodology is designed to be used onboard ships by a technician 'feeding' it with visual observations of the wave parameters, or with additional available observations of wave parameters provided by buoys, satellite and other ships. The observed wave parameters are corrections of the visual observations by established empirical relations between spectral parameters and the corresponding visual estimates, such as those provided by Nordenstroem (1973) and Guedes Soares (1986).

In the present applications the assimilated wave parameters are the significant wave height and mean wave frequency. Since the technique is independent of the type of observation, other wave parameters, such as the mean wave direction, could also be used. In fact, even the entire two-dimensional spectrum observed could be used; the reason why it is not is because it would be difficult for a ship to measure the wave spectrum, and because its knowledge is not an imperative information onboard. The use of these parameters was already justified on the previous chapters.

The input wind fields are assumed to be forecasts for the trip period, provided at the ship's departure. The assimilations can be performed along a ship route or at a fixed location or locations.

Given the forecasts, possibly over several routes, the captain can choose the most convenient route.

The wave model is only valid for deep water conditions. When the ship is in water of finite depth, *e.g.*, in the entrance of an harbour, the spectrum and the spectral parameters can be obtained by the procedure suggested in Guedes Soares and Caires (1995). From the deep water wave spectrum or spectral parameters, the finite depth wave spectrum is computed taking into account the saturation process, shoaling and refraction. The saturation process is introduced using Kitaigorodskii self similarity shape hypotheses (Kitaigorodskii et al. (1975)) to derive the finite depth wave spectrum once the deep water spectral shape is established. The shoaling and refraction effects are based on the linear wave theory. Using a refraction algorithm, the wave rays are traced and the form of the spectrum is established along the wave ortogonals, taking into account the saturation of the spectra, as well as refraction and shoaling.

6.2 Practical Applications

The examples analysed here consist of two ship journeys: a trip from Europe to North America, and the return.

The wave measurements and wind fields used for the journeys are based on synthetic data. This synthetic data consists of simulated observations provided by DOLPHIN using ECMWF analysed wind fields plus a correction coefficient, and of deviated wind fields used for the DOLPHIN first guess forecast. These first guess values are to be corrected using the BOWFOR.

To simulate a first guess wind field, the ECMWF wind fields were perturbed with fairly arbitrary but otherwise realistic errors. The wind fields were shifted over a distance of 0.5° to the East and over a distance of 0.5° to the North, and time was shifted by 3 hours. Moreover, all wind vectors were increased by 10% and a random, gaussian variation of 10% standard deviation added. Also, all wind directions were rotated 15° (*i.e.*, clockwise) and a random, gaussian variation of 30° standard deviation was added.

The wave 'observations' were simulated with the analysed wind fields from the ECMWF. The errors of this simulated series relative to the results obtained with the first guess wind fields will only be due to wind field errors. In order to introduce also wave model errors between the 'observation' and the first guess (DOLPHIN) hindcasts, the final observations are obtained from the previous series (simulated with analysed wind fields) plus a constant defined so that the difference between the mean value of the observations and Dolphin results was of *1 m* for significant wave height and *-0.02 Hz* for mean wave frequency. This difference between means is similar to that obtained in the two storms studied in Chapter 4.

If $H_{s_i}^{P}$ denote the significant wave height preliminary observations simulated with DOLPHIN from the analysed wind fields, and $H_{s_i}^{DOL}$ denote the significant wave height DOLPHIN hindcasts obtained with the perturbed wind fields (first guess wind fields), the significant wave height 'observations', $H_{s_i}^{obs}$, are given by

$$H_{s_i}^{obs} = 1 + \left(average\left(H_{s_i}^{DOL}\right) - average\left(H_{s_i}^{P}\right)\right). \qquad 6.1$$

Similarly, for the mean wave frequency 'observations', $f_{m_i}^{obs}$,

$$f_{m_i}^{obs} = -0.02 + \left(average\left(f_{m_i}^{DOL}\right) - average\left(f_{m_i}^{P}\right)\right). \qquad 6.2$$

Two journeys' wave forecasts by BOWFOR are simulated in this chapter. One of the journeys is from Ternuezen to Botwood, and the other from 47.5N 59.3W to Birkenhead. The ship route locations were provided every 6 hours by Oceanroutes. The information provided can the consulted in Appendix C. These routes are of a general cargo ship. For the cross of the Atlantic ocean towards West the vessel took 18 days, and for the cross towards Europe 12 days. The first trip was longer because of the worst weather conditions.

The ship route six hourly locations corresponding to the first trip can be seen in Figure *6.1*, with 0 a.m. of each day marked by the day number. The trip begun at 2:00 a.m. on the 25 Dec '93 and terminated at 11:40 p.m. on the 12 Jan '94. The ship went through the severe wave conditions felt on the '1st storm' at Figueira da Foz analysed in Chapter 4, of which the wind fields are shown on Appendix A.

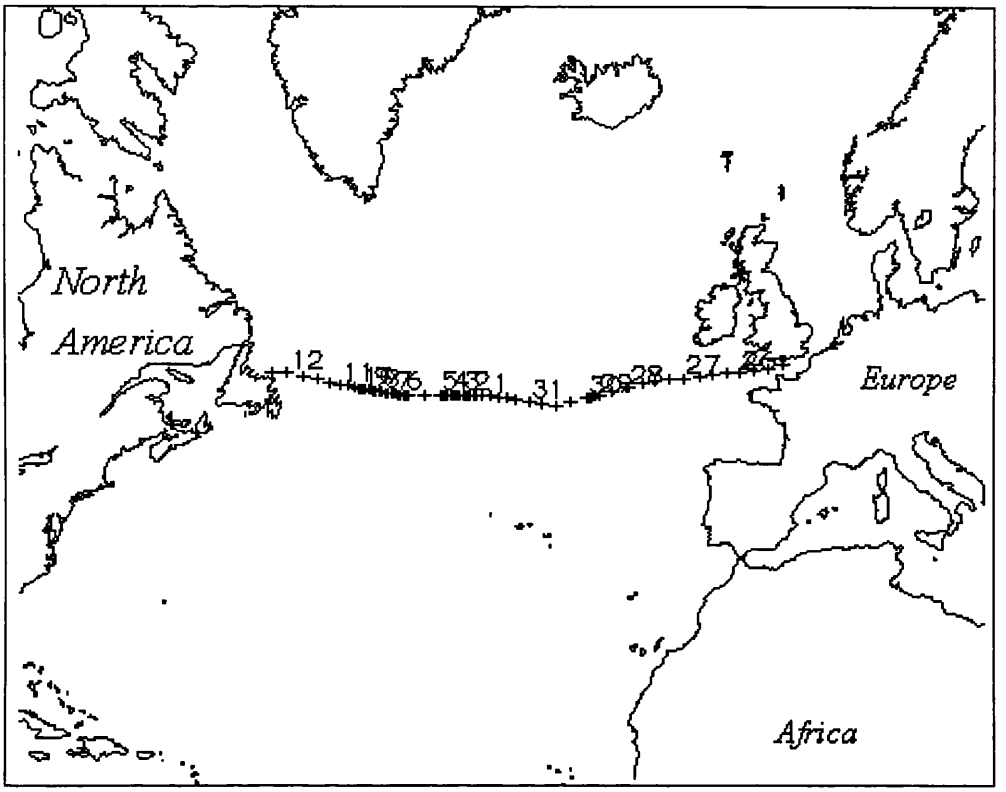

Figure 6.1 - Route location every 6 hours from Ternuezen to Botwood.

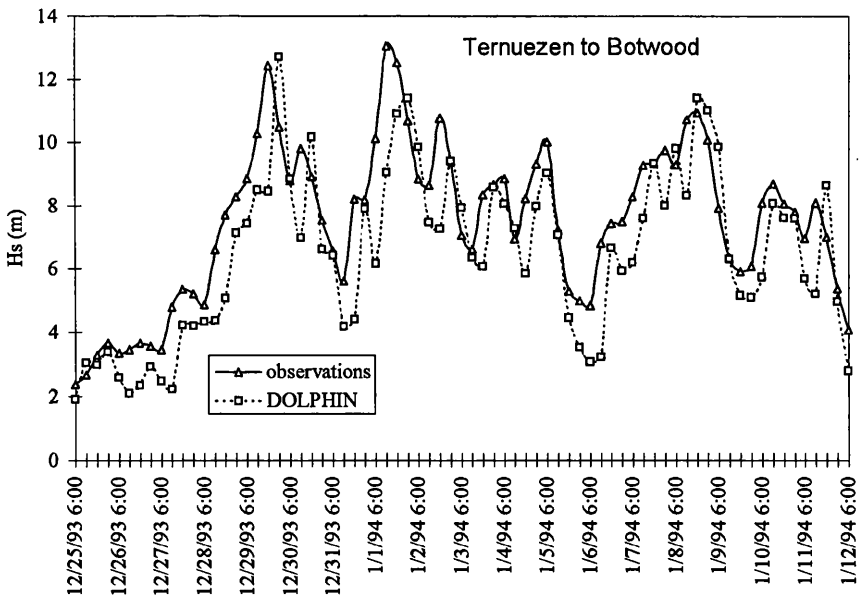

Figure 6.2 - Comparison between the simulated observations of the significant wave height and the DOLPHIN results for the journey from Ternuezen to Botwood.

The six hourly simulated 'observations' and the Dolphin results provided by the first guess deviated wind fields are presented in Figure *6.2* for the significant wave height and in Figure *6.3* for the mean wave frequency.

The significant wave height crosses the 12 meters threshold on the 29th of December and on the 1st of January. The scatter-index between 'observations' and DOLPHIN results is of 23%.

The scatter-index between the mean wave frequency 'observations' and DOLPHIN results is of 24%.

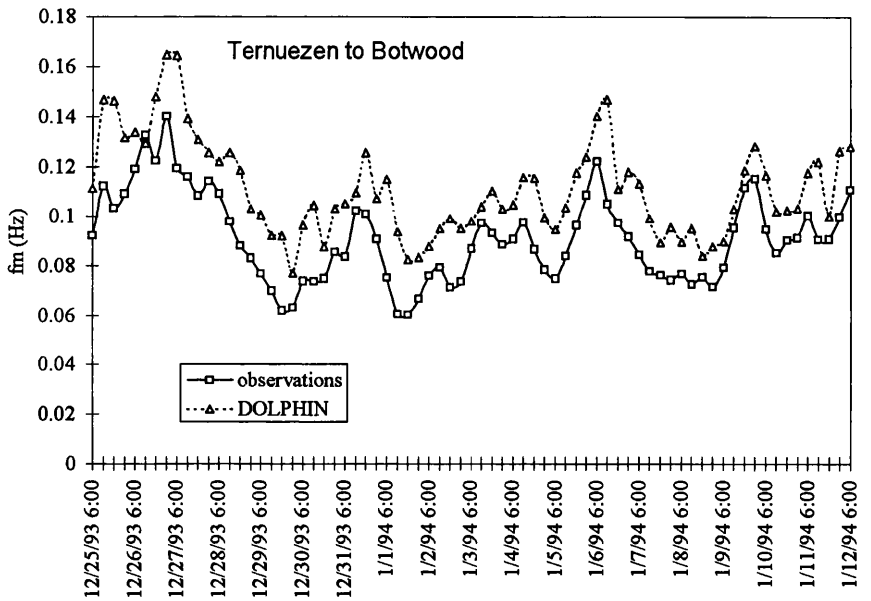

Figure 6.3 - Comparison between the simulated observations of the mean wave frequency height and the DOLPHIN results for the journey from Ternuezen to Botwood.

A BOWFOR continuous assimilation scheme like the one presented in Chapter 5 (Figure *5.6*) was used, but in this case two days, instead of one day, forecasts were made.

The ship observations are assimilated for 5 days (4 observations per day) and a two days forecast is produced. Next, the assimilation period is shifted two days and another two days forecast given. And so during all the trip.

The initial five days of assimilation are the first five days at sea, so that the forecasts can only be made from 30 Dec '93 to 11 Dec '94.

Operationally, the captain does not have to wait for five days before carrying out the first forecasts. The initial assimilations may be done with observations previously obtained by satellites, buoys or other ships.

Also, the assimilation does not have to be restricted to the 4 daily ship observations. More observations obtained in the ship, or from satellites, buoys or other ships, may also be added.

The forecast period can of course be less than two days. The choices made in these tests correspond to the most critical case, and therefore better results are expected if the number of observations of any source is increased and the period of forecast decreased.

The results of the BOWFOR method for this trip using continuous assimilation are presented in Figure *6.4* for the significant wave height. The predictions are accurate in spite of the over-prediction in the initial significant wave height peaks. It can be concluded from Figure *6.4* that the reliability of the method is high on a ship route even with this small number of observations.

Figure 6.5 compares the ship 'observations' with the DOLPHIN and BOWFOR results. Again here the forecasts provided by BOWFOR are better than those of DOLPHIN.

The estimates do not necessarily deteriorate as the end of the 2-day forecast period is approached. Thus in Figure *6.4* and Figure *6.5* the predictions in the 0h of every odd day (1,3,5,7,9 and 11), which correspond to a 48 hours forecast, are clearly compatible with all the previous estimates.

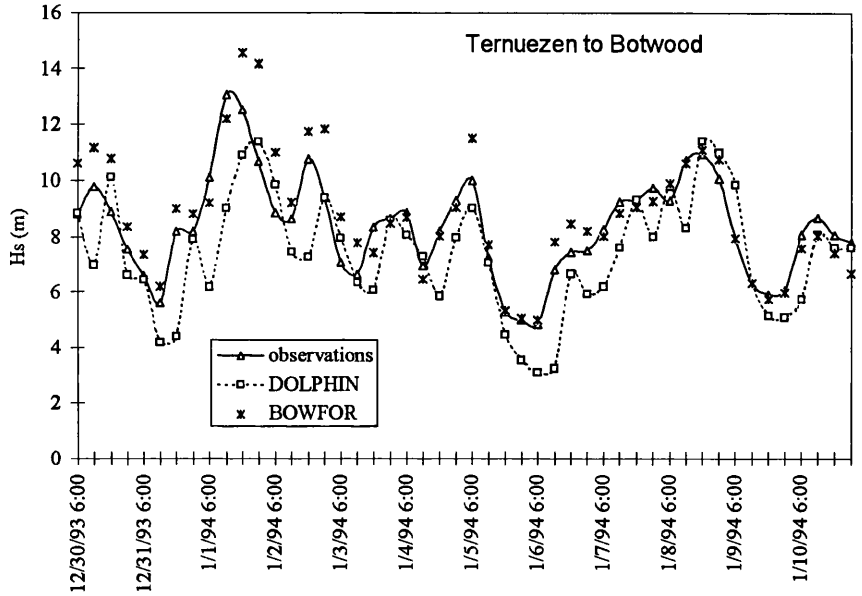

Figure 6.4 - Comparison between the simulated significant wave height observations and the DOLPHIN and BOWFOR results for the journey from Ternuezen to Botwood.

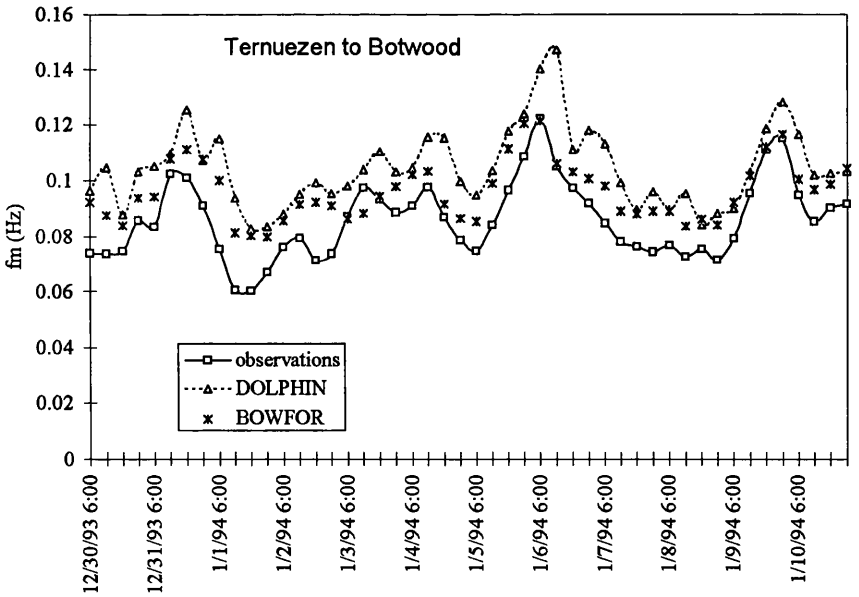

Figure 6.5 - Comparison between the simulated the mean wave frequency observations and the DOLPHIN and BOWFOR results for the journey from Ternuezen to Botwood.

Table *6.1* compares the scatter-index and root-mean-square error of the DOLPHIN and BOWFOR estimates relatively to the ship 'observations'. The scatter-index provided by BOWFOR is of 14% for the significant wave height, and of 15% for the mean wave frequency. These are very good results for wave forecasts.

	H_s			f_m		
	S.I (%)	*r.m.s* (m)	*bias* (m)	S.I (%)	*r.m.s* (Hz)	*bias* (Hz)
DOLPHIN	21.3	1.83	0.98	25.7	0.022	-0.019
BOWFOR	13.6	1.17	-0.44	15.0	0.0126	-0.010

Table 6.1 - Scatter-index, root-mean-square error and bias of DOLPHIN and BOWFOR relatively to the 'observations' for the journey from Ternuezen to Botwood.

The *bias* of the estimates is also given in Table *6.1*. This is defined by

$$bias = \frac{1}{n}\sum_{i=1}^{n}\left(\chi_i^{obs} - \chi_i\right), \qquad 6.3$$

where χ^{obs} is the observed parameter and χ the estimated parameter. The bias is a useful measure for detecting systematic over- or under-estimates.

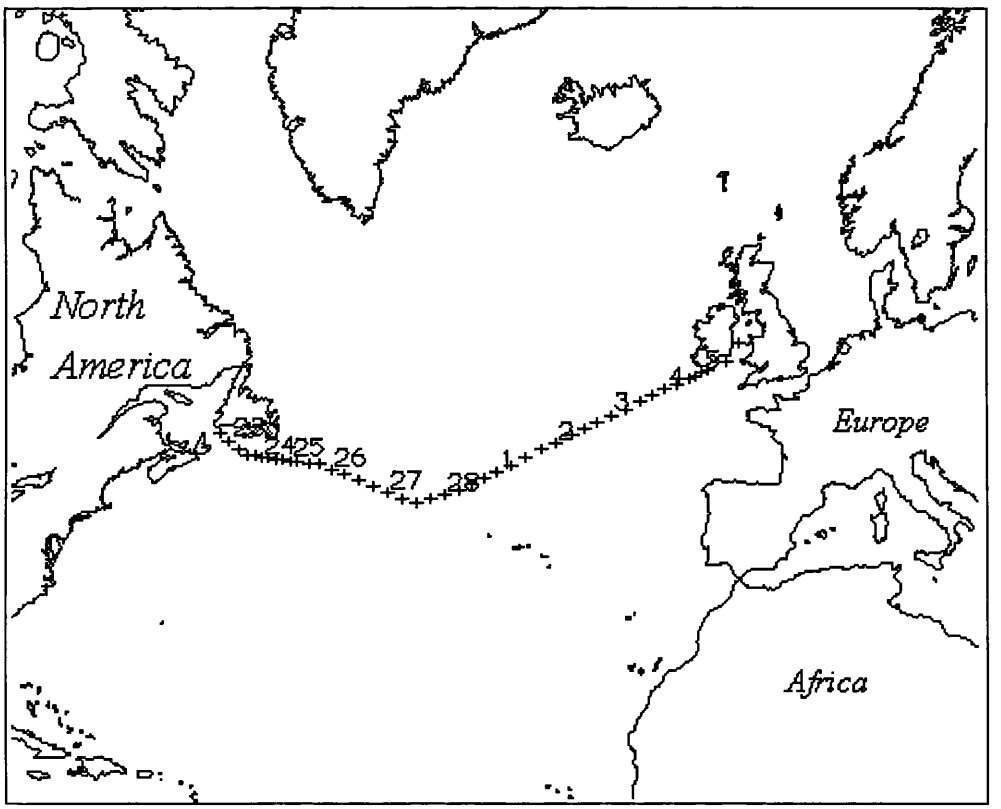

Figure 6.6 - Route location every 6 hours from 47.5N 59.3W to Birkenhead.

As seen by the previous DOLPHIN computations in Chapter 4 and Chapter 5, the model generally underestimates the significant wave height and overestimates the mean wave frequency. The results in Table *6.1* suggest that the BOWFOR method can reduce these biases. This aspect will also be examined when analysing the results of the return trip.

We now proceed with the application of the method to the trip crossing the Atlantic Ocean towards East. The 6-hourly ship route locations are presented in Figure *6.6* with 0 a.m. of each day marked with the day number.

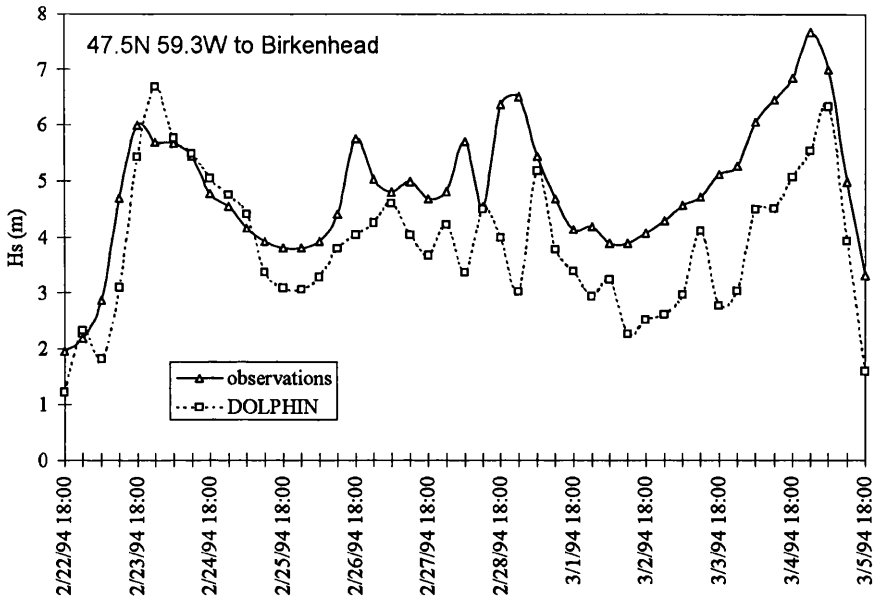

Figure 6.7 - Comparison between the simulated observations of the significant wave height and the DOLPHIN results for the journey from 47.5N, 59.3W to Birkenhead.

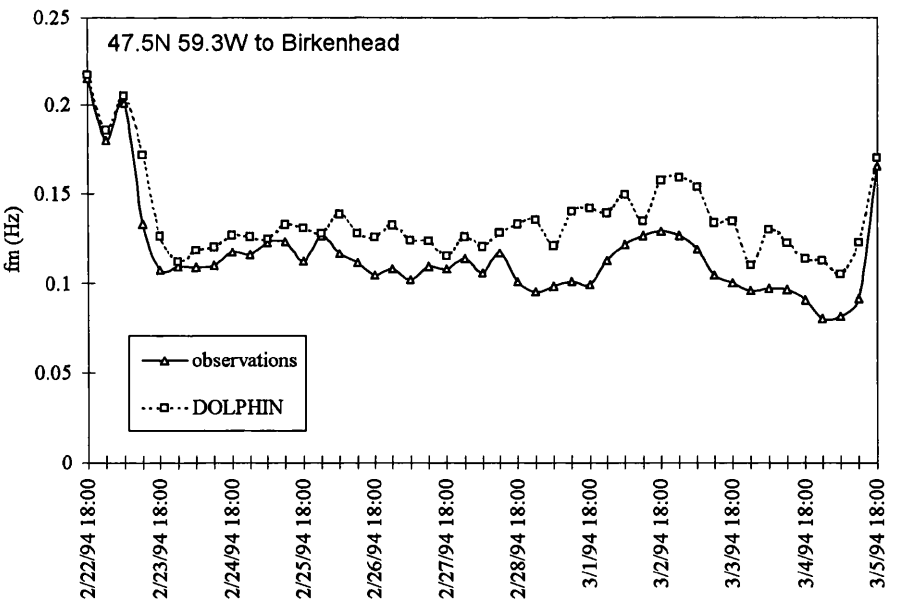

Figure 6.8 - Comparison between the simulated observations of the mean wave frequency and the DOLPHIN for the journey from 47.5N, 59.3W to Birkenhead.

The ship observations and DOLPHIN results are presented in Figure *6.7* for the significant wave height and in Figure *6.8* for the mean wave frequency. The significant wave height estimates have a scatter-index of 28%, and the mean wave frequency estimates a scatter-index of 20%.

For the assimilation period (basically the period of the journey minus 5 days) the scatter index of the DOLPHIN computations is of 32% for the significant wave height and of 27% for the mean wave frequency. These are quite large scatter indexes, and it will be interesting to see how the BOWFOR method can reduce them.

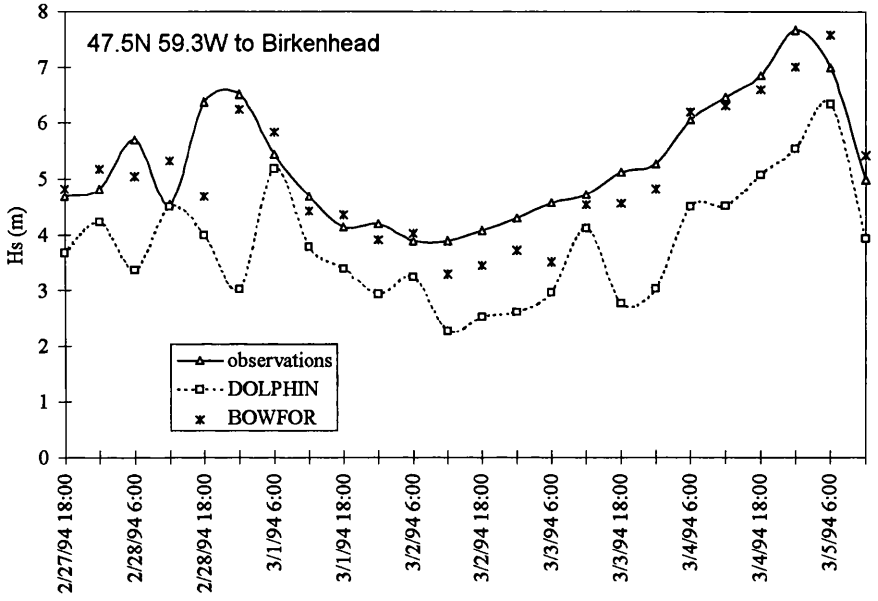

Figure 6.9 - Comparison between the simulated significant wave height observations and the DOLPHIN and BOWFOR results for the journey from 47.5N, 59.3W to Birkenhead.

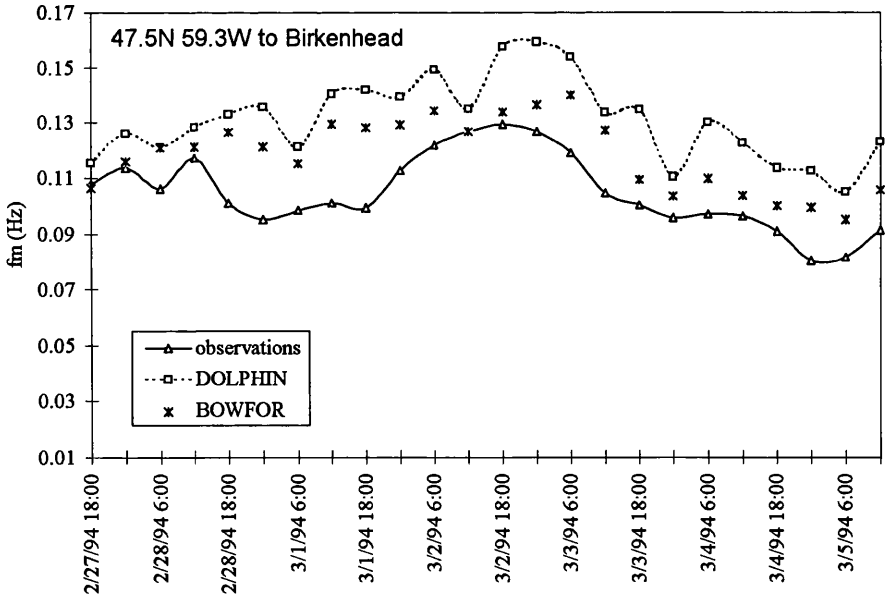

Figure 6.10 - Comparison between the simulated mean wave frequency observations and the DOLPHIN and BOWFOR results for the journey from 47.5N, 59.3W to Birkenhead.

The comparison between the DOLPHIN and BOWFOR results and the significant wave height 'observations' is shown in Figure *6.9*. The BOWFOR forecasts are better, and

have very small bias; the root-mean-square error is of 0.6m, which is an excellent result for wave height forecasts.

As seen from Figure *6.10*, the mean wave frequency BOWFOR forecasts are also encouraging.

The results are gathered in Table *6.2* in terms of the scatter-index, root-mean-square error and bias relatively to the observations.

Regarding bias, the DOLPHIN results again underestimate the significant wave height and overestimate the mean wave frequency, and in both cases the BOWFOR method reduced these biases.

	H_s			f_m		
	S.I (%)	*r.m.s* (m)	*bias* (m)	S.I (%)	*r.m.s* (Hz)	*bias* (Hz)
DOLPHIN	32.0	1.68	1.44	27.4	0.027	-0.026
BOWFOR	11.4	0.6	0.21	15.7	0.016	-0.014

Table 6.2 - Scatter-index, root-mean-square error and bias of the DOLPHIN and BOWFOR estimates relatively to the 'observations' for the journey from 47.5N, 59.3W to Birkenhead.

Comparing the BOWFOR results in Table *6.1* and Table *6.2*, one concludes that the method was more efficient during the journey from North America towards Europe than in the journey towards West. This is justified by the fact that depressions move from West to East, and that consequently the ship was running with swell, thus allowing the anticipation of the swell to be experienced further on in the journey.

Overall, the BOWFOR methodology provided very good results in both applications. The results show that the method can be fruitfully used onboard vessels.

CHAPTER 7

Achievements, Conclusions and Possible Extensions

The thesis was devoted to the set up of a forecast methodology that would provide accurate wave forecasts on board ships using a personal computer - the BOWFOR methodology.

The essentials of wave theory were given, and the evolution of wave models was outlined.

The WAM and DOLPHIN wave models were compared as possible choices for the computations required by BOWFOR.

Both models were run on a personal computer, and comparisons between the models' hindcast wave parameters, required computational time and disk space were made using data from two storms that occurred in Figueira da Foz, Portugal. The significant wave height hindcasts were shown to be reasonable, and of similar quality, with both models. The scatter-index was in both models of approximately 26%, and the root-mean-square error of around 1.3 m. The mean wave frequency WAM hindcasts were clearly superior to those of DOLPHIN, as expected by the better representation of the two-dimensional spectrum itself, inherent to third generation wave models. The DOLPHIN hindcasts had a root-mean-square error of around 0.026 Hz while with WAM this error was of around 0.01 Hz, less than half the DOLPHIN hindcast error. The mean wave direction was accurately hindcast by both models. The WAM computations were revealed to be very expensive in computational time and required disk space, and the model was consequently found less satisfactory for the purposes of BOWFOR. In the less expensive of the WAM runs, it took 4 hours to hindcast a storm for which DOLPHIN provided hindcasts in 11 minutes. The DOLPHIN model, on the other hand, while reasonably accurate, was shown to be very efficient and particularly suited for BOWFOR. Another of the advantages of DOLPHIN lies on the ray technique, which is ideal for forecasting along a ship route.

Nevertheless, the DOLPHIN forecasts had to be improved. It is generally accepted that significant improvements in wave forecasts can only be achieved through assimilation techniques, which correct the input wind fields and wave fields. While the most sophisticated assimilation techniques are very time consuming, the simplest provide only short lived improvements. The assimilation technique used in this work is a compromise between these two extremes: thanks to the choice of integral control variables, it provides long living forecasts with low computational effort.

The possibility of improving the DOLPHIN results by this assimilation technique was explored with reference to its applicability to forecasting over ship routes. Several tests were carried out to assess the effect of assimilating upwave and local observations, and satellite observations in the Indian ocean; in addition, the effectiveness of a continuous assimilation scheme applied to the two storms of Figueira da Foz, in particular regarding the joint assimilation of significant wave height and mean wave frequency, has been examined. The data used in the tests consisted of real and simulated observations of significant wave height, swell wave height and mean wave frequency.

It was found that the assimilation technique is not effective with satellite measurements, that the assimilation of measurements upwave of the forecast location is efficient, and that the validity of forecasts is of two to three days. The example of the operational (continuous) assimilation scheme demonstrated that combining the assimilation of mean wave frequency and significant wave height measurements greatly improves the forecast of the two parameters: the scatter-index of the significant wave height forecasts dropped 12% with data from one storm and 17% with data from another storm, while the corresponding improvements with the mean wave frequency were of 11% and 17%.

Finally, a practical application of the BOWFOR method was presented in Chapter 6. It consisted of a two way trip from Europe to North America, in which the location of the ship was provided 6-hourly. The example run used synthetic data of simulated wave observations and deviated wind fields. The data accounts for the major factors involved in the forecasting problem and is considered representative of a real situation.

The method was tested with continuous two days forecasts using 4 observations of significant wave height and mean wave frequency parameters per day. The resulting predictions were very good during the two trips, but in the return trip they were particularly accurate because the ship was running with the wave conditions. The forecasts had a root-mean-square error of only 0.6 m in the significant wave height and only 0.016 Hz in the mean wave frequency.

BOWFOR, the final output of the thesis, is believed to be a contribution to onboard route wave forecasts. Regarding possible extensions, both the software used and the methodology itself could be improved. Firstly, the associated software could be made more user friendly by developing interface software, enabling it to run as an application of WINDOWS 95, with windows menus. Secondly, the methodology could be integrated in a route optimising model, thus also providing the best route conditionally on a given set of variables.

References

Airy, G. B.,1845. Tides and Waves. Encycl. Metrp. London, pp. 16.

Barnett, T.P. and Wilkerson, J.C., 1967. On the Generation of Wind Waves as Inferred from Air-Borne Measurements of Fetch-Limited Spectra. J. Mar. Res., 67, pp 3095-3102.

Benney, D.J., 1962. Non-linear Gravity Wave Interactions. J. Fluid Mech., 14, pp. 577-584.

Bretschneider, C.L., 1951. The Generation and Decay of Wind Waves in Deep Waters. Tech. Rep. No. 155-46, Inst. Engineering Research.

Bretschneider, C.L., 1952. Revised Wave Forecasting Relationships. Proc. 2nd Conf. Coastal Eng., Berkley, U.S.A., pp 1-5.

Bretschneider, C.L., 1972. Prediction of Waves and Currents. Look Lab/Hawaii, 3, No.1, University of Hawai.

Cavaleri, L. and Malanotte-Rizzoli, P., 1981. Wind Wave Prediction in Shallow Water: Theory and applications. J. Geophys. Res., 89, c11, 10, 961-10, 973.

Davis, R.E., 1969. On the High Reynolds Number Flow Over A Wavy Boundary. J. Fluid Mech., 36, pp. 337-346.

Davis, R.E., 1972. On the Predictions of the Turbulent Flow Over a Wavy Boundary. J. Fluid Mech., 52, pp. 287-306.

Donelan, M.A. and Pierson, W.J., 1987. Radar Scattering and Equilibrium Ranges in Wind-Generated Waves with Application to Scatterometry. J. Geophys. Res., C92, pp. 4971-5029.

Gelci, R., Cazalé, H. and Vassal, J., 1957. Prevision de la Houle. La Méthode des Densités Spectroangulaires. Bull. Inform. Comité Central Oceanogr. d'Étude Côtes, 9, pp. 416-435.

Guedes Soares, C., 1986a. Assessment of the uncertainty in visual observations of wave height. Ocean Eng., 1986, 13, 1, pp. 37-56.

Guedes Soares, C.,1986b. Calibration of visual observations of wave period. Ocean Eng., 13, 6, pp. 539-547.

Guedes Soares, C. and Caires, S., 1995. Changes in spectral Shape Due to the Effect of Finite Water Depth. Proc. 14th Int. Conf. Offshore Mec. Artic Eng. C. Guedes Soares (Ed.), ASME, New York, II, pp 547-556.

Guedes Soares, C. and Caires, S., 1995. Calibration of a Wind Model Based on Wave Hindcast. Report TEC1.4-02(0), MAST2 Contract CT92/0025 (WAVEMOD), I.S.T.

Guedes Soares, C., Caires, S. and Calado, T. Hindcast of a Storm in the Portuguese Coast. Proc. LITTORAL '94, Lisbon, II, pp 231-245.

Hasselmann, K., 1960. Grundgleichungen der Seegangsvoraussage. Schiffstechnik, 7, pp. 191-195.

Hasselmann, K., 1961. On the Nonlinear Energy Transfer in a Wave Spectrum. Proc. Conf. Ocean Wave Spectra. Easton, Maryland, pp. 191-200.

Hasselmann, K., 1962. On the Nonlinear Energy Transfer in a Gravity Wave pectrum-Part I, General Theory. J. Fluid Mech., 12, pp.481-500

Hasselmann, K., 1963a. On the Nonlinear Energy Transfer in A Gravity-Wave Spectrum-Part 2, Conservation Theorems. J. Fluid Mech., 15, pp. 273-281.

Hasselmann, K., 1963b. On the Nonlinear Energy Transfer in a Gravity Wave Spectrum-Part 3, Computation of the Energy Flux And Swell-Sea Interaction For A Neumann Spectrum. J. Fluid Mech., 15, pp. 385-395

Hasselmann, K., 1974. On the Spectral Dissipation of Ocean Waves due to Whitecapping. Boundary-Layer Meteorology, 6, pp.107-127

Hasselmann, K., Barnett, T.P., Bouws, E., Carlson, H., Cartwright, D. E., Enke, K., Ewing, J. A., Gienapp, H., Hasselmann, D.E., Kruseman, P., Meerburg, A., Müller, P., Olbers, D.J., Richter, K., Sell, W. and Walden, H., 1973. Measurments of Wind Wave Growth and Swell Decay During the Join North Sea Wave Project (JONSWAP). Duet. Hydro. Zeit., Reich A12, 95 pp.

Hasselmann, K., Ross, D.B., Müller, P. and Sell, w., 1976. A Parameteric Wave Prediction Model, J. Phys. Ocean., 6, pp. 200-228.

Hasselmann, S., and K. Hasselmann, 1985. Computations and Parameterization of the Nonlinear Energy Transfer in a Gravity Wave Spectrum-Part 1, A New Method for Efficient Computations of the Exact Nonlinear Transfer Integral. J. Phys. Ocean., 15, pp. 1369-1377.

Heras, M.M. de las, G.J.H. Burgers and P.A.E.M. Janssen, 1994. Variational Data Assimilation in a Third Generation Wave Model. J. Atmos. Ocean. Techn., 11, 5, pp 1350-1369.

Holthuijsen, L. H. and S. de Boer, 1988. Wave forecasting for moving and stationary targets. Computer Modelling in Ocean Engineering, Eds. B. A. Schrefler and O. C. Zienkewicz, pp. 231-234

Holthuijsen, L. H., N. Booij, M. van Endt, S. Caires and C. Guedes Soares, 1996. Assimilation of Buoy and Satellite Data in Wave Forecasts with Integral Control Variables, J. Marine Systems, in press.

Jacobs, S.J., 1987. An Asymptotic Theory for the Turbulent Flow Over a Progressive Water Wave. J. Fluid Mech., 174, pp. 69-80.

Janssen, P.A.E.M., 1982. Quasilinear Approximation for the Spectrum of Wind-Generated Water Waves. J. Fluid Mech., 117, pp. 493-506.

Janssen, P.A.E.M., 1989a. Nonlinear Effects in Water Waves. Internal Report, IC/89/66. ICTP Miramare-Trieste.

Janssen, P.A.E.M., 1989b. Wave-Induced Stress and the Drag of Air Flow Over Sea Waves. J. Phys. Ocean., 21, pp. 1631-1642.

Janssen, P.A.E.M., 1991. Quasi-Linear Theory of Wind Wave Generation Applied to Wave Forecasting. J. Phys. Ocean., 21, pp. 1631-1642.

Janssen, P.A.E.M., Lionello, P., Reistad, M. and Hollingsworth, 1989. Hindcasts and Data Assimilation Studies with the WAM Model During the Seasat Period. J. Geophys. Res., C94, pp. 973-993.

Jeffreys, H., 1924. On the Formation of Water Waves by Wind. Proc. Royal Soc. A, London, 107, pp. 189-206

Jeffreys, H., 1925. On the Formation of Water Waves by Wind (second paper). Proc. Royal Soc. A, London, 110, pp. 341-347

Khandekar, M.L., 1989. Operational Analysis and Prediction of Ocean Wind Waves. Springer, New York, 214 pp.

Kitaigorodskii, S. A., Krasitskii, V.P. and Zaslavskii, M.M., 1975. On Phillips' theory of equilibrium range in the spectra of wind-generated waves. J. Phys. Oceanogr., 5, pp. 410-420.

Komen, G.J, Hasselmann, K. and Hasselmann, 1984. On the Existence of a Fully Developed Windsea Spectrum. J. Phys. Oceanogr.,14, pp 1271 1285.

Komen, G. J., Cavaleri, L., Donelan, M., Hasselmann, K., Hasselmann, S. and Janssen, P.A.E.M., 1994. Dynamics and Modelling of Ocean Waves. Cambridge Univ. Press, 532 pp.

Lighthill, M. J., 1960. Studies on magneto-hydrodynamics wave and other anisotropic wave motions. Phil. Trans. Roy. Soc., 252, 397 pp.

Lighthill, M. J., 1962. Physical Interpretation of the Mathematical Theory of Wave Generation by Wind. J. Fluid Mech., 14, pp. 385-398.

Longuet-Higgins, M.S., 1952. On the Statistical Distribution of the Heights of Sea Waves. J. Mar. Res., 11, pp. 385-398.

Longuet-Higgins, M.S., 1962. Resonant Interactions Between Two Trains of Gravity Waves. J. Fluid Mech., 12, pp. 321-347.

Longuet-Higgins, M.S., 1969. On Wave Breaking and the Equilibrium Spectrum of Wind-Generated Waves. Proc. Roy. Soc. London, A310, pp. 151-159.

Miles, J.W., 1957. On the Generation of Surface Waves by Shear Flows. J. Fluid Mech., 3, pp. 85-204.

Miles, J.W., 1959a. On the Generation of Surface Waves by Shear Flows-Part 2. J. Fluid Mech., 6, pp. 558-582.

Miles, J.W., 1959b. On the Generation of Surface Waves by Shear Flows-Part 3, Kelvin-Helmoltz Instability. J. Fluid Mech., 6, pp. 583-598.

Miles, J.W., 1967. On the Generation of Surface Waves by Shear Flows-Part 5, Kelvin-Helmoltz Instability. J. Fluid Mech., 30, pp. 163-175.

Mitsuyasu, H., Nakayama, R. and Komoni, T., 1971. Observations of the Wind and Waves in Hakata Bay. Rep. Res. Inst. Appl. Mech., Kyushu Univ., 19, pp. 37-74.

Neumann, G., 1952. On Wind Generated Ocean Waves with Special Reference to the Problem of Wave Forecasting. Rel. College of Eng. Res. Div., Dept. of Meteorol. and Oceanogr., N.Y.U., 136 pp.

Nordenstroem, N., 1973, A Method to Predict Long-Term Distributions of Waves and Wave-Induced Motions and Loads on Ships and Other Floating Structures. Det Norske Veritas, 81.

Phillips, O.M., 1957. On the Generation of Waves by Turbulent Wind. J. Fluid Mech., 2, pp. 417-445.

Phillips, O.M., 1958. The Equilibrium Range in the Spectrum of Wind-Generated Waves. J. Mar. Res., 16, pp. 231-245.

Phillips, O.M., 1960. On the Dynamics of Unsteady Gravity Waves of Finite Amplitude-Part 1. J. Fluid Mech., 9, pp. 193-217.

Phillips, O.M., 1985. Spectral and Statistical Properties of the Equilibrium Range in Wind-Generated Gravity Waves. J. Fluid Mech., 156, pp. 505-531.

Pierson, W.J., 1952. A Unified Mathematical Theory for the Analysis, Propagation and Refraction of Storm-Generated Ocean Surface Waves, Part I and II. Rel. College of Eng. Res. Div., N.Y.U., 461 pp.

Pierson, W.J., Neumann, G. and James, R.W., 1955. Practical Methods for Observing and Forecasting Ocean Waves by Means of Wave Spectra and Statistics. Pub U. S. Navy Hydrographic Office, H. O. Pub. 602, 284 pp.

Pierson, W.J. and Moskowitz, L., 1964. A Proposed Spectral Form for Fully Developed Wind Seas Based on the Similarity Theory of S.A. Kitaigorodskii. J. Geophys. Res., 69, pp. 5181-5190.

Plant, W.J., 1982. A Relation Between Wind Stress and Wave Slope. J. Geophys. Res., 87, c3, pp. 1961-1967.

Prevosto, M., Krogstad, H.E., Barstow, S., Guedes Soares, C., 1996. Observations of the High Frequency Range of the Wave Spectrum. J. Offshore Mec. Artic Eng., 118, pp. 89-95.

Rudnick, P., 1951. Correlograms for Pacific Ocean Waves. Proc. 2nd Berkeley Symposium on Mathematical Statistics and Probability, University of California Press, pp. 627-638.

Snyder, R.L. and Cox, C.S. , 1966. A Field Study of the Wind Generation of Ocean Waves. J. Mar. Res., 32, pp. 497-531.

Snyder, R. L., Dobson, F.w., Elliott, J.A. and Long, R.B., 1981. Array Measurements of Atmospheric Pressure Fluctuations Above Surface Gravity Waves. J. Fluid Mech., 102, pp. 1-59.

SPM, 1973. Shore Protection Manual. U.S. Army Coastal Engineering Research Center, Corps of Engineers.

Stewart, R. W., 1974. The Air-Sea Momentum Exchange. Boundary Layer Meteorology, Vol. 6, pp. 151-167.

Stokes, G. G., 1847. On the Theory of Oscillatory Waves. Trans. Cambridge Philos. Soc., Vol. 8, pp. 441-473.

Sverdrup, H.U. and Munk, W.H., 1974. Wind, Sea, and Swell: Theory of Relations for Forecasting. Pub. U. S. Navy Hidrographic Office, 601, 44 pp.

SWAMP Group, 1985. Ocean Wave Modelling. Plenun Press, 256 pp.

Tucker, M.J., 1991. Waves in Ocean Engineering - measurements, analysis, interpretation. Ellis Horwood, 431 pp.

WAMDI Group, 1988. The WAM model - A third generation ocean wave prediction model. J. Phys. Ocean. Res., 18, pp. 1775-1810.

Wu, J., 1982. Wind-Stress Coefficients Over Sea Surface from Breeze to Hurricane. J. Geophy. Res., C87, pp. 9704-9706.

Yuan, Y., Tung, C.C. and Huang, N.E., 1986. Statistical Characteristic of Breaking Waves, pp 265-272 in: Wave Dynamics and Radio Probing of the Ocean Surface. O.M. Phillips and K. Hasselmann (eds); Plenum, New York, 694pp.